Cell

Article

Symbiotic entrenchment through ecological Catch-22

Graphical abstract

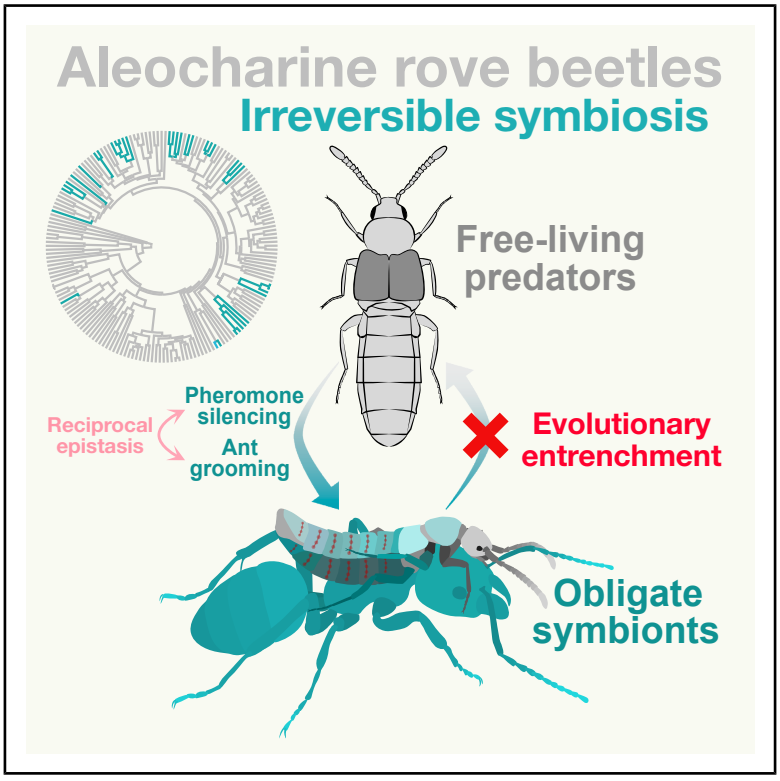

Highlights

- A rove beetle transcriptionally silences the biosynthesis of hydrocarbon pheromones
- The stealth beetle grooms ants, stealing hydrocarbons to infiltrate the ant society
- Ant hydrocarbons stop beetle desiccation, essentializing its attraction to ants
- Interdependent hydrocarbon silencing and ant attraction entrench the symbiosis

Authors

Thomas H. Naragon, Joani W. Viliunas, Mina Yousefelahiyeh, ..., Reto S. Wijker, Alex L. Sessions, Joseph Parker

Correspondence

joep@caltech.edu

In brief

A symbiotic rove beetle develops a stealth phenotype by silencing production of its hydrocarbon pheromones, enabling it to infiltrate ant colonies, steal ant pheromones, and achieve social acceptance as a parasitic impostor. Evolution of this strategy is irreversible, locking the beetle's lineage into obligate dependence on host ant societies.

Naragon et al., 2026, Cell *189*, 1228–1244
February 19, 2026
https://doi.org/10.1016/j.cell.2025.12.041

CellPress

CellPress

Cell

Article

Symbiotic entrenchment through ecological Catch-22

Thomas H. Naragon,[1] Joani W. Viliunas,[2] Mina Yousefelahiyeh,[2] Adrian Brückner,[2] Julian M. Wagner,[2] K. Esther Okamoto,[2] Hannah M. Ryon,[2] Danny Collinson,[2] Sheila A. Kitchen,[2] Reto S. Wijker,[3] Alex L. Sessions,[3] and Joseph Parker[2,4,*]

[1]Division of Chemistry and Chemical Engineering, California Institute of Technology, Pasadena, CA 91125, USA
[2]Division of Biology and Biological Engineering, California Institute of Technology, Pasadena, CA 91125, USA
[3]Division of Geological and Planetary Sciences, California Institute of Technology, Pasadena, CA 91125, USA
[4]Lead contact
*Correspondence: joep@caltech.edu
https://doi.org/10.1016/j.cell.2025.12.041

SUMMARY

Why symbiotic organisms evolve irreversible dependencies on hosts is an outstanding question. We report a biological stealth device in a beetle that permits infiltration of ant societies. Via transcriptional silencing, the beetle switches off biosynthesis of cuticular hydrocarbons (CHCs)—body surface pheromones that function pleiotropically as a waxy desiccation barrier. Silencing transforms the beetle into a chemical blank slate onto which ant CHCs are transferred via grooming behavior, leading to perfect chemical mimicry and acceptance into the colony. Silencing is irreversible, however, forcing the beetle into a chronic dependence on ants to both maintain mimicry and prevent desiccation. We show that evolutionary reversion of the silencing mechanism would render the beetle detectable to ants; conversely, reversion of the beetle's attraction to ants would render it desiccation prone. Symbiotic entrenchment can thus arise from epistasis between symbiotic traits, locking lineages into a Catch-22 that obstructs reversion to living freely.

INTRODUCTION

Obligate symbioses—where one species cannot live apart from another—have reshaped Earth's biosphere, from the endosymbiotic origins of plastids and mitochondria to innumerable lineages of pathogens, parasites, and mutualists that have emerged across all domains of life.[1–4] Complex symbiotic lifestyles are often seen as examples of irreversible evolution, as phenotypes undergo profound specialization for life within particular host niches. Diverse animal,[4,5] plant,[6,7] fungal,[8,9] and microbial[10,11] clades, spanning the spectrum of mutualism to parasitism, exist in which reversion to the free-living state is unknown or extremely rare.[12–17] Why such lifestyles resist reversal is central to understanding the conditions that stabilize symbioses, enabling major evolutionary innovations that arise through obligate species interactions. A pervasive trend in symbionts is the loss of traits[18,19] and genes[20–41] that facilitate free-living lifestyles—the outcome of relaxed selection in host environments[31,40–47] and gene-inactivating mutations that prove adaptive in specialized niches.[39,48–53] The accumulation of reductive changes is a process widely thought to entrench the association between symbionts and their hosts—that is, to counteract the probability of evolutionary reversion to living freely.[26,28,54–56] Yet, whether the loss of traits and genes is the primary cause of symbiotic entrenchment, as opposed to a reinforcing consequence, is challenging to disentangle. During the evolutionary transition to obligate symbiosis, key changes in cellular, physiological, or behavioral mechanisms arose that biased future evolution toward greater integration into the host niche, ultimately locking the phenotype into dependence on another organism. The often highly modified genomes and derived phenotypes of extant symbionts mask the causal conditions that obstruct reversion to the free-living state. Consequently, the basis of entrenchment is largely unknown for symbiotic taxa across the tree of life.

Unraveling the basis of symbiotic irreversibility may be enabled by studying convergent systems, where multiple lineages have undergone independent transitions from a free-living to a symbiotic form. Variation across such lineages may expose key evolutionary changes underlying entrenchment. Myrmecophiles are symbiotic organisms specialized for life inside ant societies and represent the archetype of dramatic symbiotic evolution.[57–59] Approximately 100,000 animal species are suspected to engage in this form of symbiosis,[60] including many that obligately depend on host colonies and are unable to live away from them. Rove beetles of the subfamily Aleocharinae comprise a unique clade where dozens of lineages have convergently evolved from free-living predators into specialized myrmecophiles that obligately assimilate into host colony social structure.[58,61–64] The transition to colony life involves a radical transformation of the phenotype, encompassing stereotyped innovations in behavior, anatomy, and chemical ecology that

enable these beetles to manipulate host ants and gain social acceptance. A common strategy encountered in aleocharine and other myrmecophiles is the mimicry of a class of pheromones on the ant's body surface named cuticular hydrocarbons (CHCs).[64–68] CHCs mediate nestmate recognition,[69,70] and mimicry of these compounds is thought to permit myrmecophiles to evade detection by ants. Yet, how CHC mimicry is achieved mechanistically, and how it evolves, remains poorly understood.

The intimate relationships and associated integration strategies of aleocharine myrmecophiles contrast with free-living species within the subfamily, which display defensive behavior toward ants—the ancestral condition in Aleocharinae.[58,71–74] At the other extreme, species with the most remarkable symbiotic phenotypes appear seamlessly socially integrated into colonies, and such taxa form clades in which there are no apparent cases of reversion to the free-living state.[63,64] This repeated trend implies that entrenchment may be inherent to the assimilation of aleocharine lineages into ant societies. Here, we leverage this beetle radiation to uncover critical changes underlying an obligate and socially complex form of symbiosis. We report a system where multiple aleocharine lineages have independently evolved to target the same host ant but show different degrees of social integration into the nest. Harnessing the comparative power of this natural experiment, we expose critical cellular, biosynthetic, and behavioral innovations in a focal rove beetle species that underlie its obligate dependence on, and social assimilation into, the ant society. Central to this relationship is the beetle's capacity to perfectly mimic ant CHCs. We demonstrate how the evolution of this lifestyle can be intrinsically irreversible, locking a lineage into perpetual symbiosis. Our findings yield a new and potentially general basis for the irreversibility of symbiotic evolution across phylogeny.

RESULTS

A convergent system of ant-myrmecophile symbiosis

We identified three aleocharine lineages that have convergently evolved to socially parasitize a dominant ant species in Southern California, the velvety tree ant (*Liometopum occidentale*).[75] Time-calibrated phylogenomic analysis reveals that the three beetles—*Platyusa sonomae* (herein "*Platyusa*"), *Sceptobius lativentris* ("*Sceptobius*"), and *Liometoxenus newtonarum* ("*Liometoxenus*")—belong to distinct aleocharine tribes (Lomechusini, Sceptobiini, and Oxypodini, respectively) and share a common ancestor ~89 mega-annum (Ma; 95% Highest Posterior Density [HPD]: 106–74 Ma) ago that was likely free living (Figures 1A, S1A, and S1B). Each lineage separately transitioned to myrmecophily, with inferred divergence times from free-living sister groups of 25.5 Ma (*Platyusa*, 95% HPD: 36–15 Ma), 30.8 Ma (*Sceptobius*, 95% HPD: 46–17 Ma), and 51 Ma (*Liometoxenus*, 95% HPD: 70–30 Ma) (Figures 1A, S1A, and S1B). These times approximate or postdate the inferred age of the genus *Liometopum* within its ant subfamily, Dolichoderinae,[76] but represent maximum age estimates. These transitions were likely more recent than inferred, as additional, closely related sister taxa not included in our phylogeny suggest later divergence times.

Convergent evolution but varying accuracy of host ant-like CHC profiles

Colonies of *Liometopum occidentale* are vast, comprising ~10^6 workers that are highly aggressive toward other organisms.[75] Our field data obtained over 8 years, plus historical collection records,[77–79] indicate that all three beetles have been found exclusively with *Liometopum* ants, either inside colonies, at nest entrances, or along foraging trails. To understand how these myrmecophiles evade detection by their host, we examined one of the primary communication systems used by ants, CHCs. CHCs are very-long-chain alkanes and alkenes that many insects use as contact pheromones.[80–82] These compounds are synthesized in abdominal cells named oenocytes[83] and secreted onto the body surface, forming a waxy coating that is also essential for desiccation avoidance.[84–87] Ants have co-opted CHCs as nestmate recognition cues, producing a complex CHC cocktail that functions as a colony identifier. Genetic and environmental factors cause the CHC template to vary between colonies and temporally within the same colony.[70] Via antennal detection, workers evaluate CHCs on the bodies of other insects, accepting nestmates that share the prevailing colony template, while aggressing against insects that present divergent profiles.[69,70]

Gas chromatography-mass spectrometry (GC-MS) analysis of body surface compounds revealed that the three myrmecophiles present CHC profiles highly similar to that of *Liometopum* workers (Figures 1B–1D). We identified each CHC compound within the host ant's profile and found that all three myrmecophiles likewise possess the same compounds, almost without exception (Table S1A). Notably, *Liometoxenus* and *Platyusa*—but not *Sceptobius*—possess a small number of additional CHCs (all alkenes) that are absent from the ant's profile (Figures 1B and 1D; Table S1A). We measured CHCs from many individuals of *Liometopum*, the three myrmecophiles, and four free-living species from across the Aleocharinae phylogeny: *Acrotona* and *Dalotia* (both tribe Athetini), *Oligota* (Hypocyphtini), and *Falagria* (Falagriini). Non-metric multidimensional scaling (NMDS) of pairwise Bray-Curtis dissimilarity measurements of the various profiles revealed that the three myrmecophile beetles are closer to, or cluster tightly with, their host ant, to the exclusion of the free-living beetles (Figure 1E). Hierarchical clustering of pairwise Bray-Curtis or Jaccard dissimilarity measures further confirmed that the CHC profiles of the myrmecophiles and *Liometopum* were more similar to each other than to those of free-living species, based on quantitative CHC composition (Figure 1F) or qualitative compound presence/absence (Figure 1G). We infer that the CHC profiles of the three myrmecophiles each independently evolved a similarity to that of their shared host ant, implying chemical mimicry.

A greater chemical resemblance was likely a key step in the symbiotic evolution of *Platyusa*, *Sceptobius*, and *Liometoxenus*, permitting closer contact with ants. The three beetles nevertheless differ in how accurately they match the ant's profile. We quantified chemical divergence between beetle and ant on a nest-by-nest basis, calculating the Bray-Curtis dissimilarity of every beetle to the mean profile of worker ants from that beetle's host colony. Strikingly, *Sceptobius* beetles and host ants exhibit equivalent dissimilarity to the mean ant profile, indicating that

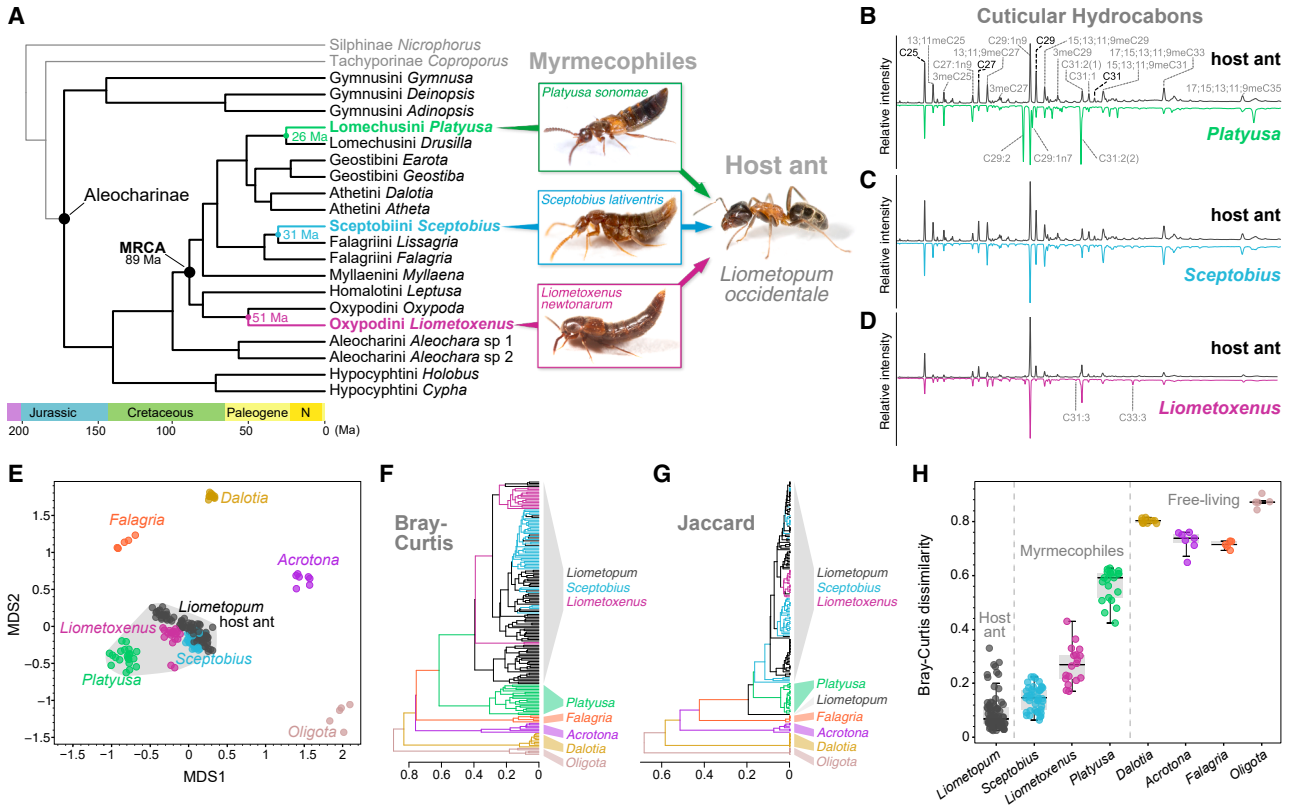

Figure 1. A convergent system of ant-myrmecophile symbiosis

(A) Dated phylogenomic tree inferred from 1,039 orthologous protein-coding loci and 12 fossil calibration points. The topology is strongly supported at all nodes (see Figure S1B).

(B–D) Gas chromatographs of CHCs from *Liometopum* host workers (top trace, with identified compounds labeled) and the myrmecophiles *Platyusa* (B), *Sceptobius* (C), and *Liometoxenus* (D). The *Sceptobius* profile closely matches the ant profile in both compound presence/absence and relative ratios, while *Platyusa* and *Liometoxenus* show certain quantitative and qualitative differences. The unique compounds absent from the ant trace are labeled for *Platyusa* and *Liometoxenus*.

(E) NMDS ordination of CHC chemical dissimilarity (pairwise Bray-Curtis) between the host ant and three myrmecophiles (demarcated by gray convex hull), as well as four free-living aleocharine species, 2D stress = 0.13.

(F and G) Hierarchical clustering of individual insect CHC profiles based on compound identity and relative abundance (Bray-Curtis) (F), and identity alone (Jaccard) (G).

(H) Bray-Curtis dissimilarity of individual ants and myrmecophiles to the mean ant profile of their colony of origin; dissimilarities of free-living beetles are to the mean ant profile calculated across colonies.

See also Figure S1 and Table S1A.

ant and beetle have effectively indistinguishable CHC profiles (Figure 1H). In contrast, the additional compounds in the profiles of *Liometoxenus* and *Platyusa* result in these species having significant dissimilarity to their host colony's mean CHC profile; in the case of *Platyusa*, differences in the ratios of some compounds common to *Platyusa* and the host ant further increase dissimilarity (Figure 1H), to the extent that the beetle falls outside of the *Liometopum* ant cluster based on Bray-Curtis and Jaccard measures (Figures 1E–1G), albeit grouping more closely with the ant than do all free-living beetles.

Due to the sensitivity of ants to even minor deviations from the CHC template,[88] these dissimilarities are likely detectable by the host ants, with consequences for the corresponding degree of integration of these myrmecophiles within the *Liometopum* society. Indeed, of the three beetles, *Sceptobius* frequents the nest proper,[77] where it feeds on host eggs and larvae, and receives food trophallactically (mouth-to-mouth) from workers, indicating complete social acceptance (Video S1). *Platyusa* and *Liometoxenus*, by contrast, are predominantly found at nest entrances and trails and feed directly on adult workers (Video S1).

Approximate chemical mimicry through *de novo* CHC synthesis

We investigated the mechanisms by which these myrmecophiles generate their CHC profiles, focusing on *Platyusa* and *Sceptobius*, which, respectively, exhibit the least and most accurate mimicry. We first determined the biosynthetic sources of the beetles' CHCs, leveraging the tendency of carbon stable isotope ratios of specific molecules to vary between organisms, depending on diet.[89] Using compound-specific gas chromatography isotope-ratio mass spectrometry (GC-IRMS), we measured the $\delta^{13}C$ values of specific CHCs present on

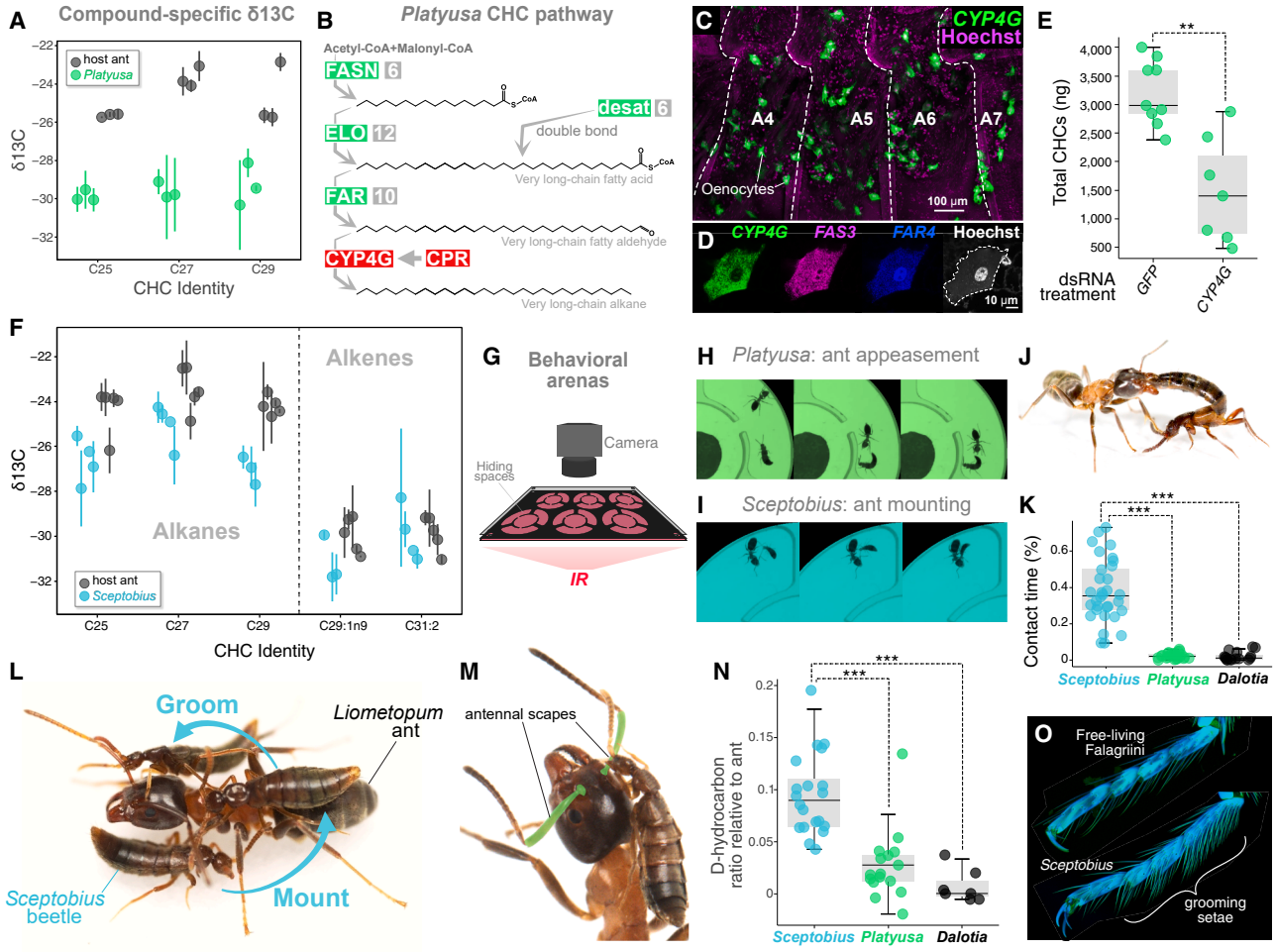

Figure 2. Distinct mechanisms of CHC mimicry

(A) $\delta^{13}C$ values of specific CHCs from *Platyusa* and *Liometopum* measured via GC-IRMS.

(B) The *Platyusa* CHC pathway. Gray boxes show number of paralogs per enzyme. CYP4G and CPR are both encoded by single-copy genes.

(C) Hybridization Chain Reaction (HCR) labeling of *CYP4G* transcripts (green) in oenocytes of the *Platyusa* abdomen (segments A4–A7 shown). Magenta, Hoechst-labeled nuclei.

(D) HCR labeling of *Platyusa CYP4G* (green), *FAS3* (magenta), *FAR4* (blue), and nuclei (white).

(E) CYP4G-RNAi in adult *Platyusa* depletes total CHCs; $p = 0.0017$.

(F) $\delta^{13}C$ values of specific CHCs from *Sceptobius* and *Liometopum* measured via GC-IRMS.

(G) Behavior arenas for tracking ant-beetle interactions.

(H) *Platyusa* demonstrating stereotyped ant appeasement behavior in arena.

(I) *Sceptobius* exhibiting stereotyped ant grooming behavior in arena.

(J) *Platyusa* appeasing *Liometopum* using substance secreted from abdomen tip.

(K) Contact time between beetles and *Liometopum* in behavioral arenas over 24 h. Asterisks denote $p < 0.0001$ in Tukey post hoc tests.

(L) *Sceptobius* climbing onto and grooming *Liometopum*.

(M) *Sceptobius* grasps the ant's antennal scape with its mandibles to permit grooming.

(N) Baseline-corrected deuterated hydrocarbon transferred from *Liometopum* to beetles in behavioral arena over 24 h. Asterisks denote $p < 0.0001$ in Tukey post hoc tests.

(O) *Sceptobius* tarsi bear dense "grooming setae," absent in free-living outgroup beetles of the tribe Falagriini.

See also Figures S2 and S3, Table S1, and Videos S2 and S3.

the two beetles and the ant. If a CHC is present on ants and beetles from the same colony but differs in $\delta^{13}C$ per mille value between the two species, it independently originated in each species; conversely, if the CHC has an identical $\delta^{13}C$ in both species, it probably came from the same biosynthetic source. We extracted CHCs from four replicates of twenty *Platyusa* beetles and twenty *Liometopum* ants from the same colony. GC-IRMS was able to achieve sufficient separation to measure $\delta^{13}C$ of three compounds shared by both species: C25, C27, and C29. For all three CHCs, we determined a large $\delta^{13}C$ offset of ~5 per mille between the *Platyusa* CHC and the corresponding compound from *Liometopum* (Figure 2A). We deduce that

Platyusa synthesizes these hydrocarbons—and likely other CHCs in its profile—*de novo*.

We further tested for *de novo* synthesis by isolating *Platyusa* from ants and found that the beetle can complete its life cycle in the laboratory in the absence of its host, reared on a diet of freshly killed *Drosophila*. Under these conditions, adult *Platyusa* present a CHC profile closely matching that of wild-caught beetles from *Liometopum* nests, albeit with altered ratios of certain compounds, implying beetles endogenously synthesize CHCs. The shifted dietary input mildly influences the profile (Figures S2A–S2D). We confirmed that *Platyusa* produces its own CHC profile by inhibiting endogenous CHC biosynthesis in this species. Insect CHCs derive from a conserved oenocyte pathway in which long-chain fatty acids are elongated and reduced to aldehydes before decarbonylation, yielding secreted, very-long-chain alkanes and, if additionally desaturated, alkenes.[82] Using RNA sequencing (RNA-seq) and differential expression analysis, we recovered an entire CHC pathway expressed in abdominal tissue, with multiple paralogs encoding enzymes for fatty acid synthesis (FASN), elongation (ELO), reduction (FAR), and desaturation (desat) (Figures 2B and S3A; Table S1B). Some of these are orthologs of enzymes previously shown to mediate CHC biosynthesis in the free-living aleocharine, *Dalotia coriaria*[73] (Table S1C). Importantly, the terminal decarbonylation step in CHC biosynthesis is performed by a single, insect-specific cytochrome P450 enzyme, CYP4G.[90] We confirmed that *Platyusa CYP4G* is expressed in large abdominal cells intermingled with fat body tissue (Figure 2C), which co-express copies of the other pathway enzymes (Figures 2D and S3C). Based on gene expression and anatomical location, we infer these cells to be oenocytes. In *Dalotia*, RNAi silencing of *CYP4G* causes loss of CHCs on the beetle's body surface,[73] and injecting double-stranded RNAi (dsRNAi) into wild-caught *Platyusa* similarly reduced the levels of all CHCs (Figures 2E and S3E). We conclude that *Platyusa* synthesizes a CHC profile *de novo* that is, at best, approximately mimetic, imperfectly matching the CHC template of any one specific host colony (Figures 1B and 1E–1H).

Accurate chemical mimicry through horizontal CHC transfer

The mode of CHC mimicry in *Sceptobius* is strikingly different from that of *Platyusa*. We were able to resolve five CHCs suitable for compound-specific GC-IRMS from *Sceptobius* beetles and ants collected from the same colony. In contrast to *Platyusa*, the $\delta^{13}C$ values of each *Sceptobius* compound overlapped with the $\delta^{13}C$ values of the corresponding ant compound, indicating a common biosynthetic origin (Figure 2F). Within a nest, *Liometopum* workers outnumber *Sceptobius* beetles by 2–3 orders of magnitude, implying that the source of *Sceptobius* CHCs is likely the ant, rather than the other way around. We explored the basis of the differing modes of CHC mimicry employed by *Sceptobius* and *Platyusa* by tracking individual beetles and ants in behavioral arenas for 24 h (Figure 2G). *Platyusa* avoided ants, spending <5% of the time in ant contact, similar to free-living *Dalotia* rove beetles (Figure 2K). During brief encounters, we observed *Platyusa* evade scrutiny by ants by "appeasing" them with secretions from the abdominal tip (Figures 2H and 2J; Video S2). Though *Platyusa*'s approximately mimetic CHC profile may confer some advantage during ant encounters, this additional behavior may function to pacify and/or distract workers that attempt to closely antennate the beetle. Comparable appeasement behavior has been observed in related aleocharines within the tribe Lomechusini,[91–94] and we speculate that these myrmecophilous associations may depend only partially on mimicry of host ant CHCs.

In contrast to *Platyusa*, *Sceptobius* spent >30% of the time in prolonged, physical contact with *Liometopum* (Figures 2I and 2K). Closer examination revealed a remarkable behavior in which *Sceptobius* mounts the dorsal ant body (Figure 2L), clasping the ant's antennae in its mandibles (Figure 2M). Anchored to the ant in this way, the beetle "grooms" the ant by scraping its tarsi repeatedly over the surface of the ant, and then the surface of its own body (Video S3; see also video S1 in Wagner et al.[95]). We established that this behavior transfers CHCs from ant to beetle. Applying deuterated hydrocarbons onto *Liometopum* workers, and then housing these ants with beetles, we measured significant transfer onto *Sceptobius* after 24 h (Figures 2N and S2E) but negligible transfer onto *Platyusa* or *Dalotia*. *Sceptobius* tarsi bear specialized "grooming setae" that likely enhance CHC transfer via increased surface area (Figure 2O). We conclude that, via interspecies grooming behavior, *Sceptobius* horizontally "steals" CHCs from ants. In this way, the beetle is capable of achieving perfect mimicry of any gestalt, colony-specific CHC template (Figures 1C and 1E–1H).

We note that the third myrmecophile lineage, *Liometoxenus*, may also acquire CHCs via physical interactions with ants. In this species, beetles crawl underneath workers, rubbing their dorsum against the ant's body (Video S4). The mimetic accuracy of *Liometoxenus* is nevertheless weaker than that of *Sceptobius* (Figures 1D–1G), with unique peaks indicating that some fraction of the profile remains endogenously synthesized (Figure 1D; Table S1A).

CHC production by *Sceptobius*

Our findings show that CHCs on the cuticle of *Sceptobius* originate from ants. Curiously, however, upon assembly of a genome and whole-body transcriptome of the beetle, we discovered an entire CHC pathway comprising intact (non-pseudogenized) loci for each catalytic enzyme. Multiple paralogs encoding FASs, ELOs, FARs, and desats are present, as well as CYP4G (Figures 3A and S3B; Table S1D). Moreover, these enzymes are co-expressed in abdominal cells that we infer to be oenocytes (Figures 3B, 3C, and S3D). This counterintuitive finding led us to consider what function CHCs may play in this species, given their tight integration inside colonies, where they horizontally acquire the colony CHC template. We speculated that the pleiotropic, non-pheromonal function of CHCs in desiccation resistance may be important (Figure 3D). Over the years of this study, we conducted natural history observations, piecing together the life cycle of *Sceptobius* (Figure 3E). We found that adult females produce giant eggs that fill the entire abdomen (Figure S4A) and contain sufficient resources to support development from egg to adult. Females oviposit in damp soil directly at nest entrances; larvae hatch from these eggs and do not

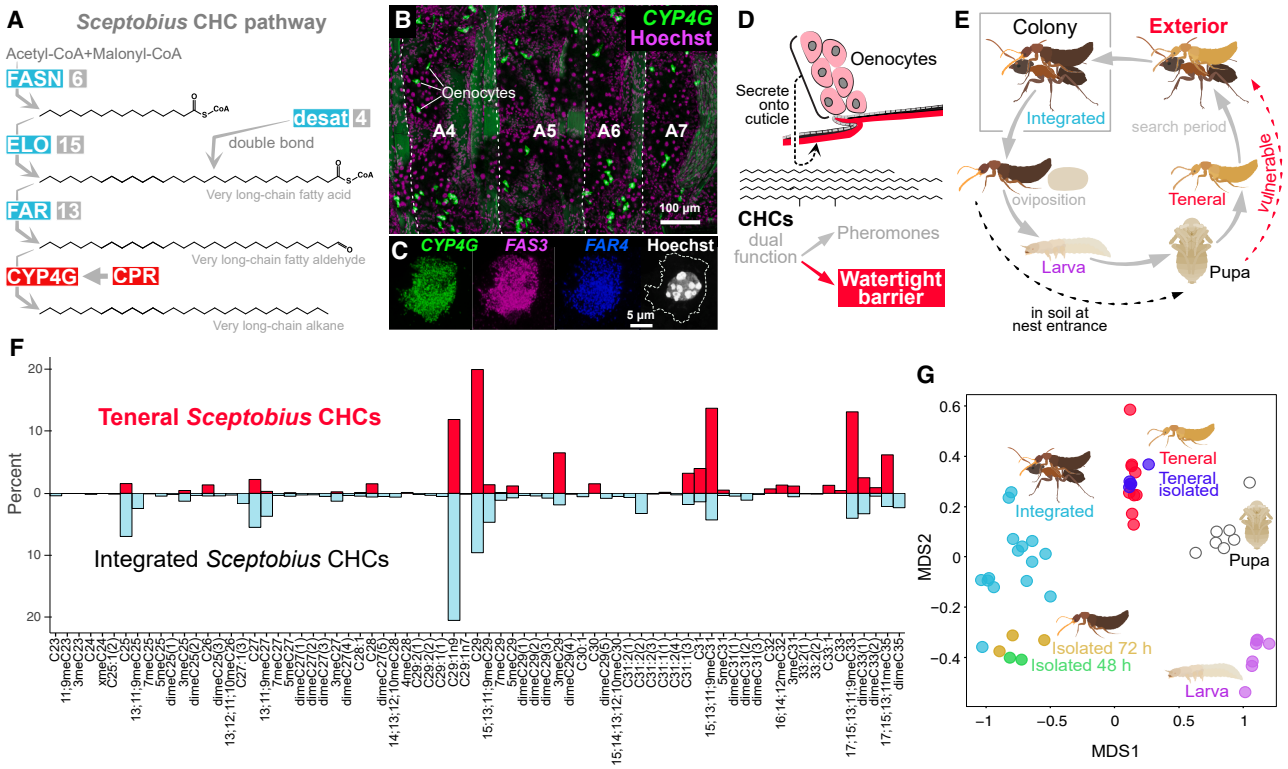

Figure 3. *Sceptobius* CHC biosynthesis

(A) *Sceptobius* CHC pathway, with paralog numbers in gray boxes.

(B) *CYP4G* HCR (green) reveals oenocytes distributed in abdominal segments A4–A7 (magenta: nuclei).

(C) HCR reveals co-expression of CHC pathway enzymes in *Sceptobius* oenocytes (green, *CYP4G*; magenta, *FAS3*; blue, *FAR4*; white, nuclei).

(D) CHCs play a dual role as contact pheromones and a desiccation barrier on the cuticle.

(E) *Sceptobius* life cycle is split between the nest interior and exterior. Oviposition as well as larval and pupal development occur outside of the nest. After eclosing, teneral beetles groom ants, integrating into the nest interior.

(F) Teneral *Sceptobius* produce a CHC profile distinct from integrated *Sceptobius*, and thus also different from the host ant.

(G) NMDS ordination of CHC profiles, measured across *Sceptobius* development, using Bray-Curtis dissimilarity, 2D stress = 0.05.

See also Figure S3 and Table S1.

need to feed, developing and pupating in soil, insulated from ants walking above them. After roughly 2 weeks, teneral (depigmented) adult beetles eclose and search for an ant to groom; due to the proximity of egg laying to *Liometopum* nests, the groomed ant will likely belong to the beetle's maternal colony, into which the beetle will integrate after "stealing" the CHC template (Figure 3E).

Sceptobius develops a "stealth" phenotype via CHC pathway silencing

Prior to grooming, the teneral beetle is highly vulnerable to desiccation, bearing no ant-derived CHCs on its body (Figure 3E). We collected *Sceptobius* eggs and larvae from *Liometopum* nest-entrance soil and transferred them to ant-free soil to undergo metamorphosis. Remarkably, teneral beetles, pre-ant contact, bear a detectable CHC profile that must be produced endogenously and is consistent across teneral beetles from different colonies (Figures 3F and 3G). The teneral profile is clearly distinct from that of a mature, integrated beetle that has obtained its CHCs via grooming (Figures 3F and 3G). The teneral profile instead appears to bear a "skeletal" similarity to the ant's profile, comprising only 31 components, almost all of which are present in *Liometopum* (Figure 3F). The profile lacks the full, 73-component complexity of a horizontally acquired CHC profile present on mature, integrated beetles (Figure 3F). CHCs are also produced by *Sceptobius* larvae and pupae—each stage synthesizing a distinct profile (Figure 3G). Hence, early *Sceptobius* life stages that inhabit the nest exterior produce CHCs, in keeping with the essential role of these compounds in desiccation resistance.

The total mass of endogenous CHCs on teneral *Sceptobius* is similar to that on *Sceptobius* larvae and pupae—and an order of magnitude less than the CHC mass acquired by integrated beetles via grooming (Figure 4A). Nevertheless, the incongruence between the teneral CHC profile and the mimetic profile obtained via grooming is of sufficient magnitude that, were these endogenous CHCs still present on the body of an integrated beetle, they would disrupt perfect mimicry (Figure 4B). NMDS ordination of the integrated *Sceptobius* CHC profile—shifted, *in silico*, by adding the average teneral beetle profile to it—would push most of the integrated profiles outside of ant CHC space (Figure 4C). How, then, does *Sceptobius* achieve perfect mimetic accuracy through grooming, when it is simultaneously

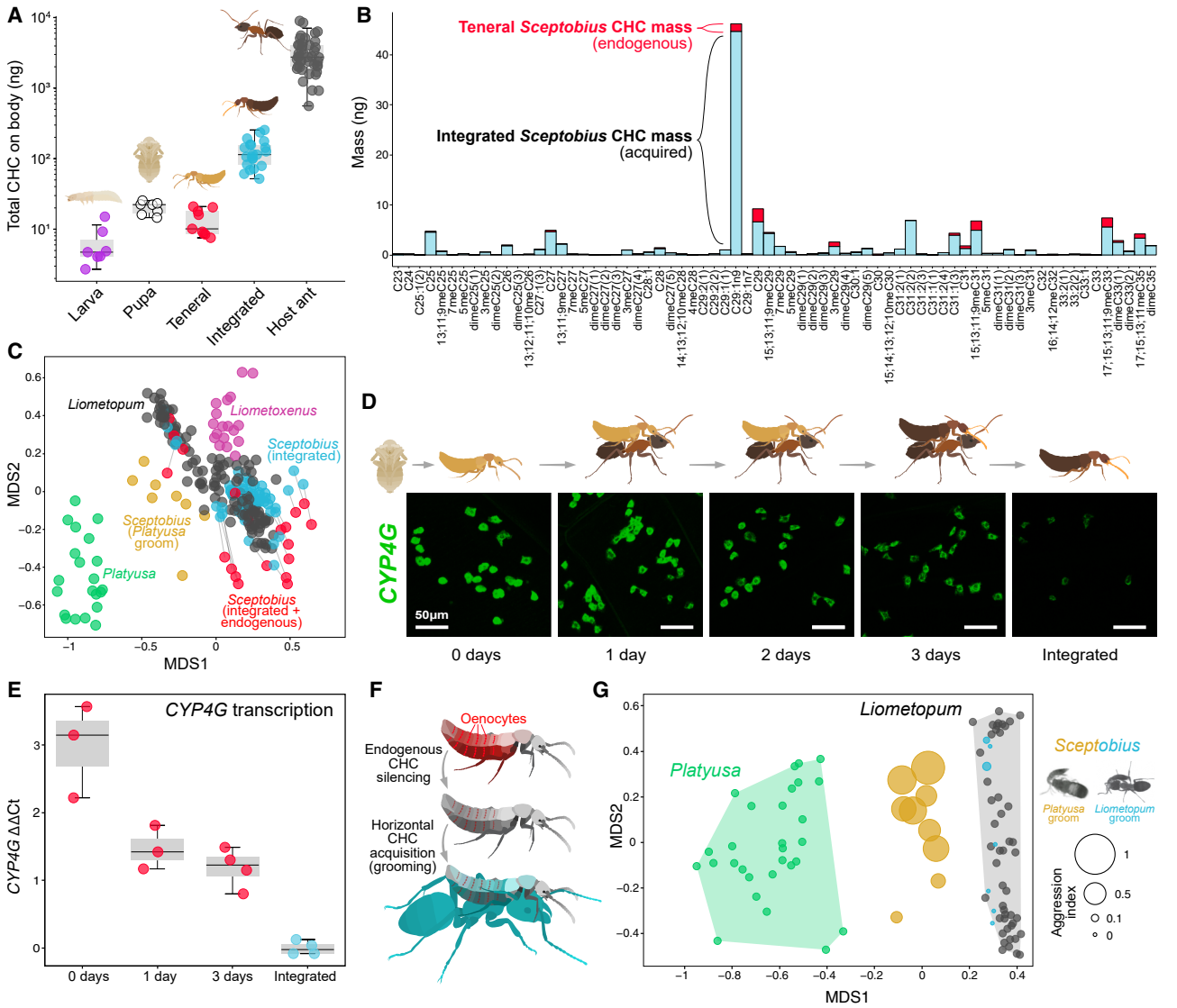

Figure 4. Adult *Sceptobius* develop a stealth phenotype

(A) Total CHC mass on *Sceptobius* life stages and *Liometopum* workers.

(B) Mean amount of each CHC on the integrated *Sceptobius* body (light blue), with the mean teneral profile stacked on top (red).

(C) NMDS ordination of *Liometopum* and myrmecophile CHC profiles (Bray-Curtis dissimilarity, 2D stress = 0.12). Blue data points are integrated *Sceptobius*; red points are combined integrated+teneral profiles (if integrated *Sceptobius* synthesized the teneral CHC profile in addition to acquiring CHCs from *Liometopum*). Gold points are profiles of *Sceptobius* that have groomed *Platyusa*.

(D) HCR time course of *CYP4G* expression levels in *Sceptobius* oenocytes, from eclosion from pupa to social integration in the nest.

(E) qPCR time course of whole-body *CYP4G* transcripts post eclosion.

(F) *Sceptobius* silences CHC biosynthesis and horizontally obtains *Liometopum* CHCs via grooming to integrate into colonies.

(G) NMDS ordination of *Platyusa*, *Sceptobius*, and *Liometopum* CHC profiles (Bray-Curtis dissimilarity, 2D stress = 0.08). CHC profiles for *Sceptobius* (with additional *Platyusa* CHCs, gold; control beetles, blue). Data point size indicates the degree of aggression experienced by each beetle in a behavioral trial with three ants from the beetle's colony of origin.

See also Figure S4.

capable of synthesizing a mimicry-disrupting, endogenous profile? We noted that, while imaging gene expression in oenocytes of mature, integrated beetles, transcript levels of CHC pathway enzymes, such as *CYP4G*, were barely detectable (Figure 4D). We quantified *CYP4G* expression over the time course of early adult life and found that expression is maximally high on eclosion from the pupa, dropping to approximately 30% by 72 h, before strongly diminishing to the baseline seen in integrated beetles (Figures 4D, 4E, and S4B–S4D). A parallel drop in gene transcription is observed for other pathway enzymes that mediate earlier steps in CHC biosynthesis (Figures S4D and S4E). CHC biosynthesis, therefore, shuts down in integrated adults. This is

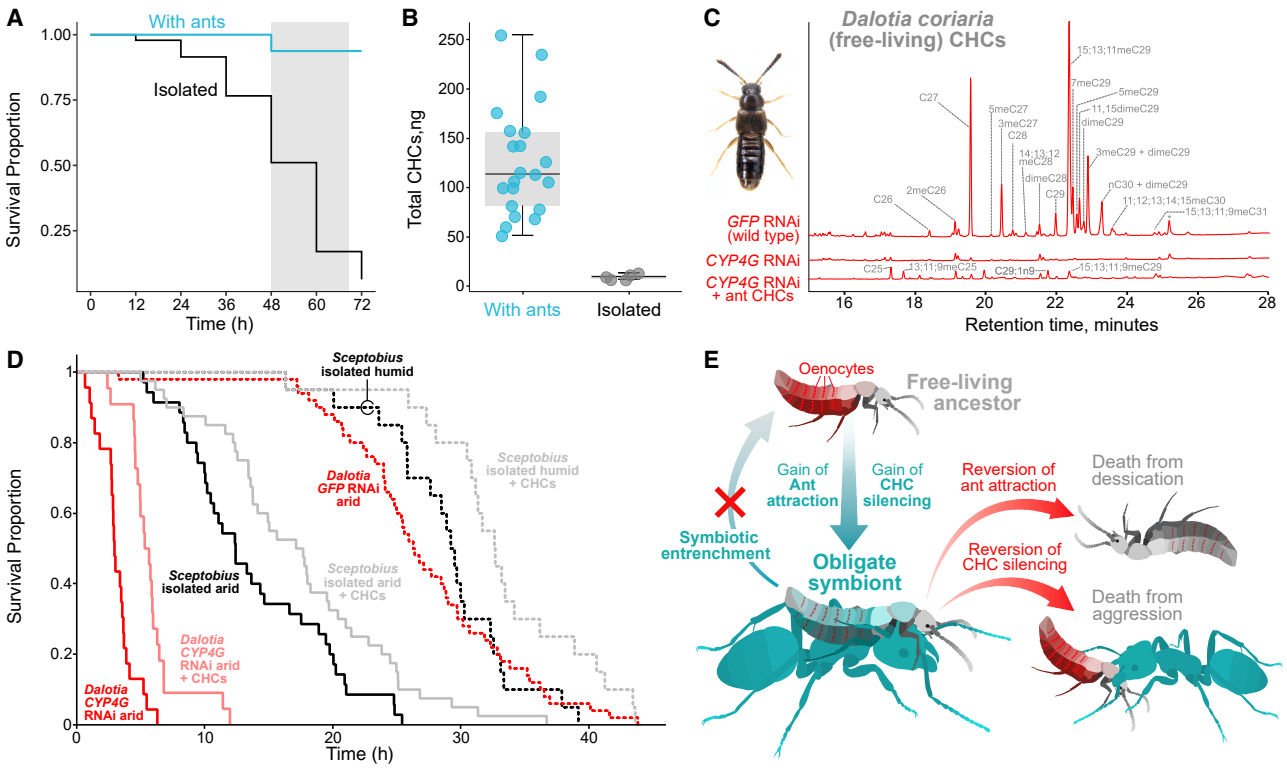

Figure 5. Entrenchment of myrmecophily

(A) *Sceptobius* undergoes rapid mortality when physically isolated from ants.

(B) Isolating *Sceptobius* results in a drastic reduction of CHCs prior to death.

(C) Free-living *Dalotia coriaria* CHC production can be silenced and replaced with a low level of *Liometopum* CHCs.

(D) Survival curves of *Sceptobius* and *Dalotia* under CHC or environmental manipulations.

(E) Entrenchment of obligate myrmecophily in *Sceptobius* through reciprocal sign epistasis between ant attraction and CHC silencing.

See also Figure S5.

achieved via transcriptional silencing of multiple CHC pathway enzymes.

We infer that *Sceptobius* produces CHCs during the vulnerable larval, pupal, and teneral life stages, which likely helps to counter desiccation (and may also be essential for successful eclosion from the pupal exuvium[96]). The teneral profile is minimal in level and possibly quasi-mimetic. During the subsequent search phase, in which the beetle locates a worker ant to groom, the CHC pathway undergoes transcriptional silencing, creating a chemically stealth beetle phenotype that can now achieve perfect chemical mimicry via grooming (Figure 4F).

We performed an experiment to demonstrate how the silencing of endogenous CHC biosynthesis is essential for the social integration of *Sceptobius* into host ant colonies. In a separate study, we found that *Sceptobius* recognizes its *Liometopum* host by detecting the ant's CHCs, which elicit the beetle's grooming behavior.[95] Because *Platyusa* presents the same CHCs as the ant, we discovered that *Sceptobius* will similarly groom this other myrmecophile species in much the same way it grooms host ants.[95] We repeated this experiment and found that grooming *Platyusa*'s "approximately" mimetic profile has the effect of pulling the CHC profiles of formerly integrated *Sceptobius* beetles outside of ant chemical space—a near-equivalent degree to the hypothetical (*in silico*) addition of the teneral profile (Figure 4C). Remarkably, disruption of the beetle's CHC profile in this way breaks the stealth beetle's cover. Such beetles are attacked repeatedly by the ant, revealing a high fitness cost to endogenous CHC production inside the nest (Figure 4G). We deduce that the stealth phenotype is critical for the viability of *Sceptobius* inside its host colony. It converts the cuticle into a chemical blank slate that evades detection by ants and permits social integration by acting as a blank canvas for the acquisition of host ant CHCs.

Horizontal acquisition of ant CHCs is essential for *Sceptobius* survival

Our findings reveal how *Sceptobius* transitioned from a free-living beetle to a myrmecophile via two phenotypic innovations: (1) a mechanism to silence endogenous CHC production and (2) a social behavioral program to obtain CHCs via ant grooming. Through these twin modifications, the beetle gained the ability to integrate into colonies. This has come at the expense of being able to live away from ants. In contrast to *Platyusa*, isolating *Sceptobius* from ants leads to rapid mortality over 12–72 h, whereas under the same laboratory conditions, the beetles survive long term if ants are present (Figure 5A). Just prior to

and immediately following death, isolated beetles exhibit negligible levels of CHCs on their bodies due to the rapid turnover of the previously acquired profile (Figure 5B). The remnant profiles are close to those of integrated beetles and clearly distinct from those of teneral beetles (Figure 3G). We infer that the silencing of endogenous CHC production is irreversible: isolated *Sceptobius* is incapable of compensatory biosynthesis of these compounds. This inability to reactivate biosynthesis implies that beetles are likely apart from ants at most transiently during adult life once integrated, removing selection pressure to endogenously produce these compounds.

We explored whether irreversible CHC loss may contribute to obligate dependence of *Sceptobius* on ants, contrasting this myrmecophile with *Dalotia*—an aleocharine approximating the free-living phenotype from which *Sceptobius* evolved.[74] *Dalotia* endogenously produces CHCs, which can be removed by silencing *CYP4G* (Figure 5C). In arid conditions, wild-type *Dalotia* survival begins dropping at ~20 h, reaching 50% at ~28 h (Figure 5D). Silencing *CYP4G* renders *Dalotia* desiccation-prone, with the beetles now reaching 50% mortality within ~5 h (Figure 5D). Application of a small level of *Liometopum* CHCs to these *Dalotia* (Figure 5C) moderately but significantly prolongs survival (Figure 5D). These results underscore the critical function that CHCs play in water balance and survival of free-living beetles.

The evolutionary loss of CHC production in mature *Sceptobius* beetles forces the beetle into a chronic dependence on CHCs acquired from ants. We permitted *Sceptobius* to groom ants and obtain a full CHC profile before isolating beetles in the same arid conditions used for *Dalotia*. Such beetles begin dying rapidly, reaching 50% mortality within 12 h, implying that ant CHCs are quickly lost (Figure 5D). As with *Dalotia*, repeating this experiment with low-level application of additional *Liometopum* CHCs moderately prolonged *Sceptobius* survival, whereas increasing humidity approximately doubled lifespan, with *Sceptobius* survival now approximating that of free-living *Dalotia* under arid conditions (Figure 5D). Some water loss through the chitinous cuticle can still occur in humid conditions,[97] hence even at elevated humidity, the application of additional *Liometopum* CHCs partially extended *Sceptobius* survival (Figure 5D).

CHCs acquired from ants are therefore essential for *Sceptobius* survival. We infer that the evolution of grooming behavior not only achieved chemical mimicry and social integration but also compensated for the loss of endogenous CHCs, which were essential for desiccation resistance in *Sceptobius*' free-living ancestors.

DISCUSSION

The phenotype we report for *Sceptobius* represents a putative syndrome that has evolved convergently in aleocharine beetles. Myrmecophile lineages that are socially integrated are often those that groom worker ants (or are groomed by them)[63,98–104] and undergo rapid mortality on isolation[98] (Figures S5A–S5C). All such clades show no instances of reversion to living freely[63]—a macroevolutionary pattern for which we offer a mechanistic explanation. We have shown that CHC silencing in adult *Sceptobius* has become an essential trait. Reversion of this phenotype to one of sustained CHC biosynthesis would be costly, breaking perfect mimicry in a beetle that has evolved to physically interact with ants (Figure 5E). Concurrently, the beetle's strong physical attraction to ants has also become essentialized. Its loss would be lethal, as the ant has become the source of CHCs that form a critical desiccation barrier (Figure 5E). *Sceptobius* is thus caught in a Catch-22,[105] where loss of either symbiotic trait renders the other deleterious. This arrangement is likely to have a ratcheting effect on evolution—the low probability of simultaneous reversion locking the lineage into obligate ant dependence (Figure 5E). All other traits being equal, the evolution of ant attraction, combined with irreversible endogenous CHC silencing, suffices to entrench the formerly free-living phenotype within ant colonies. Entrenchment may therefore be inherent to a form of social integration that has evolved convergently and irreversibly in this vast beetle subfamily. Across these convergent myrmecophile lineages, trait losses have occurred idiosyncratically, including the degeneration of eyes, wings, and the defensive tergal gland in various taxa (Figures S5D and S5E). We suspect that these losses are not themselves causal entrenching mechanisms but instead arise in entrenched lineages evolving under relaxed selection. Shedding these now-obsolete structures may also be adaptive, given their presumed metabolic cost.

We do not know the underlying genetic architecture of each symbiotic trait in *Sceptobius*, but the Catch-22 holds even if single mutational changes could eliminate either trait (or cause its reversion to the ancestral state). Reciprocal dependence between the two traits to perform their essential functions protects them from individually reverting. This condition, where two traits that permit symbiosis are functional when together but deleterious alone, is a phenotypic manifestation of "sign epistasis," in which a mutation's cost or benefit is contingent on the genetic background in which it occurs.[106] Sign epistasis underlies irreversibility at the protein level, where substitutions that alter protein function[107–109] or subunit binding[110] become entrenched through epistatic interactions with more recent substitutions. Extending the notion of epistasis to the trait level, we propose that an analog underlies cases of symbiotic entrenchment. Traits that promote interactions with other organisms may undergo loss or reversion if they are epistatically unconnected or show non-reciprocal epistasis, offering potential return paths to living freely. In *Platyusa*, closely associating with ants is likely only beneficial in the context of the beetle's ability to endogenously mimic its host's CHCs, but endogenous CHC mimicry is not itself deleterious in the absence of ants. Loss of ant attraction may therefore be possible in *Platyusa*, permitting reversion of myrmecophily in this species. By contrast, if at least two distinct symbiosis-promoting traits arise, whether through adaptive or neutral evolution, entrenchment of a symbiotic association may follow if the loss or reversion of one trait makes the other deleterious. Such is the scenario we demonstrate between ant attraction and CHC pathway silencing in *Sceptobius*.

Given the interdependence of symbiotic traits in *Sceptobius*, how each individual trait could have evolved presents a conundrum. A plausible scenario, however, is implied by considering the three myrmecophile lineages—*Platyusa*, *Liometoxenus*, and *Sceptobius*—as embodying steps along a transition from

free-living to obligate symbiont. Accordingly, *Platyusa* represents an initial step in which endogenous production of a crudely mimetic CHC profile, combined with chemical appeasement of workers, permits an ancestrally free-living beetle to shift its microhabitat to the ant-dense colony periphery. Here, the beetle interacts physically with ants via both appeasement and predation. In a subsequent step, exemplified by *Liometoxenus*, the lineage evolves greater behavioral intimacy with workers, facilitated by reduced endogenous CHC production together with the acquisition of ant CHCs by close, physical interactions (rubbing against the ant body, observed in *Liometoxenus*, may be a precursor to ultimately mounting and grooming workers). The close interactions of *Liometoxenus* occur despite some (apparent) endogenous CHC production (Figure 1D)—a situation that may be enabled by the release of a volatile secretion from the beetle's tergal gland, which appears to "intoxicate" workers,[74] attenuating their aggression and permitting the beetle to crawl below them and rub its dorsum against the ant body (Video S4). The chemical evolvability and behavioral versatility of aleocharine glands[58,64,74] may be an important facilitator behind the repeated evolution of obligate myrmecophily. Through ant-manipulating secretions, beetles gain sufficient closeness to begin acquiring host CHCs—a probable precondition for evolving social integration.

With a substantial fraction of total CHC now laterally acquired from the ant, we speculate that a further step underlies symbiotic entrenchment: the irreversible silencing of endogenous CHC production in the adult beetle. This trait may evolve through the mutation of enhancer inputs or the gain of silencing elements in CHC enzymes or their activating transcription factor(s). Because ant CHCs compensate for the lack of CHC production in adults, such genomic changes may arise and spread under neutrality.[111,112] The removal of stabilizing selection to maintain CHC biosynthesis in adult life would expose any mutational bias toward degeneration or active repression of CHC enzyme transcription. We suggest that the transient endogenous CHC profile of teneral *Sceptobius* may be interpreted as a vestige of its pre-entrenchment ancestor, before such regulatory changes accumulated. Hence, a seemingly irreducible symbiotic phenotype could arise through iterative coevolution of CHC biosynthesis mechanisms and counterbalancing changes in beetle behavior—the latter increasingly making use of the exogenous source of CHCs on host ant bodies, to the point that reliance becomes absolute.

By experimentally demonstrating a basis for entrenchment, our findings reveal how irreversible symbiosis may emerge not only through gene loss or reductive evolution but also through the evolution of essential, epistatic symbiotic traits—the interdependence between which precludes their reversal. Reciprocal sign epistasis, operating in the transition to symbiosis, is a potentially prevalent force that would bias the direction of evolution toward greater integration with hosts. Such a scenario may be widespread across symbiotic systems, from microbial to complex eukaryotic associations. We note that many symbioses, including endosymbiosis,[113,114] ecto- and endoparasitism,[115–117] and social parasitism,[65,118] hinge fundamentally on mechanisms for finding and/or physically associating with hosts, together with body- or cell-surface modifications that achieve compatibility with host immune or sensory surveillance. Pleiotropy of an organism's surface as both a barrier to the environment and the bearer of self/nonself information, positions it in potential reciprocal epistasis with host-interacting mechanisms. The Catch-22 we identify for *Sceptobius* may therefore be a common basis for symbiotic entrenchment across the tree of life.

Limitations of the study

We have investigated chemically mediated symbioses between rove beetle myrmecophiles and ants and have primarily focused on CHCs. Other cues, including non-CHC-based glandular secretions,[58,64] as well as tactile interactions,[119] have also been postulated to contribute to these symbiotic relationships. These additional channels of communication remain to be explored in the three *Liometopum* symbionts, as well as more generally in aleocharine myrmecophiles. The precise way in which *Sceptobius* mounts and grooms worker ants could also be explored in more detail. For example, *Sceptobius* tends to groom the dorsal head and thorax of worker ants, rather than their venter or abdomen. This bias may stem from the way in which *Sceptobius* usually attaches to the worker (grasping the ant's antennae). It could also reflect a preference for these regions of worker cuticle due to heterogeneity in the abundance or composition of CHCs across the ant body.[120,121] Although the main organismal subject of the current study was the myrmecophile *Sceptobius*, we employed *Platyusa* as a counterexample of non-entrenched symbiosis. Much remains to be explored about the chemical ecology of *Platyusa*, including a test of the function of its host ant-like CHC profile in chemical mimicry, an analysis of the biochemical composition of its appeasement secretion, and an understanding of the secretion's impact on ant behavior.

Finally, our study probed the basis of entrenchment of the symbiotic lifestyle of *Sceptobius* as it currently stands in the present. We argued that an analogous Catch-22 may manifest across convergent transitions to obligate myrmecophily in aleocharines; hence, the Catch-22 itself may underlie symbiotic irreversibility generally in these beetles, and we presented a hypothetical sequence by which the Catch-22 could evolve. Yet, the historical path that any one of these symbiotic lineages followed remains forever lost in time. Future studies of this convergent system will bring us closer to retracing the past from comparative patterns embedded in the Recent.

RESOURCE AVAILABILITY

Lead contact

Further information and requests for reagents and resources should be directed to and will be fulfilled by the lead contact, Joseph Parker (joep@caltech.edu).

Materials availability

Plasmids and dsRNAs generated for this study are available via request from the lead contact.

Data and code availability

- All data to support the findings of this paper were uploaded to CaltechData: https://doi.org/10.22002/3w8cz-t2g08.

- Sequence reads related to this manuscript have been deposited in the NCBI Sequence Read Archive (SRA) database under the accession numbers listed in the key resources table. New transcriptome assemblies from this study have been deposited in the NCBI TSA database, with accession numbers listed in the key resources table. Genome assemblies from other studies were downloaded from the NCBI Reference Sequence (RefSeq) database (accessions listed in key resources table). All other data were uploaded to CaltechData (see key resources table for listed DOIs) and are available as of the date of publication.
- Any additional information required to reanalyze the data reported in this paper is available from the lead contact upon request.

ACKNOWLEDGMENTS

We are grateful to Matt Pennell, Michael Dickinson, and members of the Parker lab for critical feedback on this manuscript. This study was supported by funding to J.P. from the National Science Foundation (CAREER 2047472), the Army Research Office (MURI W911NF1910269), an Alfred P. Sloan Fellowship, a Pew Biomedical Scholarship, a Rita Allen Scholarship, a Klingenstein-Simons Fellowship, and research grants from the Shurl and Kay Curci Foundation and the Okawa Foundation.

AUTHOR CONTRIBUTIONS

Conceptualization, J.P. and T.H.N.; methodology, J.P., A.L.S., S.A.K., and T.H.N.; investigation, T.H.N., J.W.V., M.Y., A.B., J.M.W., K.E.O., H.M.R., D.C., S.A.K., R.S.W., A.L.S., and J.P.; formal analysis, T.H.N., M.Y., D.C., and J.W.V.; data curation, T.H.N.; writing – original draft, J.P. and T.H.N.; writing – review & editing, J.P. and T.H.N.; supervision, J.P.; project administration, J.P.; funding acquisition, J.P.

DECLARATION OF INTERESTS

The authors declare no competing interests.

STAR★METHODS

Detailed methods are provided in the online version of this paper and include the following:

SUPPLEMENTAL INFORMATION

Supplemental information can be found online at https://doi.org/10.1016/j.cell.2025.12.041.

Received: July 18, 2025
Revised: November 19, 2025
Accepted: December 19, 2025
Published: February 5, 2026

REFERENCES

1. Margulis, L. (1970). Origin of Eukaryotic Cells: Evidence and Research Implications for a Theory of the Origin and Evolution of Microbial, Plant, and Animal Cells on the Precambrian Earth (Yale University Press).
2. Casadevall, A. (2008). Evolution of Intracellular Pathogens. Annu. Rev. Microbiol. *62*, 19–33. https://doi.org/10.1146/annurev.micro.61.080706.093305.
3. Poulin, R., and Morand, S. (2000). The Diversity of Parasites. Q. Rev. Biol. *75*, 277–293. https://doi.org/10.1086/393500.
4. Weinstein, S.B., and Kuris, A.M. (2016). Independent origins of parasitism in Animalia. Biol. Lett. *12*, 20160324. https://doi.org/10.1098/rsbl.2016.0324.
5. Poulin, R. (2007). Evolutionary Ecology of Parasites, Second Edition (Princeton University Press). https://doi.org/10.1515/9781400840809.
6. Nickrent, D.L. (2020). Parasitic angiosperms: How often and how many? Taxon *69*, 5–27. https://doi.org/10.1002/tax.12195.
7. Cai, L. (2023). Rethinking convergence in plant parasitism through the lens of molecular and population genetic processes. Am. J. Bot. *110*, e16174. https://doi.org/10.1002/ajb2.16174.
8. Tedersoo, L., May, T.W., and Smith, M.E. (2010). Ectomycorrhizal lifestyle in fungi: global diversity, distribution, and evolution of phylogenetic lineages. Mycorrhiza *20*, 217–263. https://doi.org/10.1007/s00572-009-0274-x.
9. Nygaard, S., Hu, H., Li, C., Schiøtt, M., Chen, Z., Yang, Z., Xie, Q., Ma, C., Deng, Y., Dikow, R.B., et al. (2016). Reciprocal genomic evolution in the ant–fungus agricultural symbiosis. Nat. Commun. *7*, 12233. https://doi.org/10.1038/ncomms12233.
10. Sachs, J.L., Skophammer, R.G., and Regus, J.U. (2011). Evolutionary transitions in bacterial symbiosis. Proc. Natl. Acad. Sci. USA *108*, 10800–10807. https://doi.org/10.1073/pnas.1100304108.
11. Wang, S., and Luo, H. (2025). Dating the bacterial tree of life based on ancient symbiosis. Syst. Biol. *74*, 639–655. https://doi.org/10.1093/sysbio/syae071.
12. Siddall, M.E., Brooks, D.R., and Desser, S.S. (1993). Phylogeny and the reversibility of Parasitism. Evolution *47*, 308–313. https://doi.org/10.1111/j.1558-5646.1993.tb01219.x.
13. Bert, W., Messiaen, M., Manhout, J., Houthoofd, W., and Borgonie, G. (2006). Evolutionary Loss of Parasitism by Nematodes? Discovery of a Free-Living Filaroid Nematode. J. Parasitol. *92*, 645–647. https://doi.org/10.1645/ge-672r.1.
14. Morawetz, J.J., Randle, C.P., and Wolfe, A.D. (2010). Phylogenetic relationships within the tropical clade of Orobanchaceae. Taxon *59*, 416–426. https://doi.org/10.1002/tax.592007.

15. Bochkov, A.V., and Mironov, S.V. (2013). Is parasitism of metazoa "a one-way ticket"? Èntomol. Rev. *93*, 1196–1206. https://doi.org/10.1134/s001387381309011x.

16. Klimov, P.B., and Oconnor, B. (2013). Is Permanent Parasitism Reversible?—Critical Evidence from Early Evolution of House Dust Mites. Syst. Biol. *62*, 411–423. https://doi.org/10.1093/sysbio/syt008.

17. Xu, F., Jerlström-Hultqvist, J., Kolisko, M., Simpson, A.G.B., Roger, A.J., Svärd, S.G., and Andersson, J.O. (2016). On the reversibility of parasitism: adaptation to a free-living lifestyle via gene acquisitions in the diplomonad Trepomonas sp. PC1. BMC Biol. *14*, 62. https://doi.org/10.1186/s12915-016-0284-z.

18. Ellers, J., Kiers, E.T., Currie, C.R., McDonald, B.R., and Visser, B. (2012). Ecological interactions drive evolutionary loss of traits. Ecol. Lett. *15*, 1071–1082. https://doi.org/10.1111/j.1461-0248.2012.01830.x.

19. Poulin, R., and Randhawa, H.S. (2013). Evolution of parasitism along convergent lines: from ecology to genomics. Parasitology *142*, S6–S15. https://doi.org/10.1017/s0031182013001674.

20. Searcy, D.G., and MacInnis, A.J. (1970). Measurements by DNA Renaturation of the Genetic Basis of Parasitic Reduction. Evolution *24*, 796–806. https://doi.org/10.1111/j.1558-5646.1970.tb01814.x.

21. dePamphilis, C.W., and Palmer, J.D. (1990). Loss of photosynthetic and chlororespiratory genes from the plastid genome of a parasitic flowering plant. Nature *348*, 337–339. https://doi.org/10.1038/348337a0.

22. Katinka, M.D., Duprat, S., Cornillot, E., Méténier, G., Thomarat, F., Prensier, G., Barbe, V., Peyretaillade, E., Brottier, P., Wincker, P., et al. (2001). Genome sequence and gene compaction of the eukaryote parasite Encephalitozoon cuniculi. Nature *414*, 450–453. https://doi.org/10.1038/35106579.

23. Moran, N.A. (2003). Tracing the evolution of gene loss in obligate bacterial symbionts. Curr. Opin. Microbiol. *6*, 512–518. https://doi.org/10.1016/j.mib.2003.08.001.

24. Keeling, P.J., and Slamovits, C.H. (2005). Causes and effects of nuclear genome reduction. Curr. Opin. Genet. Dev. *15*, 601–608. https://doi.org/10.1016/j.gde.2005.09.003.

25. Opperman, C.H., Bird, D.M., Williamson, V.M., Rokhsar, D.S., Burke, M., Cohn, J., Cromer, J., Diener, S., Gajan, J., Graham, S., et al. (2008). Sequence and genetic map of Meloidogyne hapla: A compact nematode genome for plant parasitism. Proc. Natl. Acad. Sci. USA *105*, 14802–14807. https://doi.org/10.1073/pnas.0805946105.

26. Merhej, V., Royer-Carenzi, M., Pontarotti, P., and Raoult, D. (2009). Massive comparative genomic analysis reveals convergent evolution of specialized bacteria. Biol. Direct *4*, 13. https://doi.org/10.1186/1745-6150-4-13.

27. Mitreva, M., Jasmer, D.P., Zarlenga, D.S., Wang, Z., Abubucker, S., Martin, J., Taylor, C.M., Yin, Y., Fulton, L., Minx, P., et al. (2011). The draft genome of the parasitic nematode Trichinella spiralis. Nat. Genet. *43*, 228–235. https://doi.org/10.1038/ng.769.

28. Wolfe, B.E., Tulloss, R.E., and Pringle, A. (2012). The Irreversible Loss of a Decomposition Pathway Marks the Single Origin of an Ectomycorrhizal Symbiosis. PLOS One *7*, e39597. https://doi.org/10.1371/journal.pone.0039597.

29. McCutcheon, J.P., and Moran, N.A. (2011). Extreme genome reduction in symbiotic bacteria. Nat. Rev. Microbiol. *10*, 13–26. https://doi.org/10.1038/nrmicro2670.

30. Xiao, J.-H., Yue, Z., Jia, L.-Y., Yang, X.-H., Niu, L.-H., Wang, Z., Zhang, P., Sun, B.-F., He, S.-M., Li, Z., et al. (2013). Obligate mutualism within a host drives the extreme specialization of a fig wasp genome. Genome Biol. *14*, R141. https://doi.org/10.1186/gb-2013-14-12-r141.

31. Wicke, S., Müller, K.F., de Pamphilis, C.W. de, Quandt, D., Wickett, N.J., Zhang, Y., Renner, S.S., and Schneeweiss, G.M. (2013). Mechanisms of functional and physical genome reduction in photosynthetic and non-photosynthetic parasitic plants of the broomrape family. Plant Cell *25*, 3711–3725. https://doi.org/10.1105/tpc.113.113373.

32. Tsai, I.J., Zarowiecki, M., Holroyd, N., Garciarrubio, A., Sánchez-Flores, A., Brooks, K.L., Tracey, A., Bobes, R.J., Fragoso, G., Sciutto, E., et al. (2013). The genomes of four tapeworm species reveal adaptations to parasitism. Nature *496*, 57–63. https://doi.org/10.1038/nature12031.

33. Cissé, O.H., Pagni, M., and Hauser, P.M. (2014). Comparative Genomics Suggests That the Human Pathogenic Fungus Pneumocystis jirovecii Acquired Obligate Biotrophy through Gene Loss. Genome Biol. Evol. *6*, 1938–1948. https://doi.org/10.1093/gbe/evu155.

34. Hendry, T.A., de Wet, J.R. de, and Dunlap, P.V. (2014). Genomic signatures of obligate host dependence in the luminous bacterial symbiont of a vertebrate. Environ. Microbiol. *16*, 2611–2622. https://doi.org/10.1111/1462-2920.12302.

35. Kohler, A., Kuo, A., Nagy, L.G., Morin, E., Barry, K.W., Buscot, F., Canbäck, B., Choi, C., Cichocki, N., Clum, A., et al. (2015). Convergent losses of decay mechanisms and rapid turnover of symbiosis genes in mycorrhizal mutualists. Nat. Genet. *47*, 410–415. https://doi.org/10.1038/ng.3223.

36. Pande, S., and Kost, C. (2017). Bacterial Unculturability and the Formation of Intercellular Metabolic Networks. Trends Microbiol. *25*, 349–361. https://doi.org/10.1016/j.tim.2017.02.015.

37. Cai, L., Arnold, B.J., Xi, Z., Khost, D.E., Patel, N., Hartmann, C.B., Manickam, S., Sasirat, S., Nikolov, L.A., Mathews, S., et al. (2021). Deeply Altered Genome Architecture in the Endoparasitic Flowering Plant Sapria himalayana Griff. (Rafflesiaceae). Curr. Biol. *31*, 1002–1011. https://doi.org/10.1016/j.cub.2020.12.045.

38. Skern-Mauritzen, R., Malde, K., Eichner, C., Dondrup, M., Furmanek, T., Besnier, F., Komisarczuk, A.Z., Nuhn, M., Dalvin, S., Edvardsen, R.B., et al. (2021). The salmon louse genome: Copepod features and parasitic adaptations. Genomics *113*, 3666–3680. https://doi.org/10.1016/j.ygeno.2021.08.002.

39. Jongepier, E., Séguret, A., Labutin, A., Feldmeyer, B., Gstöttl, C., Foitzik, S., Heinze, J., and Bornberg-Bauer, E. (2022). Convergent Loss of Chemoreceptors across Independent Origins of Slave-Making in Ants. Mol. Biol. Evol. *39*, msab305. https://doi.org/10.1093/molbev/msab305.

40. Schrader, L., Pan, H., Bollazzi, M., Schiøtt, M., Larabee, F.J., Bi, X., Deng, Y., Zhang, G., Boomsma, J.J., and Rabeling, C. (2021). Relaxed selection underlies genome erosion in socially parasitic ant species. Nat. Commun. *12*, 2918. https://doi.org/10.1038/s41467-021-23178-w.

41. Siozios, S., Nadal-Jimenez, P., Azagi, T., Sprong, H., Frost, C.L., Parratt, S.R., Taylor, G., Brettell, L., Liew, K.C., Croft, L., et al. (2024). Genome dynamics across the evolutionary transition to endosymbiosis. Curr. Biol. *34*, 5659–5670. https://doi.org/10.1016/j.cub.2024.10.044.

42. Andersson, S.G.E., and Kurland, C.G. (1998). Reductive evolution of resident genomes. Trends Microbiol. *6*, 263–268. https://doi.org/10.1016/s0966-842x(98)01312-2.

43. Mira, A., Ochman, H., and Moran, N.A. (2001). Deletional bias and the evolution of bacterial genomes. Trends Genet. *17*, 589–596. https://doi.org/10.1016/s0168-9525(01)02447-7.

44. Boscaro, V., Kolisko, M., Felletti, M., Vannini, C., Lynn, D.H., and Keeling, P.J. (2017). Parallel genome reduction in symbionts descended from closely related free-living bacteria. Nat. Ecol. Evol. *1*, 1160–1167. https://doi.org/10.1038/s41559-017-0237-0.

45. Nechitaylo, T.Y., Sandoval-Calderón, M., Engl, T., Wielsch, N., Dunn, D.M., Goesmann, A., Strohm, E., Svatoš, A., Dale, C., Weiss, R.B., et al. (2021). Incipient genome erosion and metabolic streamlining for antibiotic production in a defensive symbiont. Proc. Natl. Acad. Sci. USA *118*, e2023047118. https://doi.org/10.1073/pnas.2023047118.

46. Uthanumallian, K., Iha, C., Repetti, S.I., Chan, C.X., Bhattacharya, D., Duchene, S., and Verbruggen, H. (2022). Tightly Constrained Genome Reduction and Relaxation of Purifying Selection during Secondary Plastid Endosymbiosis. Mol. Biol. Evol. *39*, msab295. https://doi.org/10.1093/molbev/msab295.

47. Oakeson, K.F., Gil, R., Clayton, A.L., Dunn, D.M., von Niederhausern, A.C. von, Hamil, C., Aoyagi, A., Duval, B., Baca, A., Silva, F.J., et al. (2014). Genome Degeneration and Adaptation in a Nascent Stage of Symbiosis. Genome Biol. Evol. *6*, 76–93. https://doi.org/10.1093/gbe/evt210.

48. Olson, M.V. (1999). When Less Is More: Gene Loss as an Engine of Evolutionary Change. Am. J. Hum. Genet. *64*, 18–23. https://doi.org/10.1086/302219.

49. Cavalier-Smith, T. (2005). Economy, Speed and Size Matter: Evolutionary Forces Driving Nuclear Genome Miniaturization and Expansion. Ann. Bot. *95*, 147–175. https://doi.org/10.1093/aob/mci010.

50. Morris, J.J., Lenski, R.E., and Zinser, E.R. (2012). The Black Queen Hypothesis: Evolution of Dependencies through Adaptive Gene Loss. mBio *3*, e00036-12. https://doi.org/10.1128/mbio.00036-12.

51. Albalat, R., and Cañestro, C. (2016). Evolution by gene loss. Nat. Rev. Genet. *17*, 379–391. https://doi.org/10.1038/nrg.2016.39.

52. Shen, G., Liu, N., Zhang, J., Xu, Y., Baldwin, I.T., and Wu, J. (2020). Cuscuta australis (dodder) parasite eavesdrops on the host plants' FT signals to flower. Proc. Natl. Acad. Sci. USA *117*, 23125–23130. https://doi.org/10.1073/pnas.2009445117.

53. Murray, A.W. (2020). Can gene-inactivating mutations lead to evolutionary novelty? Curr. Biol. *30*, R465–R471. https://doi.org/10.1016/j.cub.2020.03.072.

54. Moran, N.A., and Wernegreen, J.J. (2000). Lifestyle evolution in symbiotic bacteria: insights from genomics. Trends Ecol. Evol. *15*, 321–326. https://doi.org/10.1016/s0169-5347(00)01902-9.

55. Wernegreen, J.J., Lazarus, A.B., and Degnan, P.H. (2002). Small genome of Candidatus Blochmannia, the bacterial endosymbiont of Camponotus, implies irreversible specialization to an intracellular lifestyle. Microbiology (Reading) *148*, 2551–2556. https://doi.org/10.1099/00221287-148-8-2551.

56. Bennett, G.M., and Moran, N.A. (2015). Heritable symbiosis: The advantages and perils of an evolutionary rabbit hole. Proc. Natl. Acad. Sci. USA *112*, 10169–10176. https://doi.org/10.1073/pnas.1421388112.

57. Kistner, D.H. (1982). The Social Insects' Bestiary. In Social Insects, H.R. Hermann, ed. (Elsevier), pp. 1–244. https://doi.org/10.1016/B978-0-12-342203-3.50008-4.

58. Parker, J. (2016). Myrmecophily in beetles (Coleoptera): evolutionary patterns and biological mechanisms. Myrmecol. News *22*, 65–108. https://doi.org/10.25849/myrmecol.news_022:065.

59. Hölldobler, B., and Kwapich, C.L. (2022). The Guests of Ants (Harvard University Press). https://doi.org/10.4159/9780674276451.

60. Elmes, G.W. (1996). Biological diversity of ants and their role in ecosystem function. In Biodiversity Research and Its Perspectives in the East Asia, B.H. Lee, T.H. Kim, and B.Y. Sun, eds. (Chonbuk National University), pp. 33–48.

61. Seevers, C.H. (1965). The systematics, evolution and zoogeography of staphylinid beetles associated with army ants (Coleoptera, Staphylinidae). Fieldiana Zool. *47*, 139–351. https://doi.org/10.5962/bhl.title.3063.

62. Kistner, D.H. (1979). Social and evolutionary significance of social insect symbionts. In Social Insects, *1*, H.R. Hermann, ed. (Elsevier), pp. 339–413. https://doi.org/10.1016/B978-0-12-342201-9.50015-X.

63. Maruyama, M., and Parker, J. (2017). Deep-Time Convergence in Rove Beetle Symbionts of Army Ants. Curr. Biol. *27*, 920–926. https://doi.org/10.1016/j.cub.2017.02.030.

64. Naragon, T.H., Wagner, J.M., and Parker, J. (2022). Parallel evolutionary paths of rove beetle myrmecophiles: replaying a deep-time tape of life. Curr. Opin. Insect Sci. *51*, 100903. https://doi.org/10.1016/j.cois.2022.100903.

65. Lenoir, A., D'Ettorre, P., Errard, C., and Hefetz, A. (2001). Chemical Ecology and Social Parasitism in Ants. Annu. Rev. Entomol. *46*, 573–599. https://doi.org/10.1146/annurev.ento.46.1.573.

66. Akino, T. (2008). Chemical strategies to deal with ants: a review of mimicry, camouflage, propaganda, and phytomimesis by ants (Hymenoptera: Formicidae) and other arthropods. Myrmecol. News *11*, 173–181.

67. Bagnères, A.-G., and Lorenzi, M.C. (2010). Chemical deception/mimicry using cuticular hydrocarbons. In Insect Hydrocarbons: Biology, Biochemistry, and Chemical Ecology, G.J. Blomquist and A.-G. Bagnères, eds. (Cambridge University Press), pp. 282–324. https://doi.org/10.1017/cbo9780511711909.015.

68. von Beeren, C., Brückner, A., Maruyama, M., Burke, G., Wieschollek, J., and Kronauer, D.J.C. (2018). Chemical and behavioral integration of army ant-associated rove beetles - a comparison between specialists and generalists. Front. Zool. *15*, 8. https://doi.org/10.1186/s12983-018-0249-x.

69. Sturgis, S.J., and Gordon, D.M. (2012). Nestmate recognition in ants (Hymenoptera: Formicidae): a review. Myrmecol. News *16*, 101–110. https://doi.org/10.25849/myrmecol.news_016:101.

70. Sprenger, P.P., and Menzel, F. (2020). Cuticular hydrocarbons in ants (Hymenoptera: Formicidae) and other insects: how and why they differ among individuals, colonies, and species. Myrmecol. News *30*, 1–26. https://doi.org/10.25849/myrmecol.news_030:001.

71. Brand, J.M., Blum, M.S., Fales, H.M., and Pasteels, J.M. (1973). The chemistry of the defensive secretion of the beetle, Drusilla canaliculata. J. Insect Physiol. *19*, 369–382. https://doi.org/10.1016/0022-1910(73)90112-1.

72. Jordan, K. (1913). Zur Morphologie und Biologie der myrmecophilen Gattungen Lomechusa und Atemeles und einiger verwandter Formen. Z. Wiss. Zool. *107*, 346–386.

73. Brückner, A., Badroos, J.M., Learsch, R.W., Yousefelahiyeh, M., Kitchen, S.A., and Parker, J. (2021). Evolutionary assembly of cooperating cell types in an animal chemical defense system. Cell *184*, 6138–6156. https://doi.org/10.1016/j.cell.2021.11.014.

74. Kitchen, S.A., Naragon, T.H., Brückner, A., Ladinsky, M.S., Quinodoz, S.A., Badroos, J.M., Viliunas, J.W., Kishi, Y., Wagner, J.M., Miller, D.R., et al. (2024). The genomic and cellular basis of biosynthetic innovation in rove beetles. Cell *187*, 3563–3584. https://doi.org/10.1016/j.cell.2024.05.012.

75. Hoey-Chamberlain, R., Rust, M.K., and Klotz, J.H. (2013). A Review of the Biology, Ecology and Behavior of Velvety Tree Ants of North America. Sociobiology *60*, 1–10. https://doi.org/10.13102/sociobiology.v60i1.1-10.

76. Ward, P.S., Brady, S.G., Fisher, B.L., and Schultz, T.R. (2010). Phylogeny and biogeography of dolichoderine ants: effects of data partitioning and relict taxa on historical inference. Syst. Biol. *59*, 342–362. https://doi.org/10.1093/sysbio/syq012.

77. Danoff-Burg, J.A. (1996). An ethogram of the ant-guest beetle tribe Sceptobiini (Coleoptera: Staphylinidae; Formicidae). Sociobiology *27*, 287–328.

78. Kistner, D.H., Jensen, E.A., and Jacobson, H.R. (2002). A new genus and two new species of myrmecophilous Staphylinidae found with Liometopum in California (Coleoptera; Hymenoptera: Formicidae). Sociobiology *39*, 291–305.

79. Caterino, M.S., and Chatzimanolis, S. (2007). Newly recorded and noteworthy California Staphylinidae. Coleopt. Bull. *61*, 398–407. https://doi.org/10.1649/0010-065x(2007)61[398:nrancs]2.0.co;2.

80. Drijfhout, F., Kather, R., and Martin, S. (2009). The role of cuticular hydrocarbons in insects. In Behavioral and Chemical Ecology (Nova Science Publishers), pp. 91–114.

81. Blomquist, G.J., and Bagnères, A.-G. (2010). Insect Hydrocarbons, G.J. Blomquist and A.-G. Bagnères, eds. (Cambridge University Press).

82. Blomquist, G.J., and Ginzel, M.D. (2021). Chemical Ecology, Biochemistry, and Molecular Biology of Insect Hydrocarbons. Annu. Rev. Entomol. *66*, 45–60. https://doi.org/10.1146/annurev-ento-031620-071754.

83. Makki, R., Cinnamon, E., and Gould, A.P. (2014). The Development and Functions of Oenocytes. Annu. Rev. Entomol. *59*, 405–425. https://doi.org/10.1146/annurev-ento-011613-162056.

84. Wigglesworth, V.B. (1945). Transpiration Through the Cuticle of Insects. J. Exp. Biol. *21*, 97–114. https://doi.org/10.1242/jeb.21.3-4.97.

85. Gibbs, A.G., and Rajpurohit, S. (2010). Cuticular lipids and water balance. In Insect Hydrocarbons, G.J. Blomquist and A.-G. Bagnères, eds. (Cambridge University Press), pp. 100–120. https://doi.org/10.1017/CBO9780511711909.007.

86. Menzel, F., Morsbach, S., Martens, J.H., Räder, P., Hadjaje, S., Poizat, M., and Abou, B. (2019). Communication versus waterproofing: the physics of insect cuticular hydrocarbons. J. Exp. Biol. *222*, jeb210807. https://doi.org/10.1242/jeb.210807.

87. Wang, Z., Receveur, J.P., Pu, J., Cong, H., Richards, C., Liang, M., and Chung, H. (2022). Desiccation resistance differences in Drosophila species can be largely explained by variations in cuticular hydrocarbons. eLife *11*, e80859. https://doi.org/10.7554/elife.80859.

88. Martin, S.J., Vitikainen, E., Helanterä, H., and Drijfhout, F.P. (2008). Chemical basis of nest-mate discrimination in the ant Formica exsecta. Proc. Biol. Sci. *275*, 1271–1278. https://doi.org/10.1098/rspb.2007.1708.

89. Fry, B., Joern, A., and Parker, P.L. (1978). Grasshopper Food Web Analysis: Use of Carbon Isotope Ratios to Examine Feeding Relationships Among Terrestrial Herbivores. Ecology *59*, 498–506. https://doi.org/10.2307/1936580.

90. Qiu, Y., Tittiger, C., Wicker-Thomas, C., Le Goff, G.L., Young, S., Wajnberg, E., Fricaux, T., Taquet, N., Blomquist, G.J., and Feyereisen, R. (2012). An insect-specific P450 oxidative decarbonylase for cuticular hydrocarbon biosynthesis. Proc. Natl. Acad. Sci. USA *109*, 14858–14863. https://doi.org/10.1073/pnas.1208650109.

91. Hölldobler, B. (1970). Zur Physiologie der Gast-Wirt-Beziehungen (myrmecophilie) bei Ameisen. Z. Vgl. Physiol. *66*, 215–250. https://doi.org/10.1007/bf00297780.

92. Hölldolber, B., Möglich, M., and Maschwitz, U. (1981). Myrmecophilic Relationship of Pella (Coleoptera: Staphylinidae) to Lasius fuliginosus (Hymenoptera: Formicidae). Psyche: J. Entomol. *88*, 347–374. https://doi.org/10.1155/1981/75317.

93. Ikeshita, Y., Taniguchi, K., Kitagawa, Y., Maruyama, M., and Ito, F. (2017). The rove beetle Drusilla sparsa (Coleoptera: Staphylinidae) is a myrmecophilous species associated with a myrmicine ant, Crematogaster osakensis (Hymenoptera: Formicidae). Entomol. Sci. *20*, 437–442. https://doi.org/10.1111/ens.12272.

94. Hölldobler, B., Kwapich, C.L., and Haight, K.L. (2018). Behavior and exocrine glands in the myrmecophilous beetle Lomechusoides strumosus (Fabricius, 1775) (formerly called Lomechusa strumosa) (Coleoptera: Staphylinidae: Aleocharinae). PLOS One *13*, e0200309. https://doi.org/10.1371/journal.pone.0200309.

95. Wagner, J.M., Wong, J.H., Millar, J.G., Haxhimali, E., Brückner, A., Naragon, T.H., Boedicker, J.Q., and Parker, J. (2025). Enforced specificity of an entrenched symbiosis. Current Biology *35*, 5965–5981. https://doi.org/10.1016/j.cub.2025.10.066.

96. Gutierrez, E., Wiggins, D., Fielding, B., and Gould, A.P. (2006). Specialized hepatocyte-like cells regulate Drosophila lipid metabolism. Nature *445*, 275–280. https://doi.org/10.1038/nature05382.

97. Kleynhans, E., and Terblanche, J.S. (2011). Complex Interactions between Temperature and Relative Humidity on Water Balance of Adult Tsetse (Glossinidae, Diptera): Implications for Climate Change. Front. Physiol. *2*, 74. https://doi.org/10.3389/fphys.2011.00074.

98. Akre, R.D., and Rettenmeyer, C.W. (1966). Behavior of Staphylinidae Associated with Army Ants (Formicidae: Ecitonini). J. Kans. Entomol. Soc. *39*, 745–782.

99. Akre, R.D., and Torgerson, R.L. (1968). The behavior of Diploeciton nevermanni, a staphylinid beetle associated with army ants. Psyche: J. Entomol. *75*, 211–215. https://doi.org/10.1155/1968/23814.

100. Kistner, D.H., and Jacobson, H.R. (1990). Cladistic analysis and taxonomic revision of the ecitophilous tribe Ecitocharini with studies of their behaviour and evolution (Coleoptera, Staphylinidae, Aleocharinae). Sociobiology *17*, 333–480.

101. Jacobson, H.R., and Kistner, D.H. (1991). Cladistic study, taxonomic restructuring, and revision of the myrmecophilous tribe Leptanillophilini with comments on its evolution and host relationships (Coleoptera: Staphylinidae; Hymenoptera: Formicidae). Sociobiology *18*, 1–150.

102. Jacobson, H.R., and Kistner, D.H. (1992). Cladistic Study, Taxonomic Restructuring, and Revision of the Myrmecophilous Tribe Crematoxenini with Comments on Its Evolution and Host Relationships (Coleoptera, Staphylinidae, Hymenoptera, Formicidae). Sociobiology *20*, 91–198.

103. Kistner, D.H. (1993). Cladistic analysis, taxonomic restructuring and revision of the Old World genera formerly classified as Dorylomimini with comments on their evolution and behavior (Coleoptera: Staphylinidae). Sociobiology *22*, 147–383.

104. Maruyama, M., Akino, T., Hashim, R., and Komatsu, T. (2009). Behavior and cuticular hydrocarbons of myrmecophilous insects (Coleoptera: Staphylinidae; Diptera: Phoridae; Thysanura) associated with Asian Aenictus army ants (Hymenoptera; Formicidae). Sociobiology *54*, 19–35.

105. Heller, J. (1961). Catch-22 (Simon & Schuster).

106. Weinreich, D.M., Watson, R.A., and Chao, L. (2005). Perspective: Sign epistasis and genetic constraint on evolutionary trajectories. Evolution *59*, 1165–1174. https://doi.org/10.1111/j.0014-3820.2005.tb01768.x.

107. Bridgham, J.T., Ortlund, E.A., and Thornton, J.W. (2009). An epistatic ratchet constrains the direction of glucocorticoid receptor evolution. Nature *461*, 515–519. https://doi.org/10.1038/nature08249.

108. Shah, P., McCandlish, D.M., and Plotkin, J.B. (2015). Contingency and entrenchment in protein evolution under purifying selection. Proc. Natl. Acad. Sci. USA *112*, E3226–E3235. https://doi.org/10.1073/pnas.1412933112.

109. Starr, T.N., Flynn, J.M., Mishra, P., Bolon, D.N.A., and Thornton, J.W. (2018). Pervasive contingency and entrenchment in a billion years of Hsp90 evolution. Proc. Natl. Acad. Sci. USA *115*, 4453–4458. https://doi.org/10.1073/pnas.1718133115.

110. Hochberg, G.K.A., Liu, Y., Marklund, E.G., Metzger, B.P.H., Laganowsky, A., and Thornton, J.W. (2020). A hydrophobic ratchet entrenches molecular complexes. Nature *588*, 503–508. https://doi.org/10.1038/s41586-020-3021-2.

111. Stoltzfus, A. (1999). On the Possibility of Constructive Neutral Evolution. J. Mol. Evol. *49*, 169–181. https://doi.org/10.1007/pl00006540.

112. Brunet, T.D.P. (2022). Higher level constructive neutral evolution. Biol. Philos. *37*, 23. https://doi.org/10.1007/s10539-022-09858-x.

113. Bublitz, D.C., Chadwick, G.L., Magyar, J.S., Sandoz, K.M., Brooks, D.M., Mesnage, S., Ladinsky, M.S., Garber, A.I., Bjorkman, P.J., Orphan, V.J., et al. (2019). Peptidoglycan Production by an Insect-Bacterial Mosaic. Cell *179*, 703–712. https://doi.org/10.1016/j.cell.2019.08.054.

114. Otten, C., Brilli, M., Vollmer, W., Viollier, P.H., and Salje, J. (2018). Peptidoglycan in obligate intracellular bacteria. Mol. Microbiol. *107*, 142–163. https://doi.org/10.1111/mmi.13880.

115. Chappell, L.H. (1980). The biology of the external surfaces of helminth parasites. Proc. Sect. B Biol. Sci. *79*, 145–172. https://doi.org/10.1017/s026972700001040x.

116. Blaxter, M.L., Page, A.P., Rudin, W., and Maizels, R.M. (1992). Nematode surface coats: Actively evading immunity. Parasitol. Today *8*, 243–247. https://doi.org/10.1016/0169-4758(92)90126-m.

117. Strand, M.R., and Pech, L.L. (1995). Immunological Basis for Compatibility in Parasitoid-Host Relationships. Annu. Rev. Èntomol *40*, 31–56. https://doi.org/10.1146/annurev.en.40.010195.000335.

118. Lorenzi, M.C., and d'Ettorre, P. (2020). Nestmate Recognition in Social Insects: What Does It Mean to Be Chemically Insignificant? Front. Ecol. Evol. *7*, 488. https://doi.org/10.3389/fevo.2019.00488.

119. Parker, J., and Rabeling, C. (2020). Evolution: Shape-Shifting Social Parasites. Curr. Biol. *30*, R1049–R1051. https://doi.org/10.1016/j.cub.2020.07.010.

120. Wang, Q., Goodger, J.Q.D., Woodrow, I.E., and Elgar, M.A. (2016). Location-specific cuticular hydrocarbon signals in a social insect. Proc. Biol. Sci. *283*, 20160310. https://doi.org/10.1098/rspb.2016.0310.

121. Sprenger, P.P., Gerbes, L.J., Sahm, J., and Menzel, F. (2021). Cuticular hydrocarbon profiles differ between ant body parts: implications for communication and our understanding of CHC diffusion. Curr. Zoöl *67*, 531–540. https://doi.org/10.1093/cz/zoab012.

122. Pimentel, H., Bray, N.L., Puente, S., Melsted, P., and Pachter, L. (2017). Differential analysis of RNA-seq incorporating quantification uncertainty. Nat. Methods *14*, 687–690. https://doi.org/10.1038/nmeth.4324.

123. Bray, N.L., Pimentel, H., Melsted, P., and Pachter, L. (2016). Near-optimal probabilistic RNA-seq quantification. Nat. Biotechnol. *34*, 525–527. https://doi.org/10.1038/nbt.3519.

124. Team, R.C. (2022). R: A Language and Environment for Statistical Computing (R Foundation for Statistical Computing).

125. Oksanen, J., Simpson, G.L., Blanchet, F.G., Kindt, R., Legendre, P., Minchin, P.R., O'Hara, R.B., Solymos, P., Stevens, M.H.H., Szoecs, E., et al. (2025) Vegan: Community Ecology Package. Zenodo.

126. Ripley, B., Venables, B., Bates, D.M., Hornik, K., Gebhardt, A., Firth, D., and Ripley, M.B. (2013). Package 'mass.'. Cran r *538*, 113–120.

127. Wickham, H. (2016). Ggplot2: Elegant graphics for data analysis (2nd ed.) [PDF] (Springer International Publishing).

128. de Vries, A., and Ripley, B.D. Ggdendro: Create Dendrograms and Tree Diagrams Using "ggplot2." CRAN.

129. Wickham, H., and Ruiz, E. (2019). Dbplyr: A "Dplyr" Back End for Databases, R Package Version 1.4. 0.

130. Galili, T. (2015). dendextend: an R package for visualizing, adjusting and comparing trees of hierarchical clustering. Bioinformatics *31*, 3718–3720. https://doi.org/10.1093/bioinformatics/btv428.

131. Harris, C.R., Millman, K.J., van der Walt, S.J., Gommers, R., Virtanen, P., Cournapeau, D., Wieser, E., Taylor, J., Berg, S., Smith, N.J., et al. (2020). Array programming with NumPy. Nature *585*, 357–362. https://doi.org/10.1038/s41586-020-2649-2.

132. Reback, J., McKinney, W., jbrockmendel, Van den Bossche, J., Augspurger, T., Cloud, P., Hawkins, S., gfyoung, Sinhrks, Roeschke, M., et al. (2021). pandas-dev/pandas: Pandas 1.2.4 (v1.2.4). Zenodo. https://doi.org/10.5281/zenodo.4681666.

133. Kluyver, T., Ragan-Kelley, B., Pérez, F., Granger, B.E., Bussonnier, M., Frederic, J., Kelley, K., Hamrick, J.B., Grout, J., Corlay, S., et al. (2016). Jupyter Notebooks – a publishing format for reproducible computational workflows. In Proceedings of the 20th International Conference on Electronic Publishing (IOS Press), pp. 87–90.

134. Levitsky, L.I., Klein, J.A., Ivanov, M.V., and Gorshkov, M.V. (2019). Pyteomics 4.0: Five Years of Development of a Python Proteomics Framework. J. Proteome Res. *18*, 709–714. https://doi.org/10.1021/acs.jproteome.8b00717.

135. Stringer, C., Wang, T., Michaelos, M., and Pachitariu, M. (2021). Cellpose: a generalist algorithm for cellular segmentation. Nat. Methods *18*, 100–106. https://doi.org/10.1038/s41592-020-01018-x.

136. Gohlke, C. Tifffile: v2022.5.4. Zenodo.

137. Rudiger, P., Stevens, J.-L., Bednar, J.A., Nijholt, B., Mease, J., Andrew, L., M., Chris, B., Randelhoff, A., Tenner, V., et al. (2022). holoviz/holoviews, Version 1.14.9. Zenodo.

138. Mathis, A., Mamidanna, P., Cury, K.M., Abe, T., Murthy, V.N., Mathis, M.W., and Bethge, M. (2018). DeepLabCut: markerless pose estimation of user-defined body parts with deep learning. Nat. Neurosci. *21*, 1281–1289. https://doi.org/10.1038/s41593-018-0209-y.

139. Nath, T., Mathis, A., Chen, A.C., Patel, A., Bethge, M., and Mathis, M.W. (2019). Using DeepLabCut for 3D markerless pose estimation across species and behaviors. Nat. Protoc. *14*, 2152–2176. https://doi.org/10.1038/s41596-019-0176-0.

140. Langmead, B., and Salzberg, S.L. (2012). Fast gapped-read alignment with Bowtie 2. Nat. Methods *9*, 357–359. https://doi.org/10.1038/nmeth.1923.

141. Song, L., and Florea, L. (2015). Rcorrector: efficient and accurate error correction for Illumina RNA-seq reads. GigaScience *4*, 48. https://doi.org/10.1186/s13742-015-0089-y.

142. Freedman, A.H., Clamp, M., and Sackton, T.B. (2021). Error, noise and bias in de novo transcriptome assemblies. Mol. Ecol. Resour. *21*, 18–29. https://doi.org/10.1111/1755-0998.13156.

143. Krueger, F. (2014). TrimGalore. GitHub. https://github.com/FelixKrueger/TrimGalore.

144. Haas, B.J., Papanicolaou, A., Yassour, M., Grabherr, M., Blood, P.D., Bowden, J., Couger, M.B., Eccles, D., Li, B., Lieber, M., et al. (2013). De novo transcript sequence reconstruction from RNA-seq using the Trinity platform for reference generation and analysis. Nat. Protoc. *8*, 1494–1512. https://doi.org/10.1038/nprot.2013.084.

145. Andrews, S. (2010). FastQC: a quality control tool for high throughput sequence data.

146. Manni, M., Berkeley, M.R., Seppey, M., Simão, F.A., and Zdobnov, E.M. (2021). BUSCO Update: Novel and Streamlined Workflows along with Broader and Deeper Phylogenetic Coverage for Scoring of Eukaryotic, Prokaryotic, and Viral Genomes. Mol. Biol. Evol. *38*, 4647–4654. https://doi.org/10.1093/molbev/msab199.

147. Haas, B.J. TransDecoder. TransDecoder.

148. Fu, L., Niu, B., Zhu, Z., Wu, S., and Li, W. (2012). CD-HIT: accelerated for clustering the next-generation sequencing data. Bioinformatics *28*, 3150–3152. https://doi.org/10.1093/bioinformatics/bts565.

149. Emms, D.M., and Kelly, S. (2015). OrthoFinder: solving fundamental biases in whole genome comparisons dramatically improves orthogroup inference accuracy. Genome Biol. *16*, 157. https://doi.org/10.1186/s13059-015-0721-2.

150. Emms, D.M., and Kelly, S. (2019). OrthoFinder: phylogenetic orthology inference for comparative genomics. Genome Biol. *20*, 238. https://doi.org/10.1186/s13059-019-1832-y.

151. Capella-Gutiérrez, S., Silla-Martínez, J.M., and Gabaldón, T. (2009). trimAl: a tool for automated alignment trimming in large-scale phylogenetic analyses. Bioinformatics *25*, 1972–1973. https://doi.org/10.1093/bioinformatics/btp348.

152. Minh, B.Q., Schmidt, H.A., Chernomor, O., Schrempf, D., Woodhams, M.D., von Haeseler, A. von, and Lanfear, R. (2020). IQ-TREE 2: New Models and Efficient Methods for Phylogenetic Inference in the Genomic Era. Mol. Biol. Evol. *37*, 1530–1534. https://doi.org/10.1093/molbev/msaa015.

153. Kocot, K.M., Citarella, M.R., Moroz, L.L., and Halanych, K.M. (2013). PhyloTreePruner: A Phylogenetic Tree-Based Approach for Selection of Orthologous Sequences for Phylogenomics. Evol. Bioinform. Online *9*, 429–435. https://doi.org/10.4137/ebo.s12813.

154. Kück, P., and Meusemann, K. (2010). FASconCAT: Convenient handling of data matrices. Mol. Phylogenet. Evol. *56*, 1115–1118. https://doi.org/10.1016/j.ympev.2010.04.024.

155. Misof, B., Meyer, B., von Reumont, B.M. von, Kück, P., Misof, K., and Meusemann, K. (2013). Selecting informative subsets of sparse supermatrices increases the chance to find correct trees. BMC Bioinform. *14*, 348. https://doi.org/10.1186/1471-2105-14-348.

156. Lanfear, R., Frandsen, P.B., Wright, A.M., Senfeld, T., and Calcott, B. (2017). PartitionFinder 2: New Methods for Selecting Partitioned Models of Evolution for Molecular and Morphological Phylogenetic

Analyses. Mol. Biol. Evol. *34*, 772–773. https://doi.org/10.1093/molbev/msw260.

157. Yang, Z. (2007). PAML 4: Phylogenetic Analysis by Maximum Likelihood. Mol. Biol. Evol. *24*, 1586–1591. https://doi.org/10.1093/molbev/msm088.

158. Puttick, M.N. (2019). MCMCtreeR: functions to prepare MCMCtree analyses and visualize posterior ages on trees. Bioinformatics *35*, 5321–5322. https://doi.org/10.1093/bioinformatics/btz554.

159. Katoh, K., and Standley, D.M. (2013). MAFFT Multiple Sequence Alignment Software Version 7: Improvements in Performance and Usability. Mol. Biol. Evol. *30*, 772–780. https://doi.org/10.1093/molbev/mst010.

160. Price, M.N., Dehal, P.S., and Arkin, A.P. (2010). FastTree 2 – Approximately Maximum-Likelihood Trees for Large Alignments. PLOS One *5*, e9490. https://doi.org/10.1371/journal.pone.0009490.

161. Friard, O., and Gamba, M. (2016). BORIS: a free, versatile open-source event-logging software for video/audio coding and live observations. Methods Ecol. Evol. *7*, 1325–1330. https://doi.org/10.1111/2041-210x.12584.

162. Dembeck, L.M., Böröczky, K., Huang, W., Schal, C., Anholt, R.R.H., and Mackay, T.F.C. (2015). Genetic architecture of natural variation in cuticular hydrocarbon composition in Drosophila melanogaster. eLife *4*, e09861. https://doi.org/10.7554/elife.09861.

163. Brückner, A. (2022). Using weapons instead of perfume: chemical association strategies of the myrmecophilous bug Scolopostethus pacificus (Rhyparochromidae). Chemoecology *32*, 147–157. https://doi.org/10.1007/s00049-022-00374-8.

164. Oksanen, J., Blanchet, F.G., Kindt, R., Legendre, P., Minchin, P., O'Hara, R., Simpson, G., Solymos, P., Henry, M., Stevens, M., et al. (2015). Vegan community ecology package: ordination methods, diversity analysis and other functions for community and vegetation ecologists. R package version 2.3.

165. Nishimura, O., Hara, Y., and Kuraku, S. (2017). gVolante for standardizing completeness assessment of genome and transcriptome assemblies. Bioinformatics *33*, 3635–3637. https://doi.org/10.1093/bioinformatics/btx445.

166. Hoang, D.T., Chernomor, O., von Haeseler, A. von, Minh, B.Q., and Vinh, L.S. (2018). UFBoot2: Improving the Ultrafast Bootstrap Approximation. Mol. Biol. Evol. *35*, 518–522. https://doi.org/10.1093/molbev/msx281.

167. Stamatakis, A. (2006). RAxML-VI-HPC: maximum likelihood-based phylogenetic analyses with thousands of taxa and mixed models. Bioinformatics *22*, 2688–2690. https://doi.org/10.1093/bioinformatics/btl446.

168. Parham, J.F., Donoghue, P.C.J., Bell, C.J., Calway, T.D., Head, J.J., Holroyd, P.A., Inoue, J.G., Irmis, R.B., Joyce, W.G., Ksepka, D.T., et al. (2012). Best practices for justifying fossil calibrations. Syst. Biol. *61*, 346–359. https://doi.org/10.1093/sysbio/syr107.

169. Misof, B., Liu, S., Meusemann, K., Peters, R.S., Donath, A., Mayer, C., Frandsen, P.B., Ware, J., Flouri, T., Beutel, R.G., et al. (2014). Phylogenomics resolves the timing and pattern of insect evolution. Science *346*, 763–767. https://doi.org/10.1126/science.1257570.

170. Kirejtshuk, A.G., Poschmann, M., Prokop, J., Garrouste, R., and Nel, A. (2014). Evolution of the elytral venation and structural adaptations in the oldest Palaeozoic beetles (Insecta: Coleoptera: Tshekardocoleidae). J. Syst. Palaeontol. *12*, 575–600. https://doi.org/10.1080/14772019.2013.821530.

171. Alexeev, A. (1993). Jurassic and lower cretaceous Buprestidae (Coleoptera) from Eurasia. Paleontol. J. *27*, 9–34.

172. Zhang, S.-Q., Che, L.-H., Li, Y., Liang, D., Pang, H., Ślipiński, A., and Zhang, P. (2018). Evolutionary history of Coleoptera revealed by extensive sampling of genes and species. Nat. Commun. *9*, 205. https://doi.org/10.1038/s41467-017-02644-4.

173. Arnol'di, L.V. (1992). Rhynchophora. In Mesozoic Coleoptera, L.V. Arnol'di, V.V. Zherikhin, L.M. Nikritin, and A.G. Ponomarenko, eds. (Smithsonian Institution), pp. 142–176.

174. McKenna, D.D., Shin, S., Ahrens, D., Balke, M., Beza-Beza, C., Clarke, D.J., Donath, A., Escalona, H.E., Friedrich, F., Letsch, H., et al. (2019). The evolution and genomic basis of beetle diversity. Proc. Natl. Acad. Sci. USA *116*, 24729–24737. https://doi.org/10.1073/pnas.1909655116.

175. Wang, B., Ma, J., McKenna, D.D., Yan, E.V., Zhang, H., and Jarzembowski, E.A. (2014). The earliest known longhorn beetle (Cerambycidae: Prioninae) and implications for the early evolution of Chrysomeloidea. J. Syst. Palaeontol. *12*, 565–574. https://doi.org/10.1080/14772019.2013.806602.

176. Liu, Y., Liu, Y., Ji, S., and Yang, Z. (2006). U-Pb zircon age for the Daohugou Biota at Ningcheng of Inner Mongolia and comments on related issues. Chin. Sci. Bull. *51*, 2634–2644. https://doi.org/10.1007/s11434-006-2165-2.

177. Cai, C.-Y., Thayer, M.K., Engel, M.S., Newton, A.F., Ortega-Blanco, J., Wang, B., Wang, X.-D., and Huang, D.-Y. (2014). Early origin of parental care in Mesozoic carrion beetles. Proc. Natl. Acad. Sci. USA *111*, 14170–14174. https://doi.org/10.1073/pnas.1412280111.

178. Bean, L.B. (2006). The leptolepid fish Cavenderichthys talbragarensis (Woodward, 1895) from the Talbragar Fish Bed (Late Jurassic) near Gulgong, New South Wales. Rec. West. Aust. Museum *23*, 43. https://doi.org/10.18195/issn.0312-3162.23(1).2006.043-076.

179. Cai, C.-Y., Yan, E.V., Beattie, R., Wang, B., and Huang, D.-Y. (2013). First rove beetles from the Jurassic Talbragar Fish Bed of Australia (Coleoptera, Staphylinidae). J. Paleontol. *87*, 650–656. https://doi.org/10.1666/12-136.

180. Yamamoto, S., and Maruyama, M. (2018). Phylogeny of the rove beetle tribe Gymnusini sensu n. (Coleoptera: Staphylinidae: Aleocharinae): implications for the early branching events of the subfamily. Syst. Entomol. *43*, 183–199. https://doi.org/10.1111/syen.12267.

181. Cai, C., and Huang, D. (2015). The oldest aleocharine rove beetle (Coleoptera, Staphylinidae) in Cretaceous Burmese amber and its implications for the early evolution of the basal group of hyper-diverse Aleocharinae. Gondwana Res. *28*, 1579–1584. https://doi.org/10.1016/j.gr.2014.09.016.

182. Shi, G., Grimaldi, D.A., Harlow, G.E., Wang, J., Wang, J., Yang, M., Lei, W., Li, Q., and Li, X. (2012). Age constraint on Burmese amber based on U–Pb dating of zircons. Cret. Res. *37*, 155–163. https://doi.org/10.1016/j.cretres.2012.03.014.

183. Zerche, L. (1999). Eine neue Art der Gattung Adinopsis Cameron aus dem Baltischen Bernstein (Coleoptera: Staphylinidae, Aleocharinae, Deinopsini). Beitr. Entomol. = Contrib. Entomol. *49*, 97–105. https://doi.org/10.21248/contrib.entomol.49.1.97-105.

184. Ritzkowski, S. (1997). K-Ar-Altersbestimmungen der bernsteinführenden Sedimente des Samlandes (Paläogen, Bezirk Kaliningrad). Metalla *66*, 19–23.

185. Paśnik, G. (2005). Fossils of Staphylinidae from Baltic amber: a new genus and three new species (Insecta, Coleoptera, Staphylinidae). Senckenberg. Biol. *85*, 97–100.

186. Paśnik, G., and Kubisz, D. (2002). A new genus and new species of Staphylinidae (Coleoptera) from Baltic amber. Eur. J. Entomol. *99*, 353–361. https://doi.org/10.14411/eje.2002.045.

187. Inoue, J., Donoghue, P.C.J., and Yang, Z. (2010). The Impact of the Representation of Fossil Calibrations on Bayesian Estimation of Species Divergence Times. Syst. Biol. *59*, 74–89. https://doi.org/10.1093/sysbio/syp078.

188. Yang, Z., and Rannala, B. (2006). Bayesian Estimation of Species Divergence Times Under a Molecular Clock Using Multiple Fossil Calibrations with Soft Bounds. Mol. Biol. Evol. *23*, 212–226. https://doi.org/10.1093/molbev/msj024.

189. Dallerac, R., Labeur, C., Jallon, J.M., Knipple, D.C., Roelofs, W.L., and Wicker-Thomas, C. (2000). A Δ9 desaturase gene with a different substrate specificity is responsible for the cuticular diene hydrocarbon polymorphism in Drosophila melanogaster. Proc. Natl. Acad. Sci. USA *97*, 9449–9454. https://doi.org/10.1073/pnas.150243997.

190. Xianglan, Z. (2006). A Female-Specific Desaturase Gene Responsible for Diene Hydrocarbon Biosynthesis and Courtship Behaviour in Drosophila melanogaster. Science *311*, 123–127.

191. MacMillan, H.A., Nørgård, M., MacLean, H.J., Overgaard, J., and Williams, C.J.A. (2017). A critical test of Drosophila anaesthetics: Isoflurane and sevoflurane are benign alternatives to cold and CO2. J. Insect Physiol. *101*, 97–106. https://doi.org/10.1016/j.jinsphys.2017.07.005.

192. Wilson, E.E., Holway, D., and Nieh, J.C. (2006). Cold anaesthesia decreases foraging recruitment in the New World bumblebee, Bombus occidentalis. J. Apic. Res. *45*, 169–172. https://doi.org/10.1080/00218839.2006.11101343.

193. Bartholomew, N.R., Burdett, J.M., VandenBrooks, J.M., Quinlan, M.C., and Call, G.B. (2015). Impaired climbing and flight behaviour in Drosophila melanogaster following carbon dioxide anaesthesia. Sci. Rep. *5*, 15298. https://doi.org/10.1038/srep15298.

194. Steidle, J.L.M., and Dettner, K. (1993). Chemistry and morphology of the tergal gland of freeliving adult Aleocharinae (Coleoptera: Staphylinidae) and its phylogenetic significance. Syst. Entomol. *18*, 149–168. https://doi.org/10.1111/j.1365-3113.1993.tb00659.x.

195. Kistner, D.H., and Jacobson, H.R. (1975). A review of the myrmecophilous Staphylinidae associated with Aenictus in Africa (Coleoptera; Hymenoptera, Formicidae). Sociobiology *1*, 20–73.

196. Kistner, D.H. (1983). A new genus and twelve new species of ant mimics associated with Pheidologeton (Coleoptera, Staphylinidae; Hymenoptera, Formicidae). Sociobiology *8*, 155–198.

197. Danoff-Burg, J.A. (1994). Evolving under myrmecophily: a cladistic revision of the symphilic beetle tribe Sceptobiini (Coleoptera: Staphylinidae: Aleocharinae). Syst. Entomol. *19*, 25–45. https://doi.org/10.1111/j.1365-3113.1994.tb00577.x.

198. Kistner, D.H. (2006). Ecitocryptus kungae – A new species of myrmecophile from Costa Rica (Coleoptera: Staphylinidae). Sociobiology *47*, 677–686.

STAR★METHODS

KEY RESOURCES TABLE

REAGENT or RESOURCE	SOURCE	IDENTIFIER
Antibodies		
Mouse monoclonal 4D9 anti-engrailed/invected	Developmental Studies Hybridoma Bank	AB_528224
Goat anti-Mouse IgG Secondary Antibody, Alexa Fluor™ 555	Thermo Fisher Scientific	Cat# A-21422
Biological samples		
Dalotia coriaria	Applied Bionomics (Canada)	https://www.appliedbio-nomics.com/; products/dalotia/
Platyusa sonomae	Wild caught by T. H. Naragon in California, USA	N/A
Sceptobius lativentris	Wild caught by T. H. Naragon, A. Brückner, and J. Wagner in California, USA	N/A
Drosophila melanogaster	Dickinson Laboratory (Caltech)	N/A
Liometopum occidentale	Wild caught by T. H. Naragon, J. Wagner, and J. Truong in California, USA	N/A
Oligota sp.	Wild caught by T. H. Naragon in California, USA	N/A
Acrotona sp.	Wild caught by T. H. Naragon in California, USA	N/A
Falagria sp.	Wild caught by K. Taro Eldredge in Massachussetts, USA	N/A
Liometoxenus newtonarum	Wild caught by T. H. Naragon in California, USA	N/A
Chemicals, peptides, and recombinant proteins		
n-hexane SupraSolv®	Sigma-Aldrich	Cat# 1.00795
octadecane analytical standard	Sigma-Aldrich	Cat# 74691-5G
tetracosane-d_{50}, 98 atom % D	Sigma-Aldrich	Cat# 451770-100MG
triacontane-d_{62}, 98 atom % D	Sigma-Aldrich	Cat# 451789-100MG
Phosphate Buffered Saline	Sigma-Aldrich	Cat# P4417
diethyl pyrocarbonate (DEPC)	Sigma-Aldrich	Cat# 40718-25ML
Tween 20	Sigma-Aldrich	Cat# 11332465001
16% Paraformaldehyde	Electron Microscopy Sciences	Cat# 15710
Proteinase K, Molecular Biology Grade (ProK), 800 U/mL	New England Biolabs	Cat# P8107S
Hoechst 33342	Thermo Fisher Scientific	Cat# 62249
Alexa 488-Wheat Germ Agglutinin conjugate	Thermo Fisher Scientific	Cat# W11261
Streptavidin, Alexa Fluor™ 647 Conjugate	Thermo Fisher Scientific	Cat# S32357
ProLong Gold Antifade Mountant	Thermo Fisher Scientific	Cat# P36934
Critical commercial assays		
ZYMO *Quick-RNA* Tissue/Insect extraction kit	ZYMO Research	Cat# R2030
NEBNext Single Cell/Low Input RNA Library Prep Kit for Illumina	New England Biolabs	Cat# E6420L
Qubit 1X High Sensitivity dsDNA kit	Thermo Fisher Scientific	Cat# Q33230
Bioanalyzer High Sensitivity DNA kit	Agilent Technologies	Cat# 5067-4626

(*Continued on next page*)

Continued

REAGENT or RESOURCE	SOURCE	IDENTIFIER
In situ HCR v3 kit for *Platyusa sonomae CYP4G1* - B4	Molecular Instruments	N/A
In situ HCR v3 kit for *Platyusa sonomae Desat1* – B3	Molecular Instruments	N/A
In situ HCR v3 kit for *Platyusa sonomae ELO4* – B1	Molecular Instruments	N/A
In situ HCR v3 kit for *Platyusa sonomae* FAS3 – B1	Molecular Instruments	N/A
In situ HCR v3 kit for *Platyusa sonomae FAR4* – B3	Molecular Instruments	N/A
In situ HCR v3 kit for *Sceptobius lativentris CYP4G1* – B4	Molecular Instruments	N/A
In situ HCR v3 kit for *Sceptobius lativentris Desat1* – B3	Molecular Instruments	N/A
In situ HCR v3 kit for *Sceptobius lativentris ELO4* – B1	Molecular Instruments	N/A
In situ HCR v3 kit for *Sceptobius lativentris* FAS3 - B1	Molecular Instruments	N/A
In situ HCR v3 kit for *Sceptobius lativentris FAR4* – B3	Molecular Instruments	N/A
HCR v3 Amplifier Hairpin System Alexa546-B1	Molecular Instruments	N/A
HCR v3 Amplifier Hairpin System Alexa488-B4	Molecular Instruments	N/A
HCR v3 Amplifier Hairpin System Alexa647-B3	Molecular Instruments	N/A
TOPO TA Cloning Kit	Thermo Fisher Scientific	Cat# 450641
MEGAscript T7 Transcription kit	Thermo Fisher Scientific	Cat# AMB13345
MEGAclear Transcription cleanup kit	Thermo Fisher Scientific	Cat# AM1908
RNeasy Mini kit	Qiagen	Cat# 74104
Superscript III kit	Thermo Fisher Scientific	Cat# 18080085
Luna Universal qPCR Master Mix	New England Biolabs	Cat# M3003L
Deposited data		
Data for figures	This study	CaltechData; https://doi.org/10.22002/3w8cz-t2g08
Oligonucleotides		
NEBNext Multiplex Oligos for Illumina (Dual Index Primers Set 1)	New England Biolabs	Cat# E7600L
NEBNext Multiplex Oligos for Illumina (Dual Index Primers Set 2)	New England Biolabs	Cat# E7780L
Dalotia coriaria oCYP4G-1 F	This Study; Integrated DNATechnologies, Inc	5'- TAATACGACTCACTATAGGGC ACTCCCTGTCGGAACCTTGGA-3'
Dalotia coriaria oCYP4G-1 R	This Study; Integrated DNATechnologies, Inc	5'-TAATACGACTCACTATAGGGT TGCGACATCCTCCACAGACGT-3'
Dalotia coriaria oCYP4G-2 F	This Study; Integrated DNATechnologies, Inc	5'-TAATACGACTCACTATAGGGA CGTCTGTGGAGGATGTCGCAA-3'
Dalotia coriaria oCYP4G-2 R	This Study; Integrated DNATechnologies, Inc	5'-TAATACGACTCACTATAGGGA TCCAAAATCCCCGGACCCGAT-3'
Platyusa sonomae oCYP4G F	This Study; Integrated DNATechnologies, Inc	5'-TAATACGACTCACTATAGGG TCTTAGGATGTACCCACCAGTG-3'
Platyusa sonomae oCYP4G R	This Study; Integrated DNATechnologies, Inc	5'-TAATACGACTCACTATAGGGT GTCGCAATGCACTCGGTAT-3'

(*Continued on next page*)

Continued

REAGENT or RESOURCE	SOURCE	IDENTIFIER
EGFP F	This Study; Integrated DNATechnologies, Inc	5'- TAATACGACTCACTATAGGG TCTTCTTCAAGGACGACGGCAACTAC -3'
EGFP R	This Study; Integrated DNATechnologies, Inc	5'- TAATACGACTCACTATAGGGT TACTTGTACAGCTCGTCCATGCCGA -3'
Sceptobius lativentris ELO4 F	This Study; Integrated DNATechnologies, Inc	5'-TTCGGTGCTGCAAGGATAA-3'
Sceptobius lativentris ELO4 R	This Study; Integrated DNATechnologies, Inc	5'-CCCAAGAGTACCACACAAGAG-3'
Sceptobius lativentris CYP4G1 F	This Study; Integrated DNATechnologies, Inc	5'-ACCCAGCTGATATTGAGGTTATC-3'
Sceptobius lativentris CYP4G1 R	This Study; Integrated DNATechnologies, Inc	5'-CTGACCAAGAGACCATTTCCA-3'
Sceptobius lativentris Desat1 F	This Study; Integrated DNATechnologies, Inc	5'-CGCTACAGCACTAACTTCACT-3'
Sceptobius lativentris Desat1 R	This Study; Integrated DNATechnologies, Inc	5'-ACACGACGCTTGACCATATC-3'
Sceptobius lativentris RPL19 F	This Study; Integrated DNATechnologies, Inc	5'-GAATGTACCGCTACTGGTTTCT-3'
Sceptobius lativentris RPL19 R	This Study; Integrated DNATechnologies, Inc	5'-CAGCCTCTGTTATGCGATGT-3'
Sceptobius lativentris RPS3 F	This Study; Integrated DNATechnologies, Inc	5'-GGTGTCGACGTAGTCGTTAATC-3'
Sceptobius lativentris RPS3 R	This Study; Integrated DNATechnologies, Inc	5'-CGAAGTAGTTGTGTCCGGTAAG-3'
Software and algorithms		
sleuth v0.30.0	Pimentel et al.[122]	https://github.com/pachterlab/sleuth
kallisto v0.46.2	Bray et al.[123]	https://github.com/pachterlab/kallisto
R v4.4.1	R Core Team[124]	https://www.R-project.org/
vegan v2.7-2	Oksanen et al.[125]	https://CRAN.R-project.org/package=vegan
MASS v7.3-65	Venables and Ripley[126]	https://cran.r-project.org/package=MASS
ggplot2 v4.0.0	Wickham[127]	https://cran.r-project.org/package=ggplot2
ggdendro	de Vries and Ripley[128]	https://CRAN.R-project.org/package=ggdendro
dplyr v1.1.4	Wickham and Ruiz[129]	https://CRAN.R-project.org/package=dplyr
dendextend v1.19.1	Galili[130]	http://cran.r-project.org/package=dendextend
python v3.7.3	Python Software Foundation	https://www.python.org/
bokeh v2.4.3	Bokeh Development Team	https://docs.bokeh.org/en/latest/
numpy v1.19.2	Charles et al.[131]	https://pypi.org/project/numpy/
pandas v1.2.4	Reback et al.[132]	https://pypi.org/project/pandas/
jupyterlab v3.6.5	Kluyver et al.[133]	https://pypi.org/project/jupyterlab/
pyteomics v4.4.0	Levitsky et al.[134]	https://pypi.org/project/pyteomics/
python 3.8.13	Python Software Foundation	https://www.python.org/
cellpose v2.0.5	Stringer et al.[135]	https://github.com/MouseLand/cellpose
tifffile v2022.5.4	Gohlke[136]	https://pypi.org/project/tifffile/
numpy v1.21.5	Charles et al.[131]	https://pypi.org/project/numpy/
holoviews 1.14.9	Rudiger et al.[137]	https://pypi.org/project/holoviews/

(*Continued on next page*)

Continued

REAGENT or RESOURCE	SOURCE	IDENTIFIER
deeplabcut v2.0.6.2	Mathis et al.,[138] Nath et al.[139]	https://github.com/DeepLabCut/DeepLabCut
tqdm v4.43.0	tqdm developers	https://pypi.org/project/tqdm/
BOWTIE2 v2.3.4.1	Langmead and Salzberg[140]	https://bowtie-bio.sourceforge.net/bowtie2/index.shtml
rCorrector v1.0.4	Li and Liliana[141]	https://github.com/mourisl/Rcorrector
TranscriptomeAssemblyTools	Freedman et al.[142]	https://github.com/harvardinformatics/TranscriptomeAssemblyTools
TrimGalore v0.6.0	Krueger github[143]	https://github.com/FelixKrueger/TrimGalore
TRINITY v2.12.0	Haas et al.[144]	https://github.com/trinityrnaseq/trinityrnaseq
FastQC v0.11.8.	Andrews[145]	https://www.bioinformatics.babraham.ac.uk/projects/fastqc/
BUSCO v5	Manni et al.[146]	https://busco.ezlab.org
transdecoder v5.5.0	Haas[147]	https://github.com/TransDecoder/Transdecoder
CDHIT v4.8.1	Fu et al.[148]	https://github.com/weizhongli/cdhit
Orthofinder v2.5.2	Emms and Kelly,[149] Emms and Kelly[150]	https://github.com/davidemms/OrthoFinder
trimal v1.4.1	Capella-Gutiérrez et al.[151]	https://github.com/inab/trimal
iqtree v1.6.8	Minh et al.[152]	http://www.iqtree.org/
PhyloTreePruner v1.2.4	Kocot et al.[153]	https://sourceforge.net/projects/phylotreepruner/
FASconCAT v1.04	Kück and Meusemann[154]	https://github.com/PatrickKueck/FASconCAT
MARE v0.1.2	Misof et al.[155]	https://bonn.leibniz-lib.de/en/research/research-centres-and-groups/mare
Partitionfinder v2.1.1	Lanfear et al.[156]	https://www.robertlanfear.com/partitionfinder/
MCMCtree	Yang[157,158]	https://github.com/abacus-gene/paml
mafft v7.453	Katoh and Standley[159]	https://mafft.cbrc.jp/alignment/software/
fasttree v2.1.10	Price et al.[160]	http://www.microbesonline.org/fasttree/
BORIS v. 8.20.1	Friard and Gamba[161]	https://www.boris.unito.it
GCMSsolution Version 4.45	Shimadzu Corporation	https://www.ssi.shimadzu.com/products/gas-chromatograph-mass-spectrometry/gc-ms-software/gcmssolution/index.html
Scripts to process data for figures	This study	CaltechData; https://doi.org/10.22002/3w8cz-t2g08
Other		
Drosophila melanogaster genome assembly	NCBI RefSeq	GCF_000001215.4
Agrilus planipennis genome assembly	NCBI RefSeq	GCF_000699045.2
Tribolium castaneum genome assembly	NCBI RefSeq	GCF_000002335.3
Aethina tumida genome assembly	NCBI RefSeq	GCF_001937115.1
Dendroctonus ponderosae genome assembly	NCBI RefSeq	GCF_000355655.1
Anoplophora glabripennis genome assembly	NCBI RefSeq	GCF_000390285.2
Leptinotarsa decemlineata genome assembly	NCBI RefSeq	GCF_000500325.1

(*Continued on next page*)

Continued

REAGENT or RESOURCE	SOURCE	IDENTIFIER
Onthophagus taurus genome assembly	NCBI RefSeq	GCF_000648695.1
Nicrophorus vespilloides genome assembly	NCBI RefSeq	GCF_001412225.1
Coproporus ventriculus genome assembly	Kitchen et al.; NCBI Genbank; NCBI SRA database	GCA_027574865.2; SRR4301367
Gymnusa sp. genome assembly	Kitchen et al.; NCBI Genbank; NCBI SRA database	GCA_030264735.1; SRR23816742
Adinopsis sp. genome assembly	Kitchen et al.; NCBI Genbank; NCBI SRA database	GCA_030264715.1; SRR23816743
Deinopsis erosa genome assembly	Kitchen et al.; NCBI Genbank; NCBI SRA database	GCA_027574845.2; SRR5176562
Cypha longicornis genome assembly	Kitchen et al.; NCBI Genbank; NCBI SRA database	GCA_030264615.1; SRR23816741
Holobus sp. genome assembly	Kitchen et al.; NCBI Genbank; NCBI SRA database	GCA_030556065.1; SRR23816746
Aleochara sp. genome assembly	Kitchen et al.; NCBI Genbank; NCBI SRA database	GCA_030264555.1; SRR23816854
Aleochara bilineata genome assembly	NCBI Genbank, reassembly in Kitchen et al. at CaltechDATA	GCA_003054995.1; CaltechDATA: https://doi.org/10.22002/k8sfv-dw648
Leptusa sp. genome assembly	Kitchen et al.; NCBI Genbank; NCBI SRA database	GCA_030264655.1; SRR23816749
Liometoxenus newtonarum genome assembly	Kitchen et al.; NCBI Genbank; NCBI SRA database	GCA_030264535.1; SRR23816853
Oxypoda opaca genome assembly	Kitchen et al.; NCBI Genbank; NCBI SRA database	GCA_030264175.1; SRR23816753
Myllaena sp. genome assembly	Kitchen et al.; NCBI Genbank; NCBI SRA database	GCA_030264135.1; SRR23816751
Falagria sp. genome assembly	Kitchen et al.; NCBI Genbank; NCBI SRA database	GCA_030556245.1; SRR23816748
Lissagria laeviuscula genome assembly	Kitchen et al.; NCBI Genbank; NCBI SRA database	GCA_030264695.1; SRR23816747
Atheta pasadenae genome assembly	Kitchen et al.; NCBI Genbank; NCBI SRA database	GCA_030264155.1; SRR23816750
Dalotia coriaria v2 genome	Kitchen et al.; this study CaltechDATA	CaltechDATA: https://doi.org/10.22002/3w8cz-t2g08
Earota dentata genome assembly	Kitchen et al.; NCBI Genbank; NCBI SRA database	GCA_027574905.2; SRR5176873
Geostiba sp. genome assembly	Kitchen et al.; NCBI Genbank; NCBI SRA database	GCA_030264215.1; SRR23816752
Platyusa sonomae bulk RNAseq reads	NCBI SRA database	SRS10254886, SRS10254885, SRS10254884, SRS10254883
Platyusa sonomae filtered bulk RNAseq reads	NCBI SRA database	SRR36026510
Drusilla canaliculata bulk RNAseq reads	NCBI SRA database	SRS10254882, SRS10254881, SRS10254880, SRS10254879
Drusilla canaliculata filtered bulk RNAseq reads	NCBI SRA database	SRR36026509
Sceptobius lativentris filtered bulk RNAseq reads	NCBI SRA database	SRR36026508, SRR36026507
Platyusa sonomae de novo transcriptome	NCBI TSA database	GLKR01000000
Sceptobius lativentris de novo transcriptome	NCBI TSA database	GLKS01000000
Drusilla canaliculata de novo transcriptome	NCBI TSA database	GLKQ01000000

(*Continued on next page*)

Continued

REAGENT or RESOURCE	SOURCE	IDENTIFIER
Platyusa sonomae tissue specific RNAseq reads	NCBI SRA database	SRR36066704, SRR36066703, SRR36066699, SRR36066698, SRR36066697
Sceptobius lativentris tissue specific RNAseq reads	NCBI SRA database	SRR36066695, SRR36066694, SRR36066693, SRR36066696, SRR36066692, SRR36066702, SRR36066701, SRR36066700
InsectaSlip/Fluon	Bioquip, CA	Discontinued
ZB-5MS fused silica capillary column for GCMS (30m x 0.25mm ID, df=0.25μm)	Phenomenex	7HG-G010-11
ZB-5MS fused silica capillary column for GCMS (30m x 0.25mm ID, df=1μm)	Phenomenex	7HG-G010-22
F8 standard mix	Arndt Schimmelman, Indiana University	https://hcnisotopes.earth.indiana.edu/reference-materials/materials-descriptions/fatty-acid-esters.html
Mono camera: BFS-U3-51S5M-C: 5.0 MP	Flir	BFS-U3-51S5M-C
Pentax 12mm 1:1.2 TV lens	Ricoh	FL-HC1212B-VG
BFS-U3-16S2C-CS: 1.6 MP	Flir	BFS-U3-16S2C-CS
InfiniGage lens	Infinity Photo-Optical	N/A
Plexiglass IR acrylic 3143	ePlastics	ACRY31430.125PM24X48
BFS-U3-04S2M-CS: 0.4 MP	Flir	BFS-U3-04S2M-CS

EXPERIMENTAL MODEL AND STUDY PARTICIPANT DETAILS

Liometopum occidentale

Liometopum occidentale ants were collected from nests in the Angeles National forest. All collected individuals were female workers.

Sceptobius lativentris

Sceptobius lativentris were collected from *Liometopum occidentale* nests in the Angeles National Forest. For genome/transcriptome sequencing, *S. lativentris* could be sexed using dimorphic dense setae present on the third antennomere of males and not females (personal observation). For other experiments, individuals from both sexes were pooled due to the lack of obvious dimorphism in their chemical ecological and symbiotic behavioral interactions with ants.

Platyusa sonomae

Platyusa sonomae were collected from *Liometopum occidentale* nests in the Angeles National forest. For transcriptome sequencing, *P. sonomae* could be sexed using dimorphic dense setae present on the third, fourth, and fifth antennomeres of males and not females (personal observation). For other experiments, individuals from both sexes were pooled due to the lack of obvious dimorphism in their chemical ecological and symbiotic behavioral interactions with ants.

Liometoxenus newtonarum

Liometoxenus newtonarum were collected from *Liometopum occidentale* nests in the Angeles National Forest. Individuals from both sexes were pooled for all experiments due to undetectable sexual dimorphism in chemical ecology and symbiotic behavior.

Drusilla canaliculata

Drusilla canaliculata were collected in Belgium and maintained on a diet of frozen *Drosophila melanogaster*. For transcriptome sequencing, beetles were sexed based on abdominal morphology and genitalia prior to RNA extraction.

Oligota sp.

Oligota beetles were collected from soil in the vicinity of *Liometopum occidentale* nests in the Angeles National Forest. Animals from both sexes were pooled for CHC analysis due to negligible CHC dimorphism.

Acrotona sp.

Acrotona beetles were collected from leaf litter in the Angeles National Forest. Animals from both sexes were pooled for CHC analysis due to negligible CHC dimorphism.

Falagria sp.

Falagria beetles were collected in Massachusetts. Animals from both sexes were pooled for CHC analysis due to negligible CHC dimorphism.

Dalotia coriaria

Dalotia coriaria were from a laboratory culture maintained in the Parker lab. As with other species in this study, sex was not a factor in experiments involving *Dalotia*, so animals from both sexes were pooled for experiments.

Specimen collection

Beetles and ants were collected from *Liometopum occidentale* nests in the Angeles National Forest between 2017 and 2024. *Liometopum* nests were most commonly located in Coast Live Oak (*Quercus agrifolia*) and California Bay Laurel (*Umbellularia californica*). Specimens of all three rove beetle species were primarily collected by sieving leaf litter and soil surrounding nests at the bases of trees. *Sceptobius* was also collected from internal nest material, while both *Sceptobius* and *Liometoxenus* were additionally collected from nest entrances. *Platyusa* eggs and larvae were collected in leaf litter surrounding *Liometopum* nests. *Sceptobius* eggs and larvae were collected in damp soil directly at nest entrances, comprising frass formed from the heartwood excavated by *Liometopum*. *Platyusa* and *Sceptobius* were collected year-round (peaking between February and August). *Liometoxenus* is seasonal and was only collected between February and May. Beetles and ants were aspirated and placed into 50 ml tubes filled with damp kimwipes and transported back to the laboratory.

Myrmecophile culture

In lab, beetles were maintained in large plastic bins (Rubbermaid) until they were used in experiments. *Platyusa* were reared without ants in containers with a layer of densely packed, damp coconut fiber. Frozen *Drosophila melanogaster* or *Liometopum occidentale* workers were placed in containers on pieces of foil as a food source. *Platyusa* reared in lab would periodically lay viable eggs that would develop into adults. *Platyusa* eggs and larvae were additionally collected in leaf litter at the field sites, or in leaf litter brought back to the lab and sorted under a microscope. They were maintained in lab on damp coconut fiber substrate in the same containers as adult *Platyusa*. Larvae were fed frozen *Drosophila* and proceeded through three larval instars prior to pupation. Both *Sceptobius* and *Liometoxenus* were kept in containers with *Liometopum* workers collected from the same nest. The walls of these containers were coated in InsectaSlip/Fluon (Bioquip, CA) to prevent ant escapes. Ants were provided with sucrose solution and glass tubes partially filled with water and cotton ball stoppers to provide moisture. Soil was brought back to lab where *Sceptobius* eggs and larvae were located in soil using a stereomicroscope. Eggs were stored on slightly damp filter paper in petri dishes and observed daily for the presence of freshly hatched larvae. Larvae were transferred to fresh petri dishes with damp filter paper. Attempts to identify a food source for *Sceptobius* larvae were unsuccessful; it was found that *Sceptobius* larvae do not require feeding to successfully pupate. Prior to pupation, the larvae pass through two larval instars. The container of pupae was checked twice daily for the presence of freshly eclosed teneral *Sceptobius*. Teneral *Sceptobius* died rapidly if not introduced to *Liometopum* within a day of eclosing. Teneral *Sceptobius* not being sampled on the day of eclosion were placed in petri dishes with damp filter paper and five *Liometopum* workers. The ants were kept alive by placing sucrose solution-soaked filter paper squares on pieces of foil in petri dishes.

METHOD DETAILS

Cuticular Hydrocarbon analysis

Insects were extracted in 70 μL hexane (n-hexane SupraSolv®, Sigma Aldrich, MO) for 20 min. Samples for which semi-quantification of CHC amounts was required were extracted in hexane containing a 10 nanogram-per-microliter octadecane (C18, Sigma Aldrich, MO) internal standard. Crude extracts (2μL) were then injected into a Shimadzu QP2020 GCMS with an AOC-20i Shimadzu autosampler. The instrument was equipped with Helium as a carrier gas and a Phenomenex (Torrance, CA) ZB-5MS fused silica capillary column (30m x 0.25 mm ID, df=0.25μm). The injection port was operated at 310°C in splitless mode, with a column flow rate of 2.15 mL/min. The column was held at 40°C for 1 minute, ramped at 20°C/min to 250°C, ramped at 5°C/min up to 320°C, and then held at 320°C for 7.5 minutes. The transfer line was held at 320°C and the ion source temperature was held at 230°C. Electron ionization was carried out at an ion source voltage of 70eV, and MS scans were collected between 40 m/z and 650 m/z at a scan rate of 2 scans per second.

For some organisms, including *Oligota* and some of the *Sceptobius* samples, beetles were extracted in 10 microliters of hexane due to the low amount of CHCs on the organisms. When quantification of these samples was required, hexane with a 1 ng/microliter C18 internal standard was used. Low volume samples were manually injected into the GCMS. Identification of individual CHC compounds was determined based on retention index as well as diagnostic ions, and comparison to previously described *Liometopum* and *Drosophila* GCMS data.[162,163] GC peaks were manually integrated using LabSolutions Postrun Analysis (Shimadzu, Kyōto, Japan). Alkene double bond position was previously identified for a number of *Liometopum* compounds.[163] Absolute CHC amounts were calculated by taking the ratio of the area of each peak to the C18 internal standard peak area, and multiplying by the total mass of internal standard in the extraction. CHC measurements were converted to percent composition for each spectrum. Pairwise Bray-Curtis dissimilarity was calculated across all samples, and then non-metric multidimension scaling (NMDS) ordination was

performed using the metaMDS function from the vegan R package.[164] The R function hclust was used to perform hierarchical clustering of the pairwise Bray-Curtis dissimilarity matrix. Hierarchical clustering was additionally performed on the pairwise Jaccard dissimilarity matrix of the binarized CHC data.

Gas Chromatography Isotope Ratio Mass Spectrometry (GCIRMS)

Due to the high concentrations required for accurate measurement, ants and beetles were pooled with conspecifics from the same nest/collecting trip for stable isotope measurements. Between 28-50 ants, 9-64 *Sceptobius*, and 20 *Platyusa* were pooled for each extraction. Insects were extracted in 1mL of hexane, which was then evaporated under a stream of nitrogen to a volume of roughly 100 microliters. Samples were then analyzed on a GC-combustion-IRMS system composed of a Thermo Trace GC_{ultra} (Thermo Fisher, CA) interfaced to a Thermo-Scientific $Delta_+XP$ IRMS (Thermo Fisher, CA) equipped with a ZB-5MS column (30m x 0.25 mm ID, df=1μm, Phenomenex). Samples were injected in splitless mode into a PTV injection port with He as the carrier gas. The column was initially held at a temperature of 80°C for 1 minute, followed by a 20°C/min ramp up to 250°C and then a 3°C/min ramp up to 320°C, which was held for 12 minutes. A CO_2 reference gas ($\delta^{13}C$ = -32.4‰) was co-injected during each sample run, generating four reference peaks against which sample $\delta^{13}C$ was calculated relative to VPDB (Vienna Pee Dee Belemnite). An external standard containing ethyl icosanoate (from the 'F8 mix' of Arndt Schimmelmann, Indiana University), which has a known $\delta^{13}C$ value of -26.1‰, was run every eight samples. The difference between the measured value and true value of the ethyl icosanoate standards bounding each set of eight runs was used to correct the $\delta^{13}C$ values of the intervening samples. Samples were measured in triplicate and arithmetic means are reported. Peaks were identified by comparison to GCMS measurements and the stereotypical elution order of the CHCs of the three organisms.

Life stage analysis

First and second instar larvae, as well as prepupal larvae were extracted in 10 microliters of hexane containing 1 ng/microliter C18 for 20 minutes. The extracts were then manually injected (3μL) into the GCMS and run with the CHC-GCMS program described above. Neither the first, nor the early second instar larvae possessed measurable CHCs. To obtain pupae for CHC analysis, prepupal larvae were left on damp filter paper in petri dishes at room temperature. Pupae were collected within one day of pupation and extracted and run on the GCMS in the same manner as the *Sceptobius* larvae. Teneral *Sceptobius* were generated by allowing larvae to pupate in soil, which had been cleared of *Liometopum*. As individual teneral beetles eclosed, they were collected and either immediately extracted for CHCs, placed into petri dishes with damp filter paper for isolation analysis, or placed into petri dishes with damp filter paper and multiple *Liometopum*, for later time point measurements. Isolated teneral *Sceptobius* were kept on damp filter paper in Petri dishes for 24 hours, after which they were extracted and run on the GCMS using the same method as the *Sceptobius* larvae and pupae. High mortality was observed for the teneral beetles during this 24-h isolation period.

Deuterium transfer

Approximately 0.5 milligrams of fully deuterated tetracosane and triacontane (triacontane-d_{62} and tetracosane-d_{50}, 98 atom % D, Sigma-Aldrich, MO) were added to a 5 mL glass vial along with 1 mL of hexane to fully dissolve the hydrocarbons. The hexane was then evaporated off under a steady stream of nitrogen gas leaving a thin film of the two deuterated hydrocarbons on the inner wall of the vial. *Liometopum* were added to the vial and then shaken for ~1 minute to transfer the labeled hydrocarbons to the surface of the ants. Uncoated control ants were prepared in a similar fashion, using a vial treated only with hexane. Deuterated hydrocarbon labelled and control *Liometopum* were paired with either *Platyusa, Sceptobius*, or *Dalotia* in wells within an IR transparent black acrylic arena, Figure 2G. Interactions were recorded in the dark at 1 hz under IR illumination using a FLIR camera (BFS-U3-51S5M-C: 5.0 MP) with a Pentax 12mm 1:1.2 TV lens (Ricoh, FL-HC1212B-VG). After 24 hours, the arena was removed and ants and beetles were extracted in 70 microliters of hexane with 25ng/microliter of octadecane as an internal standard. Samples were run on Shimadzu QP2020 GCMS equipped with helium as a carrier gas and a Phenomenex ZB-5MS fused silica capillary column (30m x 0.25 mm ID, df=0.25μm). The injection port was operated at 310°C in splitless mode, with a column flow rate of 2.15 mL/min. The column oven was held at 40°C for 1 minute, followed by a 40°C/min ramp up to 250°C, a 20°C/min ramp up to 320°C, and then a 5 minute hold at 320°C. The transfer line was held at 320°C and the ion source temperature was held at 230°C. The MS was operated at an ion source voltage of 70eV and scans were collected in selected ion monitoring mode (SIM), monitoring m/z 66, 85, 98, 254, 389, and 485 at 3.33 scans per second. Videos were reviewed and only interactions in which the beetles had not been killed were used.

The C18, triacontane-d_{62}, and tetracosane-d_{50} peaks were manually integrated (sum of the selected ion counts, and the absolute amounts of the deuterated hydrocarbons were calculated by taking the ratio of the area of each peak to the C18 internal standard peak area, and multiplying by the total mass of internal standard in the extraction. The average background signal was calculated for the control ants and beetles and subtracted from the corresponding treatment groups. The background-corrected deuterated hydrocarbon mass on each beetle was then divided by the corresponding measurement from the paired ant to calculate the ratio of deuterated hydrocarbon transferred in each interaction well. Differences in the transfer ratio between the three beetles were compared using an ANOVA test with a Tukey *post hoc* test in R.

Phylogenomics

For phylogenomic inference, transcriptomes were first generated for *Sceptobius, Platyusa*, and *Drusilla*. These three transcriptomes were then combined with gene predictions from 26 other beetles, including the v2 *Dalotia coriaria* genome (CaltechData, https://doi.org/10.22002/3w8cz-t2g08 Dalotia_coriaria_v2_genome), and *Drosophila melanogaster*. Orthologous sequences were identified from the 3 transcriptomes and 27 genome samples and a maximum likelihood species tree was calculated from a supermatrix constructed from single-copy gene families.

Platyusa sonomae and *Sceptobius lativentris* were collected at Chaney Canyon, Angeles National Forest, California (34°13'00.9"N 118°09'09.9"W) during the summer of 2018-2019. *Drusilla canaliculata* specimens were collected by Tim Struyve (locality: Moerbeke, Belgium, 51°10'37.2"N 3°54'32.4"E, 04 iv 2017). *Sceptobius* were dissected and pooled to create body part specific libraries, which were sequenced separately and then combined in transcriptome assembly. From 120 *Sceptobius*, all 6th and 7th abdominal segments were pooled and all 8th abdominal segments were pooled. Additionally legs and antennae from the 120 beetles were separately pooled, also being separated by sex. An additional 20 male and female *Sceptobius* were collected and separated into pools of legs, antennae, and the rest of the body, separated by sex. One each of male and female *Platyusa* and *Drusilla* were separated into heads and bodies. Total RNA was extracted from live or flash frozen materials stored at -80°C using a ZYMO *Quick-RNA* Tissue/Insect extraction kit (ZYMO Research, CA). RNA quantity was assessed with a Nanodrop (Thermo Fisher, CA). *Sceptobius* 150bp libraries were prepared and sequenced paired end, 100 million reads and *Platyusa* and *Drusilla* 150bp libraries were prepared and sequenced paired end, 100 million reads, all by Omega bioservices. The *Platyusa* and *Drusilla* reads were initially filtered by mapping raw reads from both species onto a concatenated *Platyusa*/*Drusilla* genome (generated previously[74]) using BOWTIE2 v2.3.4.1[140] to account for any cross contamination of the samples during library prep. Only reads mapping to the correct portion of the combined genomes were used in subsequent analysis. Similarly, *Sceptobius* reads were filtered by mapping raw reads from all libraries onto a concatenated *Sceptobius*/*Dalotia coriaria* genome and only reads mapping to the correct species were used in downstream analysis. The filtered reads from *Platyusa, Drusilla*, and *Sceptobius* were assessed for quality with FastQC v0.11.8. and then filtered using rCorrector v1.0.4 to remove erroneous k-mers and then run through the FilterUncorrectabledPE-fastq.py script from https://github.com/harvardinformatics/TranscriptomeAssemblyTools to remove uncorrectable reads. TrimGalore v0.6.0[143] was used to remove any remaining adaptors from the reads. The *Platyusa, Drusilla*, and *Sceptobius* libraries were then fed to TRINITY v2.12.0[144] for de Novo transcriptome assembly with Jaccard clipping. Assembled transcriptomes were assessed for completeness via gVolante[165] using BUSCO v5[146] with the Arthropoda ortholog set. BUSCO scores for *Platyusa*, *Drusilla*, and *Sceptobius* were 99.9%, 99.9%, and 100% respectively for the 1013 core genes analyzed. The *de novo* transcriptomes were then processed with transdecoder v5.5.0 to predict open reading frames and run through CDHIT v4.8.1[148] using a 98% sequence identity threshold, -p 1 -d 0 -b 3 -T 10, to remove duplicate sequences.

The three transcriptomes were combined with gene predictions from 27 other genomes, including the dipteran outgroup *Drosophila melanogaster*, various free-living beetles spanning the suborder Polyphaga, and the myrmecophile *Liometoxenus newtonarum*, all of which were collated or assembled previously.[74] Protein-coding sequences for the 30 species were processed with Orthofinder v2.5.2[149,150] (-M msa -S diamond -A mafft -T fasttree) to find orthologous sequences. The orthogroups can be found at CaltechData (https://doi.org/10.22002/3w8cz-t2g08, Figure S3A). The resulting MAFFT amino acid sequence alignments for the orthogroups containing at least one sequence for at least 24 of the species were then trimmed with the trimal v1.4.1[151] gappyout method, resulting in 2064 orthologous protein coding loci. Maximum likelihood trees were generated for all trimmed alignments using iqtree v1.6.8[152,166] with 1000 bootstraps, restricted to the models WAG,LG,JTT, and Dayhoff. The trees were pruned to strictly orthologous sequences using PhyloTreePruner v1.2.4[153] with a minimum number of taxa cutoff of 24 (80%) and a bootstrap cutoff of 0.7. The resulting pruned alignments were concatenated with FASconCAT v1.04,[154] resulting in a supermatrix containing 750,163 amino acid sites with 2,063 gene partitions. MARE v0.1.2[155] was used to improve the phylogenetic signal of the partitions, resulting in a supermatrix containing 374,139 amino acid sites with 1,039 gene partitions. Partitionfinder v2.1.1[156] was then used with raxml[167] and otherwise default parameters to identify an optimal partitioning scheme and corresponding set of molecular evolution models for the gene partitions. A maximum likelihood species tree was generated from the supermatrix and partition scheme using iqtree v1.6.8 with 1000 bootstrap replicates. The supermatrix, partition scheme, and maximum-likelihood species tree can be found at (CaltechData https://doi.org/10.22002/3w8cz-t2g08, Figure 1A). The tree was rooted using *Drosophila melanogaster*.

In order to constrain divergence times on the species tree, twelve fossil calibrations were selected to place bounds on specific nodes in the tree. For all fossils, the youngest age interpretation of the fossil was used, following best practices.[168] The corresponding nodes are labeled in Figure S1A.

A. MRCA of Diptera and Coleoptera

An upper bound was placed on the root of the tree using the median age estimate of holometabola (345 Ma).[169] A lower bound was set using the stem group beetle *Coleopsis archaica* (293.8 Ma).[170]

B. MRCA of Buprestoidea and all other beetles in this study:

A lower bound was placed on the node at which *A. planipennis* branches, using the stem Buprestid fossil, *Ancestrimorpha volgensis* (164.7Ma).[171,172]

C. MRCA of Curculionoidea and Chrysomeloidea:

A lower bound was placed on the MRCA of Curculionoidea and Chrysomeloidea using both *Archaeorrhynchus* sp. and *Eobelus* sp. (157.3Ma).[173,174]

D. MRCA of Chrysomeloidea:

A lower bound was placed on crown Chrysomeloidea using *Cretoprionus liutiaogouensis* (122.5 Ma).[174,175]

E. MRCA of Staphylinidae:

A lower bound was placed on the MRCA of Staphylinidae using undescribed Silphids (152 Ma).[176,177]

F. MRCA of Aleocharinae and Tachyporinae:

A lower bound was placed on the MRCA of Aleocharinae and Tachyporinae using the Tachyporine beetle *Protachinus minor* (147.28 Ma).[178,179]

G. MRCA of Gymnusini:

A lower bound was placed on the Gymnusini MRCA using *Cretodeinopsis aenigmatica* (98.17 Ma).[180–182]

H. MRCA of *Adinopsis* and *Deinopsis*:

A lower bound was placed on the MRCA of *Adinopsis* and *Deinopsis* using *Adinopsis groehni* (43.1 Ma).[183]

I. MRCA of Hypocyphtini:

A lower bound was placed on the MRCA of the hypocyphtines using *Baltioligota electrica* (43.1 Ma).[184,185]

J. Aleocharini stem:

A lower bound was placed on the *Aleochara* stem based on *Aleochara baltica* (43.1 Ma).[186]

K. MRCA of Oxypodini and Homalotini:

A lower bound was placed on the MRCA of Homalotini and Oxypodini using *Phymatura electrica* (43.1 Ma).[186]

L. MRCA of Athetini and Geostibini:

A lower bound was placed on the MRCA of Athetini and Geostibini using *Atheta jantarica*. *Dalotia coriaria* is most likely a member of the *Atheta*, thus the calibration point was moved one node deeper from the Athetini MRCA (43.1 Ma).[185]

MCMCtree and codeml, from PAML v4.9,[157] were used to perform divergence time analysis, using the previously generated maximum likelihood species tree, the associated supermatrix, and the above fossil calibration points. Branch lengths were initially approximated in codeml by maximum likelihood (ML) using the WAG empirical rate matrix with gamma rates among sites, approximated with four rate categories. The gradient and Hessian of the likelihood function at the ML branch length estimates were then used to run MCMCtree with the approximate method. The relevant model parameters were clock = 2, cleandata = 0, BDparas = 1 1 0.1, rgene_gamma = 2 20 1, sigma2_gamma = 1 10 1, and finetune = 1:.1.1.1.1.01.05. All fossil calibration points were modelled as truncated Cauchy distributions,[187] defined with default MCMCtree parameters, with the exception of the root, which was defined as a uniform distribution between the upper and lower bound with tails on either side of the bounds.[188] After a burn in of 20,000 iterations, 200,000 samples were collected, sampling every 100 iterations. Divergence time estimates were compared between multiple runs to verify that the MCMC chains had converged to a stable posterior distribution. The time calibrated species tree data can be found at CaltechData (https://doi.org/10.22002/3w8cz-t2g08, Figure 1A).

SMART-seq transcriptome sequencing

The abdominal fat body and entire crushed pronotum were dissected from individual *Platyusa*, and the 5^{th}-7^{th} abdominal segments, with gut removed, and the entire crushed pronotum were dissected from *Sceptobius* in ice-cold DEPC PBS, flash frozen in a dry ice/ethanol bath, and stored at -80°C until processing. Library preparation was carried out using the NEBNext Single Cell/Low Input RNA Library Prep Kit for Illumina, using NEBNext Multiplex Oligos (New England Biolab, MA) following the manufacturers protocol (NEB #E6420). The number of PCR cycles during cDNA amplification was 9 for *Sceptobius* samples and 14 for *Platyusa* samples. Final library amplification was either 8 or 12 cycles for all libraries, depending on the intermediate library concentration at this step. The quality of all libraries was assessed by running samples on a Qubit High Sensitivity dsDNA kit (Thermo Fisher, CA) and Agilent Bioanalyzer High Sensitivity DNA assay (Agilent, CA). The libraries were sequenced, either 50 bp for *Platyusa* or 100 bp for *Sceptobius*,

single end to a read depth of 20-25 million reads on an Illumina HiSeq2500 (Illumina, CA) at the Millard and Muriel Jacobs Genetics and Genomics Laboratory at Caltech.

Differential Expression Analysis

SMART-seq reads were pseudoaligned to transcriptomes of *Sceptobius* and *Platyusa* using kallisto v0.46.2, with 100 bootstraps, single end flag, an average fragment length of between 339-450bp with a standard deviation of 27-41 bp. Two paired *Sceptobius* samples from the same animal were removed after mapping, due to the small percentage of reads that pseudoaligned (<4% vs 20-40% for all other samples). Next, sleuth v0.30.0 was run, using a full model of condition (pronotum or fat body) plus animal (paired samples were collected from each beetle) and a reduced model of animal. A likelihood ratio test was run using the two models to identify differentially expressed transcripts, which were then filtered by the sign of the average transcripts per million (TPM) for the transcript in the abdominal fat body minus the average TPM for the transcript in the pronotum.

Identification of CHC pathway enzymes

All transcripts in the *Sceptobius* and *Platyusa* transcriptomes were searched against the NCBI nr (February 2019) and UniProt (February 2019) databases, taking the top five hits and using an evalue cutoff of 1e-05. The top hit for each transcript ID, sorted by highest bitscore, lowest evalue, and highest percent identify, was determined for both the NCBI nr and Uniprot results. The differentially expressed smartseq transcripts were then filtered by the NCBI nr and Uniprot annotations, selecting those transcripts annotated as elongation of very long chain fatty acids, fatty acyl-CoA reductase, fatty acid synthase, acyl-CoA desaturase, stearoyl-CoA desaturase, cytochrome P450 4G1/4G15, or NADPH-cytochrome P450 reductase. The orthogroups containing these potential CHC pathway enzymes were identified.

The enzyme list generated via differential expression analysis was supplemented with a homology based approach, drawing from cuticular hydrocarbon biosynthesis literature in *Drosophila melanogaster*[189,190] and the closely related rove beetle, *Dalotia coriaria*.[73] Orthogroups containing known *Dalotia* and *Drosophila* CHC biosynthesis enzymes as well as the differentially expressed *Sceptobius* and *Platyusa* enzymes were analyzed by aligning the sequences in each orthogroup using mafft v7.453[159] and then generating phylogenetic trees using fasttree v2.1.10.[160] The resulting gene trees were manually curated, pruning analogous branches, removing short sequences that appeared to be fragmented, removing or splitting long sequences that appeared to be mis-predicted chimeras of adjacent genes in the genome, removing identical or nearly identical sequences, and in some cases replacing misassembled transcripts with gene predictions from the corresponding draft genomes. All *Sceptobius* and *Platyusa* sequences in each gene tree were assumed to be potential CHC biosynthesis enzymes. Curated transcriptomes for both *Sceptobius* and *Platyusa* were generated by replacing or removing those sequences modified or removed in the process of generating the gene trees. The smartseq reads were then remapped, in a similar fashion as described above, to these curated transcriptomes and differential expression analysis was performed. Heatmaps of TPM for the full complement of enzymes as well as their differentially expressed status in *Sceptobius* and *Platyusa* are shown in Figures S3A and S3B. Gene trees, curated transcriptomes, and lists of CHC biosynthesis enzymes can be found at CaltechData (https://doi.org/10.22002/3w8cz-t2g08, Figures S3A and S3B).

Hybridization Chain Reaction (HCR)

Probe sets, HCR hairpins, as well as amplification buffer, hybridization buffer, wash buffer were purchased from Molecular Instruments (Beckman Institute at Caltech; www.moleculartechnologies.org) for each transcript. Representative transcripts were chosen from each gene family in *Sceptobius* and *Platyusa* using several criteria. As the only representative of its family, *CYP4G1* was chosen. *Desat1* is homologous to *Drosophila desatF*, *desat1*, *desat2*, and thus was chosen as a likely oenocyte enzyme candidate. *ELO4* was chosen due to its known expression and function in *Dalotia* oenocytes (the orthologous gene is named elo-708 in Brückner et al.[73]). *FAS3* and *FAR4* were chosen due to their differential expression in the abdomen as well as minimal expression in the pronotum control tissue.

Samples were dissected in DEPC treated PBS with a small amount of DEPC PBST (0.1% Tween) added. Beetles were CO_2 anesthetized and then transferred to a dissecting dish and the head was removed with dissecting scissors. Grasping the thorax and abdominal segments 9 and 10 with forceps, the abdominal tip, gut, and genitalia were removed through the tip of the abdomen. The abdomen was then either separated along the sagittal plane or ventrally and dorsally with dissecting scissors. Samples were placed in ice-cold DEPC-PBST until fixing. Abdominal segments were fixed in 4% PFA in DEPC-PBST for 25 minutes at room temperature and subsequently rinsed three times with fresh DEPC-PBST. Samples were then dehydrated by washing with a DEPC-PBST/methanol series, finishing with a 100% methanol wash. At this step, samples were either stored at -20°C or rehydrated using a methanol/DEPC-PBST series. Samples were rinsed two additional times for five minutes each at room temperature and then washed with a 0.01% Proteinase K solution in DEPC-PBST for five minutes at room temperature. Samples were then rinsed twice with fresh DEPC-PBST and post-fixed with a 4% PFA in DEPC-PBST solution for 25 minutes at room temperature. Samples were rinsed again with DEPC-PBST and then incubated with hybridization buffer at 37°C for 30 min. The probe solution was preheated during this period, combining two microliters of both even and odd HCR probes with 100 μL of hybridization buffer at 37°C. The hybridization buffer was removed from the sample and replaced with probe solution.

Samples were incubated overnight at 37°C. No-probe control samples were incubated overnight at 37°C in hybridization buffer in the absence of probes. The following day, samples were washed with preheated wash buffer, twice for five minutes and twice for

30 minutes, both at 37°C. During the last wash, hairpins were snap cooled (90 seconds at 95°C and then 30 min room temp in the dark). Samples were incubated with amplification buffer for 10 min, after which the old amplification buffer was replaced with 100 μL of fresh amplification buffer and the hairpins. Amplification occurred overnight in the dark at room temp. Multiple combinations of B1, B3, and B4 amplifiers with Alexa 488, Alexa 546, and Alexa 647 fluorophores were used. Samples were then washed with SSCT (saline sodium citrate with Tween) twice for five minutes in the dark. Samples were incubated for two hours at room temperature with Hoechst 33342 (1:2000, Thermo Fisher, CA) to mark nuclei, Alexa 488-Wheat Germ Agglutinin conjugate (WGA; 1:500, Thermo Fisher, CA) to mark cell membranes, streptavidin Alexa 647 (Thermo Fisher, CA) to mark sites of biotin accumulation (e.g. fatty acid biosynthesis in fat body, 1:500), and then washed four more times with SSCT, twice for five minutes and twice for 30 minutes. Samples were mounted in ProLong Gold Antifade Mountant (Thermo Fisher, CA), and imaged using a Zeiss LSM 880 with Airyscan fast at 10x and 40x.

Tissue imaging and confocal microscopy

Beetles were dissected in PBS with a small amount of PBST added. Dissections were carried out in a similar fashion to those described under HCR. Samples were stored in ice cold PBST until all samples had been dissected. Samples were then fixed in 4% PFA with PBST for 25 minutes at room temperature. Samples were then quickly washed by exchanging the PBST three times, and then incubated with an anti-Engrailed 4D9 (1:5, DSHB, IA) mouse primary antibody in PBST overnight at 4°C. The following day, samples were rinsed quickly three times by replacing the PBST. Samples were then nutated 3 times for 20 minutes at room temperature with fresh PBST. Samples were then incubated with Alexa-488-Wheat Germ Agglutinin conjugate (WGA; 1:500), Hoechst 33342 (1:2000) to mark nuclei, and secondary antibody (Alexafluor-555 goat anti-mouse; 1:500, Thermo Fisher, CA) at room temperature for two hours. Samples were washed three times rapidly by replacing PBST, three 20 minute washes with PBST at room temp, and then were mounted in ProLong gold Antifade Mountant (Thermo Fisher, CA), and imaged using a Zeiss LSM 880 confocal microscope with Airyscan fast at 10x and 40x.

Gene silencing by RNAi

Double-stranded RNA constructs were prepared as previously described.[73] Target sequences were cloned into a pCR2.1 TOPO vector (Thermo Fisher, CA) with primers containing T7 linkers. The following primers were used:

Dcor* oCYP4G-*1

F: 5'- TAATACGACTCACTATAGGGCACTCCCTGTCGGAACCTTGGA-3'
R: 5'-TAATACGACTCACTATAGGGTTGCGACATCCTCCACAGACGT-3'

Dcor* oCYP4G-*2

F: 5'-TAATACGACTCACTATAGGGACGTCTGTGGAGGATGTCGCAA-3'
R: 5'-TAATACGACTCACTATAGGGATCCAAAATCCCCGGACCCGAT-3'

***Pson* oCYP4G**

F: 5'-TAATACGACTCACTATAGGGTCTTAGGATGTACCCACCAGTG-3'
R: 5'-TAATACGACTCACTATAGGGTGTCGCAATGCACTCGGTAT-3'

EGFP

F: 5'- TAATACGACTCACTATAGGGTCTTCTTCAAGGACGACGGCAACTAC -3'
R: 5'- TAATACGACTCACTATAGGGTTACTTGTACAGCTCGTCCATGCCGA -3'

The MEGAscript T7 Transcription kit (Thermo Fisher, CA) was used to synthesize dsRNA, which was cleaned using MEGAclear Transcription cleanup kit (Thermo Fisher, CA), and quantified via NanoDrop (Thermo Fisher, CA). Target dsRNA and control dsRNA, targeting green fluorescent protein (GFP), were diluted in DEPC-treated PBS and green food dye to a concentration of ~2mg/mL. Constructs were microinjected into third instar *Dalotia* larvae and adult *Platyusa*. *Dalotia* larvae were reared in 5cm Petri dishes with clean filter paper until they pupated and eclosed, after which they were fed frozen fruit flies until they were used in experiments. Injected *Dalotia* were used in experiments within 5-10 days of eclosing. *Platyusa* were maintained in Rubbermaid containers with a bed of packed damp coconut husk fiber and a diet of fruit flies. Beetles were sacrificed at 10 days and extracted in 100 microliters of hexane with a 10ng/microliter octadecane internal standard and analyzed via the CHC-GCMS method previously described. Total CHCs were compared between *oCYP4G*-KD and *GFP Platyusa* using a Welch's t-test in R.

qPCR of CHC pathway enzymes

Teneral *Sceptobius* were collected and reared as previously described. Three or four beetles were sampled each from zero, one, and three days post-eclosion as well as fully integrated beetles. All beetles were frozen at -80°C prior to RNA extraction. RNA was extracted and purified with the RNeasy purification kit (Qiagen, Germany). cDNA was then prepared using a Superscript III kit (Thermo Fisher, CA). The resulting cDNA was analyzed via qPCR. Briefly, 1 μL of cDNA template was combined with 6.5 μL of Luna® Universal qPCR master mix (New England BioLabs), 2 μL of combined forward and reverse primer (10μM, Integrated DNA Technologies, IA), and 10.5 μL of dH_2O per well. Samples were run on an Applied Biosystems StepOnePlus Real Time PCR System (Thermo Fisher, CA) using the following conditions: 95°C for 1 minute, 40 cycles at 95° for 15 s, 59°C for 30s. Melt curve analysis was performed by holding for 15s at 95°C followed by 30s at 60°C and 15s at 95°C. Primers were designed for three *Sceptobius* CHC enzymes and two *Sceptobius* housekeeping genes, Ribosomal protein S3 and Ribosomal Protein L19.

The following primers were used:

Sceptobius *ELO4*

F: 5'-TTCGGTGCTGCAAGGATAA-3'

R: 5'-CCCAAGAGTACCACACAAGAG-3'

Sceptobius *CYP4G1*

F: 5'-ACCCAGCTGATATTGAGGTTATC-3'

R: 5'-CTGACCAAGAGACCATTTCCA-3'

Sceptobius *Desat1*

F: 5'-CGCTACAGCACTAACTTCACT-3'

R: 5'-ACACGACGCTTGACCATATC-3'

Sceptobius *RPL19*

F: 5'-GAATGTACCGCTACTGGTTTCT-3'

R: 5'-CAGCCTCTGTTATGCGATGT-3'

Sceptobius RPS3

F: 5'-GGTGTCGACGTAGTCGTTAATC-3'

R: 5'-CGAAGTAGTTGTGTCCGGTAAG-3'

Each sample was run in duplicate, and the geometric means of the technical replicates were determined. The ΔΔct calculation was then used to determine fold change of samples relative to the integrated condition. The difference between the cycle threshold for the genes of interest and the geometric mean of the two housekeeping genes was first calculated for each sample. From this difference in cycle threshold for each gene, the geometric mean of the cycle threshold difference in the integrated condition was subtracted. Multiplying the resulting values by negative one yielded the approximate fold change in expression for each time point compared to the integrated condition.

Fluorescence quantification of CHC pathway enzyme expression levels

Teneral *Sceptobius* were collected and reared as previously described. Three beetles were sampled each from zero, one, two, three, and eight days post-eclosion. Four fully integrated *Sceptobius* were also collected. Due to the difficulty of obtaining larvae for the experiment, beetles were accumulated over the span of multiple weeks. As they were collected, samples were processed immediately via the previously mentioned HCR protocol up through the methanol dehydration step, at which point they were stored at -20°C. Once all samples had been collected, the remaining steps in the HCR process were carried out in parallel for all samples, with all beetles from the same time point being processed in the same tube. All sample tubes were incubated with identical probe and hairpin solution concentrations, targeting *Desat1*, *ELO4* and *CYP4G1*. Samples were mounted together and imaged on a Zeiss 880 confocal microscope (Zeiss, Germany) in Airyscan fast mode using identical imaging parameters. The integrated fluorescence signal was then calculated for all oenocytes in the resulting micrographs. Image stacks were converted to Tiffs and masks for oenocytes were determined using the *CYP4G1* channel and the python package Cellpose v.2.0.5[135] in Python v3.8.13. Image stacks were first projected along the z-axis by summing over all slices in the stack and then cells were identified with the 'cyto' model in Cellpose using a diameter of 35, flow threshold of 0.1, minimum size of 200, cell probability threshold of 0.8, and interp and neg_avg set to true. The resulting oenocyte cell masks were used to filter the *CYP4G1* channel by calculating the percentage of the z-projected frame occupied by all cell masks, and then setting a pixel intensity threshold that excludes the same percentage of voxels across the *CYP4G1* channel slices. The threshold mask determined with the *CYP4G1* channel was then applied to the *ELO4* and *Desat1* channels. Next, the cell masks were applied to each filtered channel, integrating over the fluorescence intensity in each slice to recover the total fluorescence intensity in each oenocyte, for the three channels. Oenocyte HCR fluorescence micrographs can be found at CaltechData (https://doi.org/10.22002/3w8cz-t2g08, Figures S4B–S4D, confocal_data).

Aggression analysis

Wild caught *Sceptobius*, *Liometopum*, and *Platyusa* were transported to the lab as previously described and maintained until they were used in behavior experiments. *Liometopum* and *Sceptobius* were used in behavioral arenas within a week of collecting to avoid shifts in CHC profiles that arise from the standard lab feeding setup. *Sceptobius* were coated with *Platyusa* CHCs by placing *Sceptobius* in 5 mL vials with 7-8 *Platyusa* for 2 hours. The number of *Platyusa* was sufficient to fill the entire bottom of the vial, ensuring that *Sceptobius* was in contact with *Platyusa* for the entire 2-hour period, regardless of grooming status. Control *Sceptobius* were placed in empty vials for 2 hours. Following the coating procedure, *Sceptobius* was loaded into a behavioral arena with three *Liometopum* collected contemporaneously from the same colony as the beetle. The behavioral arena was constructed from acrylic, with a 5cm diameter and a sliding door to allow acclimation of the beetle and ants in the arena prior to being introduced to each other. Beetles and ants were loaded into the arena unanesthetized, to avoid changes in behavior that arise from CO_2 or cold anesthesia.[191–193] After a 2-minute acclimation period, the sliding door was opened, allowing the beetle and the ants to interact for a 5-minute interaction period. Behavior was recorded on a FLIR camera (BFS-U3-16S2C-CS: 1.6 MP) with an InfiniGage lens (Infinity Photo-Optical, CO), at 60hz. Aggression behavior videos can be found at CaltechData (https://doi.org/10.22002/3w8cz-t2g08, Figure 4G_videos).

After each run, *Sceptobius* and the three *Liometopum* CHCs were analyzed via GCMS. Each beetle was extracted in 10 microliters of hexane for 20 minutes and three microliters of extract were analyzed. *Liometopum* samples were extracted in 70 microliters of

hexane for 20 minutes and two microliters were analyzed. CHCs were run on the GCMS, identified, and integrated as described previously. Scoring of behavioral interactions was carried out in BORIS v. 8.20.1.[161] A simple ethogram consisting of biting, mandible flaring, and neutral interaction (any instance where no biting or mandible flaring was observed) was used. Interactions were scored any time that any ant's antenna made contact with *Sceptobius*. An aggression index was calculated as the sum of mandible flaring events and two times the number of biting events, divided by the sum of mandible flaring events, two times the number of biting events, and neutral events. Aggression values can thus take any value between zero, i.e. none of the interactions were aggressive, and one, i.e. every interaction was aggressive.

Behavioral analysis of beetle-ant physical interactions

A multi-well behavior arena was constructed from 1/8th inch infrared transparent acrylic (Plexiglass IR acrylic 3143) and was backlit with infrared LED panel. To ensure that runs were conducted in complete darkness, the arena was placed inside an incubator in a dark room. The arena was 4 cm in diameter, split into multiple chambers to give the beetles places to hide from their paired ant. Small, ~5 mm diameter, pieces of damp filter paper were added to each well to increase humidity within wells. Single *Sceptobius lativentris, Dalotia coriaria*, and *Platyusa sonomae* were cold anesthetized, and then loaded into individual arena wells, along with one cold anesthetized *Liometopum occidentale*. Beetles were recorded at 1 hz for 24 hours using a FLIR camera (BFS-U3-51S5M-C: 5.0 MP) with a Pentax 12 mm 1:1.2 TV lens (Ricoh, FL-HC1212B-VG). Videos were cropped down to individual wells and analyzed with Deeplabcut v2.0.6.2.[138,139] Distinct network models, using a default ResNet50 network, were trained for each beetle, consisting of two labels for the head and abdominal tip of both *Liometopum* and *Platyusa*, and one label for the head of *Sceptobius* and *Dalotia*. The networks were trained on ~500 labeled frames for the *Platyusa* model, ~150 frames for the *Sceptobius* model, and ~50 frames for the *Dalotia* model. All of the models were trained over multiple iterations and the *Dalotia* model used the training weights from the final *Sceptobius* model as its initial weights. The training and test errors were 1.27 and 0.92 pixels for the *Platyusa* model, 1.03 and 2.79 pixels for the *Sceptobius* model, and 2.13 and 3.55 pixels for the *Dalotia* model. The three networks were used to analyze all of the videos of their respective beetles.

Position data was filtered for frames in which the ant prediction is likely accurate by calculating the length of each ant, and then choosing an upper threshold that excludes outliers for all ants collected in a given behavioral run. Then an ellipse was drawn around the ant for each labelled video frame, such that the sum of the distances between any point on the perimeter of the ellipse and the head and abdominal tip of the ant summed to 1.4 times the ant length in that frame. If the beetle's head, or head or tail for *Platyusa*, fell within the ellipse for that frame, the beetle was considered to be touching the ant. The percent of frames in which the beetle was touching the ant was then calculated for each well. Differences in the touching percent between the three beetles were compared using an ANOVA with a Tukey *post hoc* test in R.

Desiccation analysis

Desiccation resistance was measured in *Sceptobius* using an acrylic desiccation arena. The arena consisted of two sheets of 3/8 inch acrylic both containing six wells with a diameter of one centimeter each. The two sets of wells sandwiched a piece of filter paper, which acted as the floor for the beetles, located in the upper set of wells. The lower set of wells was used to introduce wetted circles of filter paper as a humidity source. The well setup was then sandwiched between two sets of IR pass-through acrylic, creating a dark behavior arena. The desiccation arena was lit from below by LED lights, which emitted partially in the IR range.

To test the effect of superphysiological levels of CHCs on *Sceptobius*, beetles were coated in *Liometopum* CHCs, which were extracted and fractionated previously.[95] Briefly, surface chemicals were extracted from tens of thousands of *Liometopum*, and were subsequently separated via vacuum flash chromatography and eluted with hexane and cyclohexane. The resulting purified CHC extracts contained approximately 250 ant equivalents per milliliter. Roughly 25 ant equivalents of *Liometopum* CHCs were then applied to the inside of a 5mL glass vial and the hexane was evaporated off under a stream of N_2. This process resulted in a thin coating of *Liometopum* CHCs on the inner surface of the vial. *Sceptobius* were collected at multiple nest-sites, and were pooled for each run. Beetles were either placed in the CHC coated vial, or in a blank control vial, for an hour. *Sceptobius* in the CHC coated vial moved around enough to transfer CHCs from the walls of the vial to their cuticle. Groups of five beetles were then loaded into each well in the arena. Beetles were run in groups to avoid confounding effects from social isolation. Desiccation trials were run at room temperature under a FLIR camera (BFS-U3-04S2M-CS: 0.4 MP) with an InfiniGage lens (Infinity Photo-Optical, CO) running at 1 hz. Recordings were collected until all beetles in the desiccation arena were dead, typically 20-40 hours.

For runs with higher humidity, 10 pieces of hole punched filter paper were placed in the lower chamber below each well and 50μl of water were added to the pieces of filter paper. To replicate the effects of CHC addition on another beetle species, we knocked down *CYP4G1* in *Dalotia coriaria*, using the RNAi protocol described above. Control beetles were injected with dsRNA for *GFP*, and thus had a species typical CHC profile. We then took the *CYP4G* KD *Dalotia* and coated them in ant CHCs, as described above. *GFP* RNAi *Dalotia*, *CYP4G* RNAi *Dalotia*, and *CYP4G* RNAi *Dalotia* with *Liometopum* CHCs were then run in the desiccation arena. After each run, *Dalotia* were extracted in 70 microliters of hexane containing an internal octadecane standard and analyzed with the CHC-GCMS method describe above to verify that the knockdowns were successful. Beetles for which the wild type CHC profile was detectible were excluded from downstream analysis.

Sceptobius and *Platyusa* isolation from *Liometopum*

Sceptobius were maintained in a container of damp coconut fiber in an incubator at 24°C and 90-95% relative humidity. Control beetles were kept in similar containers containing 12 *Liometopum* workers. Boxes were monitored twice daily for beetle death. CHC amounts were quantified for living or recently deceased *Sceptobius* at 48 and 72 hours of isolation by extracting beetles in 10 microliters of hexane containing 1ng/microliter of C18 for 20 minutes followed by GCMS analysis using the previously described CHC-GCMS method. Wild caught *Platyusa* were reared for a month on a diet of frozen *Drosophila melanogaster* in the absence of *Liometopum occidentale*. *Platyusa* and *Drosophila* were then extracted in 70 microliters of hexane containing 10 ng/microliter C18 for 20 minutes and run on the GCMS using the previously described CHC GCMS method. CHC profiles of the *Drosophila* fed *Platyusa* were compared to CHC profiles of *Platyusa* fed frozen *Liometopum occidentale* for the same period.

QUANTIFICATION AND STATISTICAL ANALYSIS

The comparison of the touching percent and deuterated hydrocarbon transfer data in Figures 2K and 2N was performed using an ANOVA with Tukey post-hoc test in R, v4.4.1. The comparison of CHCs in *oCYP4G*-KD and *GFP* injected *Platyusa* in Figure 2E was performed using Welch's t-test in R, v4.4.1. An alpha level less than or equal to 0.05 was used to determine significance. Differential expression analysis of tissue specific RNA-seq data from Figures S3A and S3B was performed in sleuth v0.30.0, using a likelihood ratio test comparing the full model (condition + animal) and the reduced model (animal).

Supplemental figures

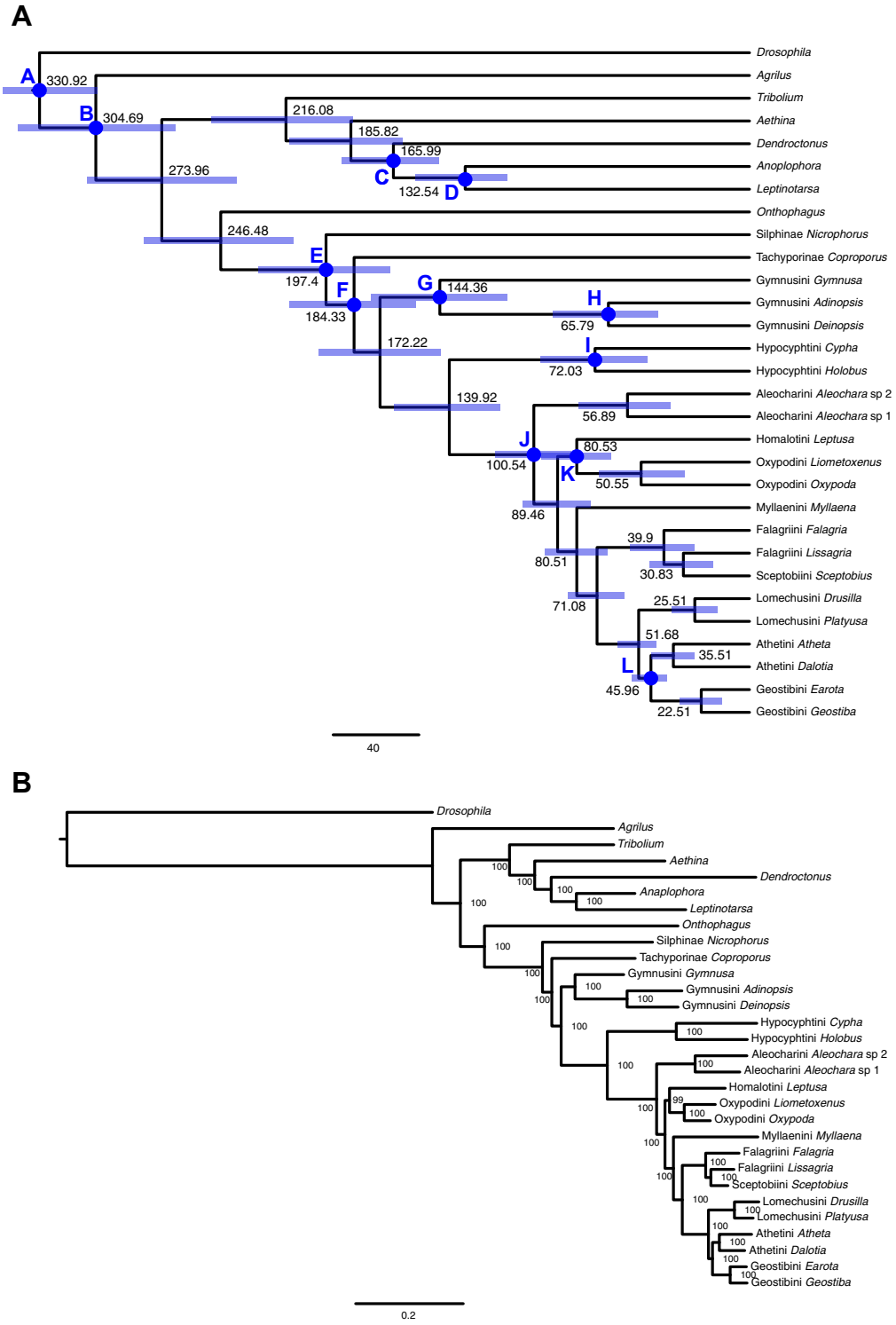

(legend on next page)

Figure S1. Additional species trees, related to Figure 1

(A) A time-calibrated species tree generated with the approximate Bayesian method in MCMCTree. Divergence times are listed in millions of years (Ma), blue bars represent 95% credibility intervals on divergence times, and labeled blue dots specify fossil calibration points, listed in STAR Methods.

(B) A maximum likelihood species tree, with bootstrap support listed at each node.

Trees in (A) and (B) were rooted using *Drosophila* as the outgroup.

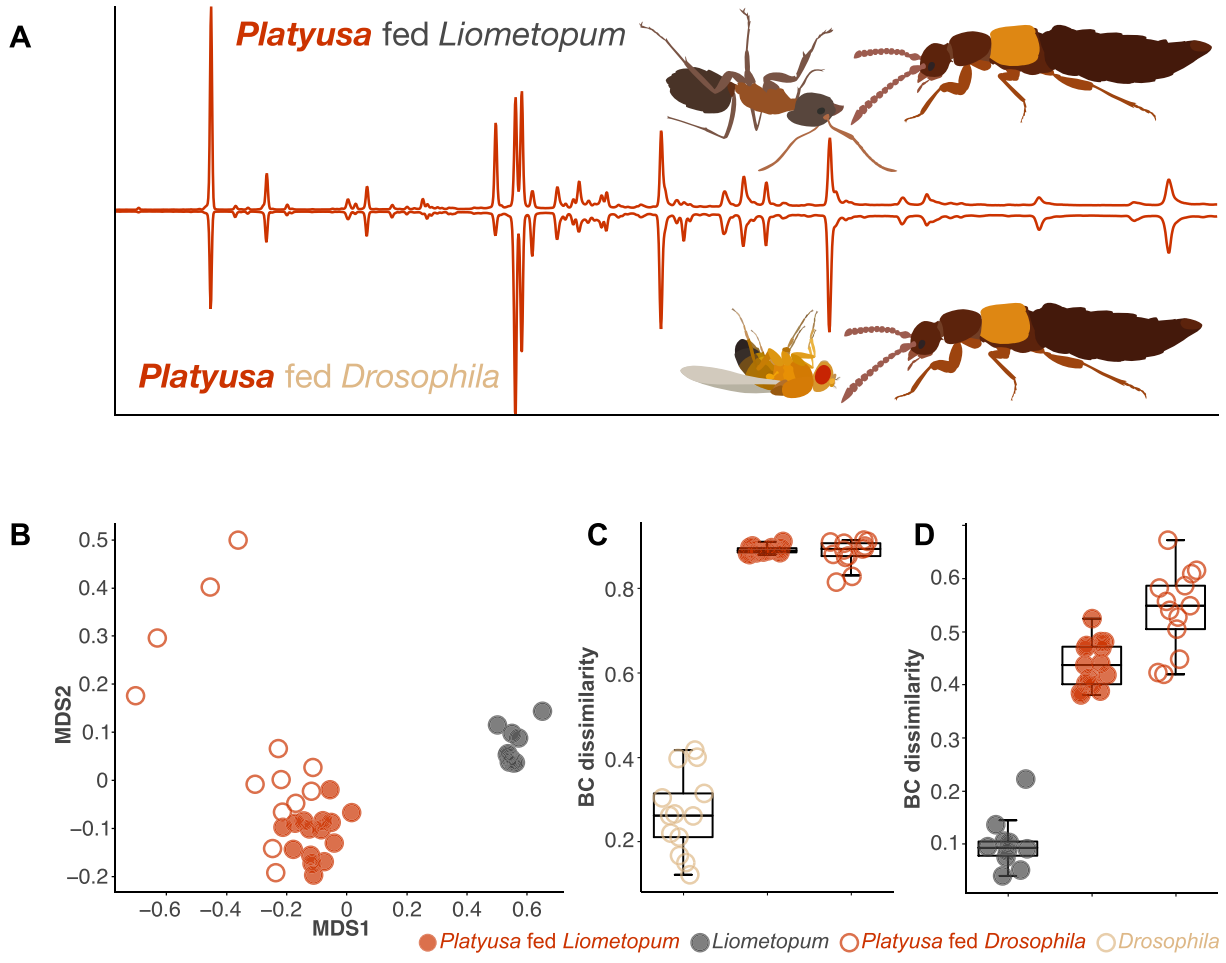

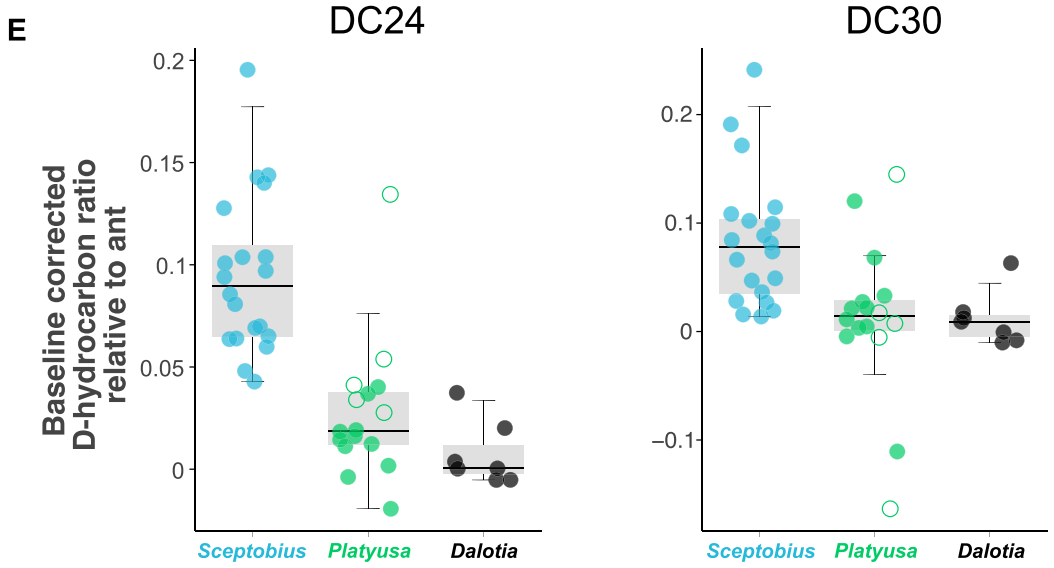

(legend on next page)

Figure S2. Additional tests of CHC mimicry mechanisms, related to Figure 2

(A) Representative GC traces showing the CHC profile of *Platyusa* fed *Liometopum* or isolated *Platyusa* fed *Drosophila* for 1 month.

(B) NMDS ordination plot of pairwise Bray-Curtis dissimilarity measurements of *Liometopum*, *Platyusa* fed *Liometopum* for 1 month, and *Platyusa* fed *Drosophila* for 1 month (stress = 0.0859).

(C) Bray-Curtis dissimilarity between the two *Platyusa* treatments and the average *Drosophila* CHC profile. *Drosophila* samples were also compared with the average *Drosophila* profile.

(D) Bray-Curtis dissimilarity between the two *Platyusa* treatments and the average *Liometopum* CHC profile. *Liometopum* samples were also compared with the average *Liometopum* profile.

(E) Baseline-corrected deuterated hydrocarbon transferred from *Liometopum* to beetles during 24-h interaction period using tetracosane-d_{50} (DC24) and triacontane-d_{62} (DC30). Open circles represent trials in which *Platyusa* ate the paired ant. The DC24 plot is the same as Figure 2N, with the additional information of ant predation by *Platyusa*.

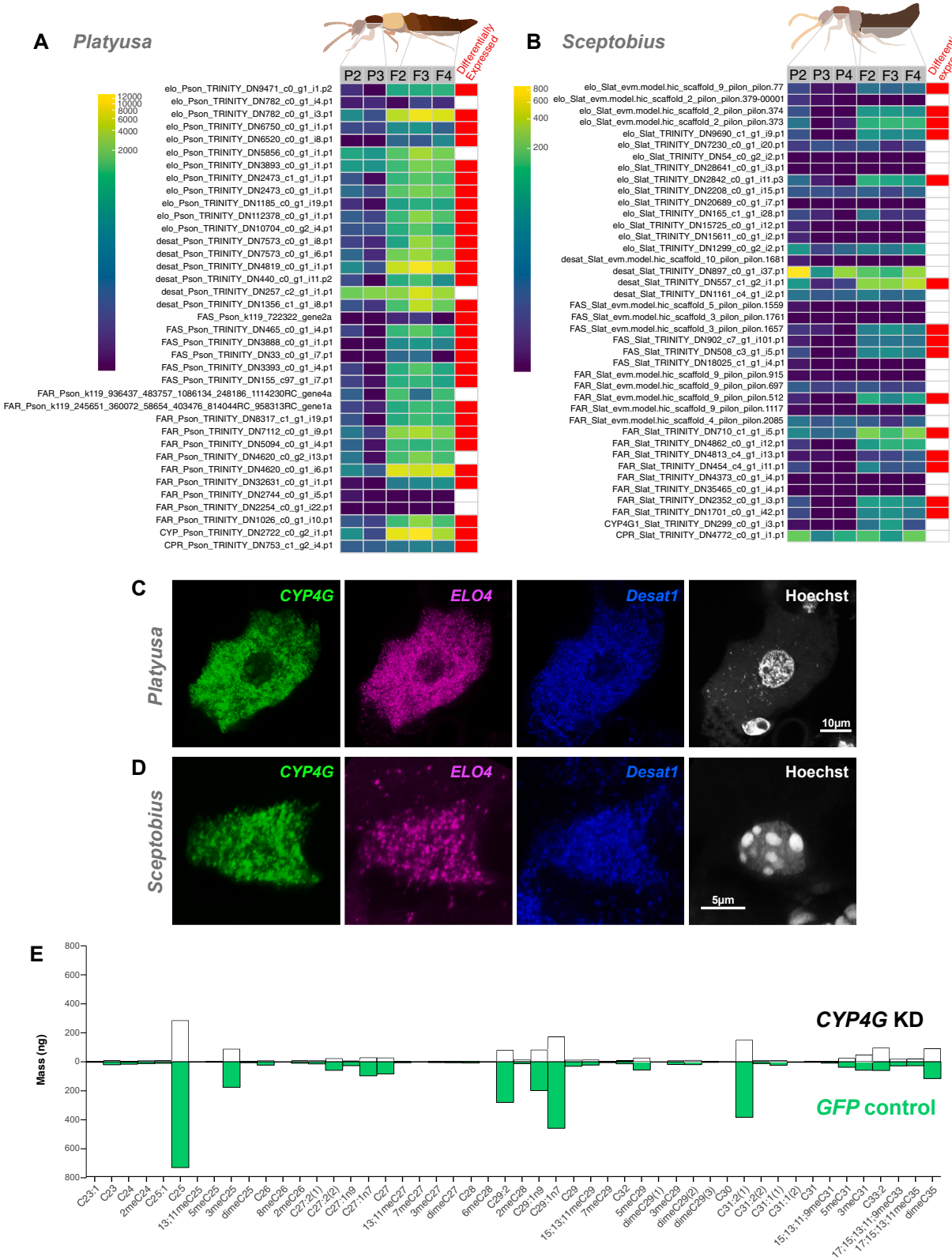

(legend on next page)

Figure S3. CHC biosynthesis pathway validation, related to Figures 2 and 3

(A and B) Heatmaps of CHC enzyme expression in (A) *Platyusa sonomae* and (B) *Sceptobius lativentris* in transcripts per million (TPM) for control tissue (pronotum, P) and test tissue (fat body, F). Numbers next to the treatment group correspond to the ID of the single beetle dissected for that sample. Differentially expressed transcripts are shown in red.

(C and D) (C) HCR labeling of *CYP4G* (green), *ELO4* (magenta), *Desat1* (blue), and Hoechst (white) in an oenocyte in *Platyusa sonomae* and (D) *Sceptobius lativentris*.

(E) The average mass of each CHC extracted from wild-caught *Platyusa sonomae* 10 days after injection with dsRNA targeting *CYP4G* or *GFP*.

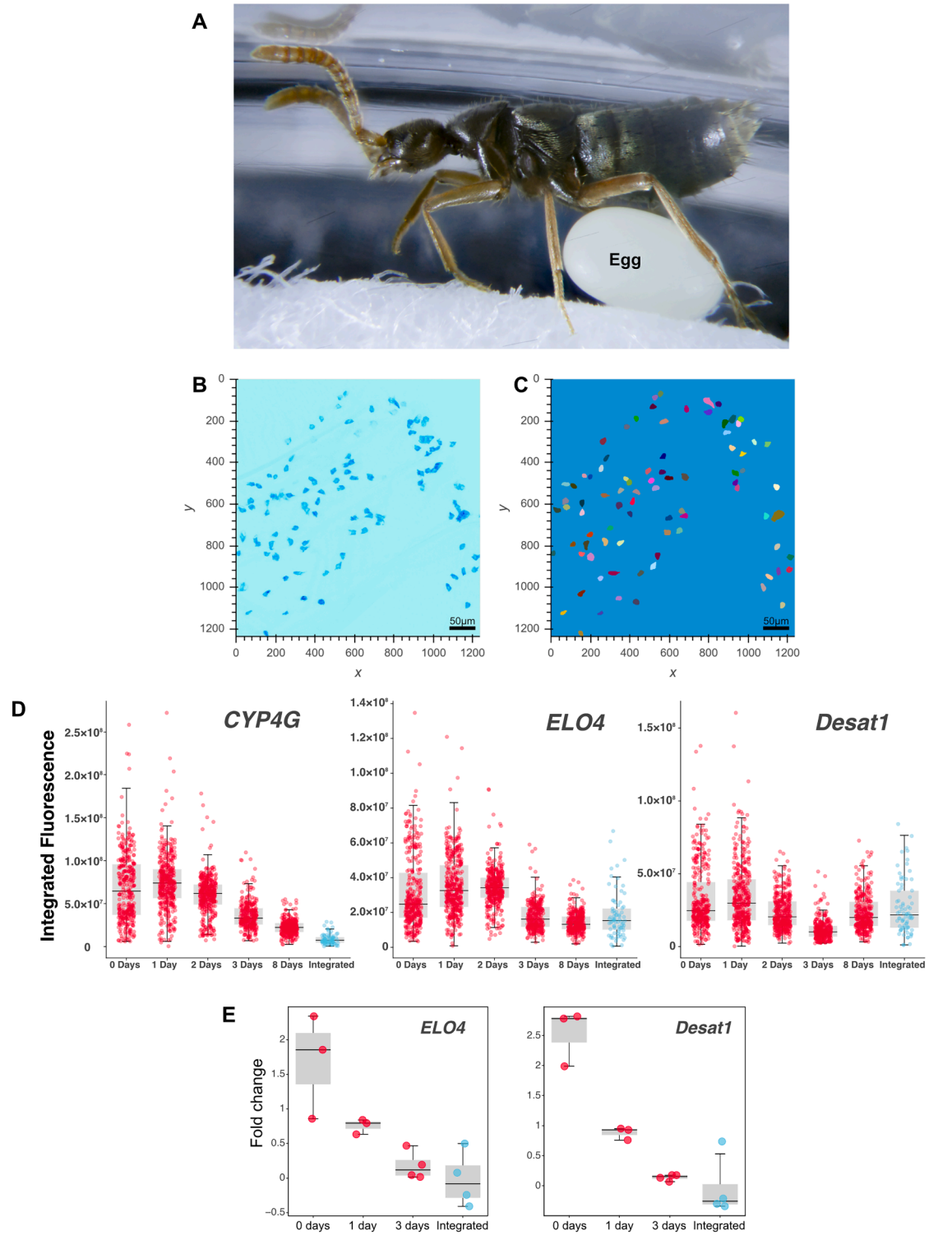

Figure S4. The imprint of myrmecophily in *Sceptobius lativentris* development, related to Figure 4

(A) A deceased female *Sceptobius* next to her recently laid egg. *Sceptobius* invest heavily in individual eggs that are of a comparable size to the non-gravid female abdomen.

(legend continued on next page)

(B) Summed projection of a representative z stack of HCR targeting *CYP4G* expression in teneral *Sceptobius*.
(C) Cellpose cell masks generated for the same sample.
(D) Integrated fluorescence intensity of HCR probes targeting *CYP4G*, *ELO4*, and *Desat1* in individual oenocytes at multiple time points after *Sceptobius* eclosion.
(E) qPCR measurements of *ELO4* and *Desat1* transcription in whole-body extractions of *Sceptobius* at multiple time points following eclosion.

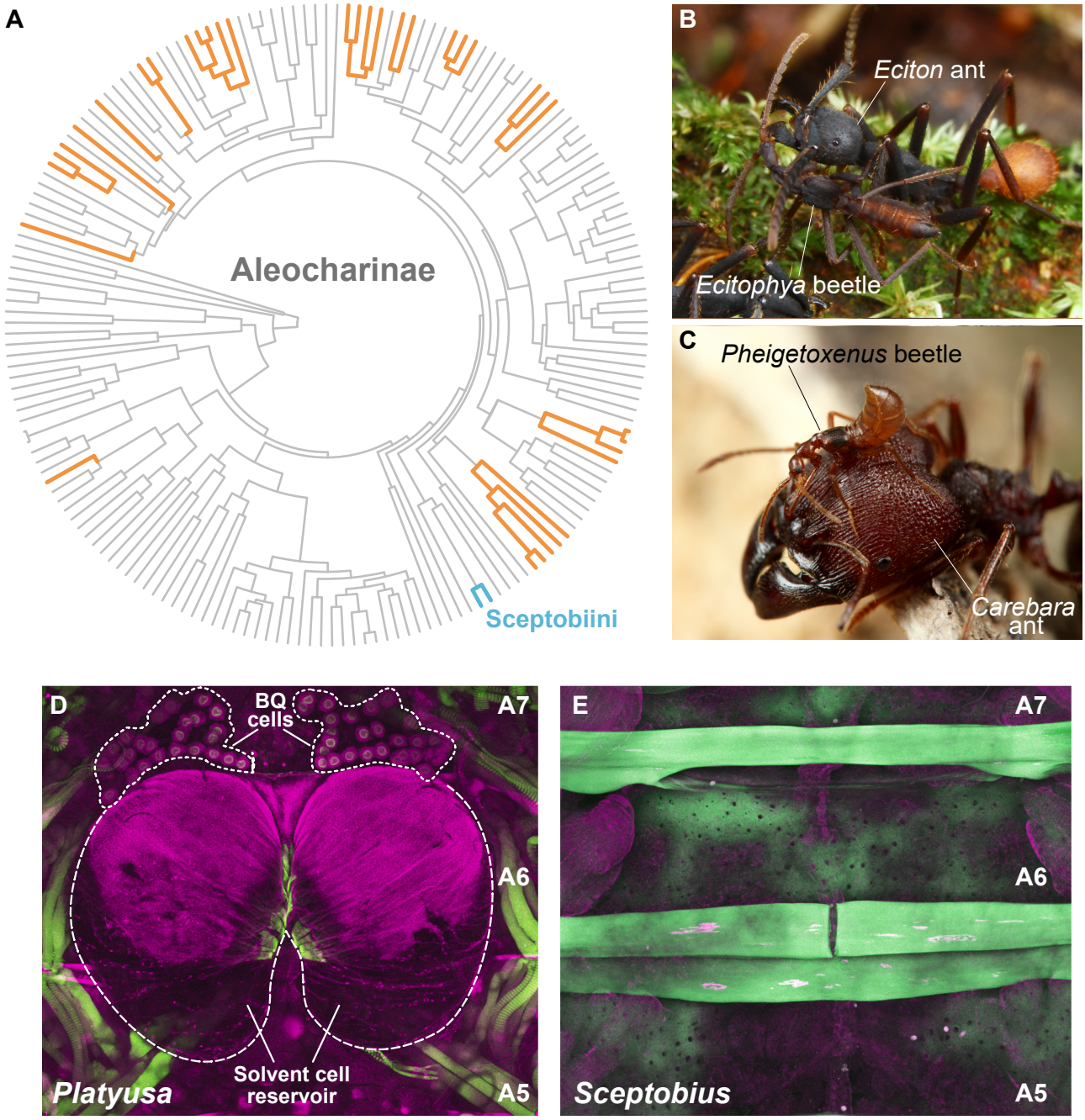

Figure S5. The Catch-22 syndrome across Aleocharinae, related to Figure 5

(A) Aleocharinae phylogeny showing socially integrated clades, with *Sceptobius*-like biology labeled orange—or blue for Sceptobiini. Within these clades, no instances of reversion to a free-living lifestyle have been described. The topology is from Maruyama and Parker.[63]

(B and C) Examples of aleocharine myrmecophiles that have converged on a similar, obligately symbiotic phenotype to *Sceptobius*.

(B) *Ecitophya* grooming its host ant, *Eciton burchellii*. Credit: T. Komatsu.

(C) *Pheigetoxenus* on a major worker of its host ant, *Carebara diversa*. Credit: Taku Shimada.

(D) The defensive tergal gland in *Platyusa sonomae*, which is present in all higher Aleocharinae (magenta, engrailed antibody and autofluorescence, general structures; green, phalloidin, muscles). The gland comprises two cell types: benzoquinone-secreting BQ (benzoquine) cells and alkane/ester-secreting solvent cells, which form a large chemical reservoir inside the body cavity.[73,74,194] A5–A7 represent abdominal segments 5 to 7.

(E) The tergal gland has been evolutionarily lost in *Sceptobius lativentris* (green, autofluorescence; magenta, engrailed antibody and autofluorescence). Numbers represent abdominal segments. The gland has been convergently lost among the orange clades in (A).[100–103,195–198]